Trapping effects on axion dark matter by shift symmetry breaking and their cosmological implications

Ph.D thesis

Trapping effects on axion dark matter by shift symmetry breaking and their cosmological implications

Shota Nakagawa

Department of Physics, Tohoku University

Abstract

One of the most leading candidates for dark matter (DM) is QCD axion. In addition to nonperturbative effects of QCD, the QCD axion could acquire extra potentials from the other explicit breaking effects of shift symmetry that is nothing but the Peccei-Quinn (PQ) symmetry. Such extra PQ breaking potentials must be suppressed to satisfy the experimental bound on the neutron electric dipole moment. However, the axion potential from QCD is negligibly small at high temperatures in the early universe, and therefore the extra potentials can have a sizable effect on the dynamics of axion. In particular, when the axion is temporarily trapped by the extra PQ breaking potential, the dynamics is expected to be significantly modified compared to the conventional scenario. This is the trapping effect. In this thesis, we study the trapping effect on the dynamics of the QCD axion and identify a viable parameter region in which the axion can explain DM. We begin with investigating the fundamental properties of the trapping effect in a general setup. Thanks to the analysis, we find that the adiabaticity in the physical system is an important factor in determining the dynamics of axion. To study the detail further, we consider two types of extra PQ breaking potential. First, we consider the case when the axion acquires a time-independent potential with multiple minima. We find that the abundance of axion can be enhanced or suppressed, depending on the initial position of axion, and that the isocurvature perturbation can be significantly suppressed. In particular, when the axion is temporarily trapped around a wrong vacuum, the abundance is independent of the decay constant as long as the trapping effect is strong enough. As a result, the axion can explain DM for arbitrary decay constant f_ϕ without isocurvature problem. It is nontrivial that the axion with small f_ϕ can saturate the total DM abundance, and such axions have relatively strong couplings with the SM particles, so that they can be probed by future haloscope experiments, such as MADMAX and BREAD. Second, we consider a time-dependent extra potential from the Witten effect of hidden monopoles. In this work, we investigate the trapping effect by the Witten effect in a broader parameter region of $\theta_{\rm ini}$ than previous studies. We find that the abundance can be suppressed as long as the trapping effect is sufficiently strong. The analysis of these two concrete cases helps us understand how the violation of adiabaticity affects the axion dynamics. We clarify that the trapping effect by extra PQ breaking has a significant impact on the viable parameter region for QCD axion DM, and the new predictions of axion DM motivate experiments scanning a different parameter region from the conventional QCD axion DM.

Contents

Chapter 1

Introduction

1.1 Overview and motivation

The existence of dark matter (DM) has been established by various observations. For instance, cosmic microwave background radiation (CMB) [1], rotational curves of spiral galaxies [2], and the bullet cluster [3], and so on. From these observational results, we have known some information on DM. First, DM is almost electrically neutral and has very feeble or possibly no interactions other than gravity. Second, it is so stable that the lifetime is much longer than the age of the current universe. According to some literature, e.g. [4, 5, 6], if DM particle is allowed to decay into dark radiation, the lifetime must be at least 10 times longer than the cosmic age. Third, the energy density amounts to about a quarter of the total one, $\Omega_{\rm DM} \sim 0.24$ [1]. Here the density parameter is defined as $\Omega_{\rm DM} \equiv \rho_{\rm DM0}/\rho_{\rm crit}$, where $\rho_{\rm DM0}$ is the present energy density of DM and $\rho_{\rm crit}$ is the critical energy density. Also, DM is cold i.e. non-relativistic so that it plays an important role in structure formation.

Nevertheless, the detailed properties of DM are yet unknown: "What is it composed of?", "How does it couple to known particles?", "How is it produced?", etc. To answer these questions, it is essential to make a plausible hypothesis based on new experimental fact and propose theoretical predictions. At first, such hypotheses must satisfy the properties or conditions described above. So far, various possibilities have been proposed. If DM is composed of some particle, a new undiscovered particle beyond SM (BSM) physics is necessary, because there is no DM candidate in the SM.[1] One of the well-studied candidates is Weakly Interacting Massive Particles (WIMP). WIMP is predicted in many BSM physics such as a supersymmetric extension. WIMP is assumed to be in thermally equilibrium with the SM particles in the early universe. When the universe cools down below the WIMP mass and WIMP is decoupled from thermal bath, the thermal relic explains DM. Interestingly, for the annihilation cross section $\langle \sigma v \rangle \sim 10^{-9}$ GeV^{-2}, it is consistent with the observed abundance. However, WIMP with an expected mass ($\mathcal{O}(10 - 100)$ GeV) is tightly constrained by direct DM search experiments. Thus, it is timely to explore alternative DM candidates and the corresponding BSM physics.

In addition to WIMP DM, very light particles are attractive. A typical example of light DM is QCD axion. The QCD axion is a pseudo Nambu-Goldstone boson associated

[1] As a possibility of non-particle DM, a primordial black hole has been proposed. It is assumed to be produced from some dense region of energy density in the early universe.

with spontaneous breaking of a global U(1) symmetry, the so-called Peccei-Quinn (PQ) symmetry [7, 8, 9, 10]. The first motivation of axion is to solve the Strong CP problem. The discovery of QCD anomaly [11, 12] and nontrivial vacuum structure [13, 14, 15] has revealed that the strong CP phase $\bar{\theta}$ has observable effects [16, 17, 18]. However, measurements of the neutron electric dipole moment (nEDM) constrains the CP phase as $|\bar{\theta}| \lesssim 10^{-10}$ [19]. This fine-tuning problem is the Strong CP problem. The axion acquires a potential from nonperturbative effects of QCD and settles down at the CP conserving minimum of the potential. In this way, the axion can solve the Strong CP problem. Note that the 'axion' often includes the QCD axion and axion-like particles (ALP). The QCD axion is the main subject in this thesis, but ALP will be also discussed later. ALP is a pseudo-scalar field theoretically predicted by BSM physics such as the string theory [20]. It has properties similar to the QCD axion, but is not necessarily related to the Strong CP problem.

The QCD axion has various cosmological implications, and there are two different types of cosmological scenarios. The first scenario is the case in which the PQ symmetry is spontaneously broken after inflation or, even if the PQ symmetry is broken during inflation, it is restored after inflation. This is known as the post-inflationary scenario. The axions are initially positioned near some different minima, and domain walls attached by cosmic strings appear, which contributes to the axion density. The second scenario is the case in which the PQ symmetry is already spontaneously broken during inflation and not restored afterwards. This is called pre-inflationary scenario. In this case, the axion acquires quantum fluctuations during inflation. Such fluctuations give rise to a different contribution to cosmological structure from the currently observed fluctuation induced by the inflaton field. The axionic fluctuation induces what is called isocurvature perturbation. The isocurvature fluctuation is severely constrained by observation, which can be recast as the upper bound on the inflation scale. In this thesis, we focus on the pre-inflationary scenario.

In the pre-inflationary scenario, the initial position $\theta_{\rm ini}$ of axion is a free parameter that is naturally expected to be of the order of unity. At the QCD phase transition, the axion starts to oscillate due to the potential induced from nonperturbative effects of QCD, and is nonthermally produced as nonrelativistic matter. This production mechanism is known as the misalignment mechanism [21, 22, 23]. The energy density of axion is given by the oscillation energy, and if the initial amplitude $\theta_{\rm ini}$ is of order unity, the axion with $f_\phi \lesssim 10^{12}$ GeV is consistent with the observed DM abundance. Here, f_ϕ is the decay constant which is close to the PQ symmetry breaking scale in a simple setup. Also, the stability of axion is attributed to the light mass thanks to the shift symmetry, and the interactions with other particles are suppressed by the decay constant f_ϕ. This is why the QCD axion is a leading DM candidate. The cosmologically viable range of the decay constant is known as the QCD axion window,

$$10^8 \text{ GeV} \lesssim f_\phi \lesssim 10^{12} \text{ GeV}. \tag{1.1}$$

While the upper bound is set by the axion DM abundance for $\theta_{\rm ini} = \mathcal{O}(1)$, the lower bound is given by the stellar cooling argument [24, 25, 26, 27, 28, 29, 30, 31, 32].

For $f_\phi \lesssim 10^{12}$ GeV, the axion abundance is not enough to explain DM in the case of $\theta_{\rm ini} = \mathcal{O}(1)$. One solution is to take the initial position of axion near the top of potential. Then, the delay of commencement of oscillations significantly enhances the abundance.

This is known as the anharmonic effect [33, 34, 35, 36, 37, 38, 39]. However, the isocurvature perturbation is also enhanced, and we need some prescription for overcoming this drawback. For $f_\phi \gtrsim 10^{12}$ GeV, we can simply take small $\theta_{\rm ini}$ to reduce the abundance. For instance, considering the stochastic dynamics of axion during inflation, the initial amplitude can be suppressed, as long as the inflation scale is lower than the QCD scale [40, 41] (cf. [42, 43] for ALP DM).

The axion could acquire an additional potential from the other shift symmetry (PQ symmetry) breaking than the QCD effect. In order for the PQ mechanism to work well, the PQ symmetry has to be of high quality. However, quantum gravity theory predicts that any global symmetry is explicitly broken [44, 45, 46, 47, 48]. Thus the QCD axion may acquire a small extra potential in addition to the potential from the QCD effect. Such a potential would not seem to affect the axion dynamics, because it should be tightly constrained by experiments of nEDM. However, it is premature to make a conclusion. This is because the QCD potential is negligibly small well before the QCD phase transition. If the axion is temporarily trapped by the additional potential, the dynamics would be completely different. We call this phenomenon the trapping effect. In this thesis, we study the trapping effect on the abundance and isocurvature perturbation of the QCD axion.

In Chapter 3, we will analytically study the trapping effect by a general extra potential. What is important here is the adiabaticity that is an essential property of the system and determines if an extra oscillation of the axion is induced. When the adiabaticity is broken, an extra oscillation occurs and enhances the abundance. We will find that the dynamics can be systematically categorized into two regimes by the adiabaticity. However, we need the model-dependent analysis to understand what determines the adiabaticity, in which parameter region DM can be explained, and how much the isocurvature perturbation is produced. To answer these question, Chapter 4 and 5 are devoted to the analysis in specific situations.

First, we consider a time-independent extra potential with multiple minima [49]. In order for the PQ mechanism to work well, extra potentials should be tiny compared to the potential by nonperturbative effects of QCD. Even such small potentials can affect the axion dynamics, because of the asymptotic freedom of QCD. In fact, we will see in Chapter 4 that the axion dynamics is significantly altered by the extra PQ breaking potential. We will clarify the allowed parameter region for explaining DM and identify the bound by the isocurvature perturbations.

Second, we consider a time-dependent extra potential from the Witten effect [50, 51] of hidden monopole [52, 53]. The effective mass is proportional to the number density of monopole, and the axion is strongly trapped in the early universe. In the previous literature [54, 55], the authors assumed that the axion is initially around the minimum of QCD potential. In this case, the trapped axion adiabatically follows the temporal minimum after the QCD phase transition, so that any additional amplitude is not generated and the abundance is suppressed. This is called adiabatic suppression mechanism [56, 57, 54, 55, 58]. In Chapter 5, taking a broader region of $\theta_{\rm ini}$, we will study whether the adiabatic suppression mechanism works well in the presence of the anharmonic effect, based on [58].

These two specific analysis will provide us with the further understanding of the trapping effect. In particular, we will reveal in which case the adiabaticity is broken.

1.2 Organization

This thesis is organized as follows. In Chapter 2, we review the standard arguments on the QCD axion. In Chapter 3, we introduce other PQ symmetry breaking potentials, and summarize the fundamental properties of the trapping effect by an extra PQ breaking potential. We discuss specific models : a time-independent potential (in Chapter 4) and a time-dependent potential (in Chapter 5). We conclude the thesis in Chapter 6.

1.3 Notations

- The natural unit is used, $c = \hbar = k_B = 1$.
- The reduced Planck mass is defined by $M_{\rm Pl} \equiv 1/\sqrt{8\pi G}$ with G the Newton constant.
- We adopt the mostly minuses, $(+,-,-,-)$, except for Appendix D.
- The Euclidean action is defined as

$$S_E \equiv -iS|^{A_0 \to -iA_4}_{t \to -ix_4}, \tag{1.2}$$

  where A_0 is the time component of gauge field.

- The Pauli matrices are defined as

$$\sigma_1 = \begin{pmatrix} 0 & 1 \\ 1 & 0 \end{pmatrix}, \quad \sigma_2 = \begin{pmatrix} 0 & -i \\ i & 0 \end{pmatrix}, \quad \sigma_3 = \begin{pmatrix} 1 & 0 \\ 0 & -1 \end{pmatrix}. \tag{1.3}$$

- The density parameter of some component is defined as $\Omega_i \equiv \rho_{i0}/\rho_{\rm crit}$, where ρ_{i0} is the present energy density and $\rho_{\rm crit}$ is the critical energy density.

Chapter 2

QCD axion

It is known that there is nontrivial vacuum structure in QCD sector, which implies the nonzero contribution to CP violation of the Chern-Simons term (also called the θ-term). The CP violation mainly induces neutron electric dipole moment as observables, but it must be tightly suppressed in accord with current experimental results. The puzzle of why CP is preserved to such a high accuracy in QCD is called the Strong CP problem. The most plausible solution is to introduce a pseudo-Nambu-Goldstone boson, i.e. QCD axion, which is associated with spontaneous breakdown of a global U(1) symmetry. The QCD axion acquires a potential with CP conserving minima by nonperturbative effects of QCD. The dynamics on the potential also plays an essential role in a nonthermal production of axion DM. Thus the QCD axion is highly motivated by the solution to the Strong CP problem and DM, and a number of experiments and observations have been carried out and planned rigorously.

In this chapter, we summarize properties of the QCD axion (for more details, see e.g. [59, 60, 61, 62, 63, 64]). First we explain the Strong CP problem and the solution by the Peccei-Quinn (PQ) mechanism in Sec. 2.1 and 2.2. After introducing the axion potential induced from QCD nonperturbative effect in Sec. 2.3, the axion DM is discussed in Sec. 2.4, which includes the non-thermal production mechanism of axion DM, known as the misalignment mechanism, and generation of axionic isocurvature perturbation. Finally, focusing on the axion-photon coupling, we will briefly summarize the experiments and observations of axion detection in Sec. 2.5.

2.1 Strong CP problem

The QCD is based on an SU(3) gauge group, which describes well various phenomena associated with the strong interaction among quarks and gluons. To introduce the Strong CP problem, let us begin with discussing the field configuration of gluons. The gauge invariance and the renormalizability give the following terms,

$$\mathcal{L}_{\rm gauge} = -\frac{1}{4} G^a_{\mu\nu} G^{a\mu\nu} - \theta \frac{g_s^2}{32\pi^2} G^a_{\mu\nu} \tilde{G}^{a\mu\nu}, \tag{2.1}$$

where the gluon field strength and its dual are respectively written as $G^a_{\mu\nu} = \partial_\mu A^a_\nu - \partial_\nu A^a_\mu + g_s f^{abc} A^b_\mu A^c_\nu$ and $\tilde{G}^a_{\mu\nu} = \frac{1}{2}\epsilon_{\mu\nu\alpha\beta} G^{a\alpha\beta}$. g_s is the gauge coupling constant, and f^{abc} denotes the structure constant for SU(3). The second term is a pseudo-scalar term whose

coefficient is an arbitrary parameter, and is called the Chern-Simons term (or the θ-term). Actually, the θ term is ineffective to observables in perturbation theory. It is written in terms of the Chern-Simons current K^μ as [65]

$$G^a_{\mu\nu}\tilde{G}^{a\mu\nu} = \partial_\mu K^\mu = \partial_\mu \epsilon^{\mu\alpha\beta\gamma}\left(A^a_\alpha G^a_{\beta\gamma} - \frac{g_s}{3} f_{abc} A^a_\alpha A^b_\beta A^c_\gamma\right), \tag{2.2}$$

which seems not to contribute to path integral as long as we consider a trivial configuration of gluon fields, $A^a_\mu = 0$, at the boundary in Euclidean space, since it is a total derivative. However, it is found that there exist nontrivial field configurations of the Yang-Mills gauge field, or instanton solution [13, 14, 15], such that the θ-term provides a nonzero contribution,

$$\frac{g_s^2}{32\pi^2}\int d^4x G^a_{\mu\nu}\tilde{G}^{a\mu\nu} = \nu, \tag{2.3}$$

with an integer ν being the winding number. The winding number ν categorizes the topologically stable vacua which cannot be continuously deformed into each other by small gauge transformation. For the discussion of the QCD nontrivial vacuum structure, see Appendix B.

In addition to the Chern-Simons term, the QCD possesses another CP violation source in the quark mass phases. In the SM, quarks acquire a mass through the Yukawa coupling to the Higgs field, and the quark mass term can be described by $-\mathcal{L}_{\text{mass}} = \bar{q}_L M_q q_R + \text{h.c.}$, where M_q is the complex, $n_f \times n_f$ mass matrix with n_f being the number of flavor. The right- (left-) handed quark field is defined by multiplying projection operators $(1 + (-)\gamma_5)/2$ to Dirac spinors. However, it is nontrivial whether these two sources of CP violation are physical or not. Consider the axial U(1) transformation, $q_i \to e^{i\alpha_i\gamma_5/2}q_i$ with α_i a constant parameter for each flavor labeled by i. The axial U(1) symmetry is anomalous as represented by triangle diagrams [11, 12], and in fact, the coefficient of the Chern-Simons term is transformed as $\theta \to \theta - \sum_i \alpha_i$. We can understand it explicitly in terms of the transformation of the functional measure,[1] [66]

$$D\bar{q}_i Dq_i \to D\bar{q}_i Dq_i \exp\left[-i\sum_i \alpha_i \frac{g_s^2}{32\pi^2}\int d^4x G^a_{\mu\nu}\tilde{G}^{a\mu\nu}\right]. \tag{2.4}$$

Thus the θ-term can be removed by the chiral rotation, but instead, the quark mass phase is induced and the CP violations never vanish unless the two contributions cancel each other. Diagonalizing the quark mass matrix by using unitary matrices, we obtain $-\mathcal{L}_{\text{mass}} = \sum_i \bar{q}^m_{iL} m_i e^{i\theta_i} q^m_{iR} + \text{h.c.}$, where m_i and θ_i are a mass and a phase of each flavor. Imposing the axial U(1) transformation, the mass phase is shifted as $\theta_i \to \theta_i + \alpha_i$. The combination $\bar{\theta} \equiv \theta + \sum \theta_i = \theta + \arg(\det M_q)$ is the only physical contribution of CP violation and is invariant under the chiral rotation.

The most sensitive observable of $\bar{\theta}$ is the neutron electric dipole moment (nEDM). The nEDM is defined by the non-relativistic Hamiltonian for the interaction between a neutron and an external electric field, $\mathcal{H} = -d_n \vec{E}\cdot\hat{S}$, where $\vec{E}$ denotes the electric field

[1] The electromagnetic anomaly is also induced, but it does not give any contribution to the action, because it is a total derivative. However, if magnetic monopole exists, the anomalous term can contribute to physics. See Sec. 3.2 for hidden U(1) anomaly.

and $\hat{S} \equiv \vec{S}/|\vec{S}|$ is a normalized spin vector. The strong CP phase $\bar{\theta}$ gives rise to the nEDM as [17]

$$|d_n| = 1.2 \times 10^{-16} |\bar{\theta}| e \text{ cm}. \tag{2.5}$$

The nEDM is tightly constrained according to the current experimental result, $|d_n^{(\text{exp})}| < 1.8 \times 10^{-26} e$ cm [19], which can be recast to the bound on $\bar{\theta}$,

$$|\bar{\theta}| \lesssim 10^{-10}. \tag{2.6}$$

It is a puzzle in QCD why the strong CP phase $\bar{\theta}$ is so suppressed. This fine tuning problem is called the Strong CP problem.

2.2 Peccei-Quinn mechanism

The most plausible solution to the Strong CP problem[2] is to introduce a pseudo-scalar boson, the QCD axion [7, 8, 9, 10]. Introducing an axion and using the chiral rotation to put all the quark mass phases collectively into the Chern-Simons term, the Lagrangian is written as

$$\mathcal{L}_{\text{QCD}+\phi} = \frac{1}{2}\partial_\mu \phi \partial^\mu \phi + \sum_i \bar{q}_i (i\not{D} - m_i) q_i - \frac{1}{4} G^a_{\mu\nu} G^{a\mu\nu} - \left(\bar{\theta} + \frac{\phi}{f_\phi}\right) \frac{g_s^2}{32\pi^2} G^a_{\mu\nu} \tilde{G}^{a\mu\nu}, \tag{2.7}$$

where $\phi(t, \vec{x})$ denotes the axion field and f_ϕ is called the decay constant which determines the strength of the axion coupling to other particles. The Lagrangian is invariant under the shift transformation $\phi \to \phi + \kappa f_\phi$ up to the last term, where κ is an arbitrary constant. The axion corresponds to a Nambu-Goldstone boson associated with the spontaneous breaking of a global U(1) symmetry which is called the PQ symmetry $\text{U}(1)_{\text{PQ}}$. We can choose the parameter κ so that $\bar{\theta}$ is removed. This prescription means that the parameter $\bar{\theta}$ is promoted to a dynamical field ϕ and the effective θ-parameter becomes $\langle\phi\rangle$.

It is shown that the QCD instanton effect provides the potential energy whose minimum is exactly at $\phi = 0$, leading to the strong CP conservation [72, 73]. To see it without the direct calculation of potential, let us analyze the Euclidean functional derivative. In the Euclidean space, integrating out the quark and gluon, we can write the effective potential $V(\phi)$ as

$$\begin{aligned}
& \exp\left(-\int d^4 x_{\text{E}} V(\phi)\right) \\
= & \int DAD\bar{q}Dq \exp\left[-\int dx^4_{\text{E}} \left(\sum_i \bar{q}_i (\not{D}_{\text{E}} + m_i) q_i + \frac{1}{4} G^a_{\mu\nu} G^a_{\mu\nu} - \frac{i\phi}{f_\phi} \frac{g_s^2}{32\pi^2} G^a_{\mu\nu} \tilde{G}^a_{\mu\nu}\right)\right] \\
= & \int DA \prod_i \text{Det}(\not{D}_{\text{E}} + m_i) \exp\left[-\int dx^4_{\text{E}} \left(\frac{1}{4} G^a_{\mu\nu} G^a_{\mu\nu} - \frac{i\phi}{f_\phi} \frac{g_s^2}{32\pi^2} G^a_{\mu\nu} \tilde{G}^a_{\mu\nu}\right)\right],
\end{aligned} \tag{2.8}$$

[2]There are some other possibilities left. For instance, one possibility is a scenario that CP symmetry is exact symmetry and $\bar{\theta} = 0$ in high energy scale, and then is spontaneously broken to induce the expected $\bar{\theta}$ [67, 68, 69, 70, 71].

where Euclidean values are labeled by the subscript 'E'. In the second equality, the Gaussian integration is performed. The gamma matrices in the Euclidean space can be represented by $\gamma_4^{\rm E} = \gamma^0$ and $\gamma_i^{\rm E} = -i\gamma^i$, and thus, $i\not{D}$ is a Hermitian operator whose eigenvalues λ are real. Writing the eigenfunction as ψ, $(i\not{D}_{\rm E})(\gamma^5\psi) = -\lambda(\gamma^5\psi)$ when $(i\not{D}_{\rm E})\psi = \lambda\psi$ is satisfied. Then the determinant of the Dirac operator is given by

$$\mathrm{Det}(\not{D} + m_i) = \prod_{\lambda}(-i\lambda + m_i) = (m_i)^{N_0}\prod_{\lambda>0}(\lambda^2 + m_i^2) > 0, \tag{2.9}$$

where N_0 is the number of zero mode. Using this results and applying the Schwarz inequality to the absolute value of (2.8), we obtain the relation of the potential, $|\exp\left(-\int V(\phi)\right)| \leq |\exp\left(-\int V(0)\right)|$, i.e. $V(0) \leq V(\phi)$. The minimum of the potential is at $\phi = 0$ which preserves the strong CP symmetry. As a result, the axion is dynamically stabilized there and can resolve the Strong CP problem. This is called the PQ mechanism.

Lastly, let us comment on UV completed models of the axion. To obtain the axion with an anomalous coupling to gluons, we should introduce the PQ symmetry. In the framework, the axion is identified with a Nambu-Goldstone mode of the additional Higgs field. The model depends on how to construct the Higgs sector and how the PQ charges are assigned to the Higgs and quarks running in the loop of triangle diagrams. There are two benchmark models, KSVZ model and DFSZ model, named after the initials of the authors of [74, 75] and [76, 77], respectively. However, the following discussion of this thesis can be applied to both models, and therefore, we do not assume any specific model.

2.3 Axion potential from QCD effect

The QCD axion acquires an effective potential from nonperturbative effects of the QCD. At temperatures lower than the QCD phase transition, i.e. at $T \ll \Lambda_{\rm QCD}$, where $\Lambda_{\rm QCD}$ is the confinement scale, we can evaluate the potential using the chiral effective Lagrangian [9, 78, 79, 80]. Considering the two-light-flavor (u and d) effective field theory [78, 79], the potential at zero temperature is given by

$$V_{\rm ChPT}(\phi) = -m_\pi^2 f_\pi^2\sqrt{1 - \frac{4m_u m_d}{(m_u+m_d)^2}\sin^2\left(\frac{\phi}{2f_\phi}\right)}, \tag{2.10}$$

where $f_\pi = 92.21$ MeV is the pion decay constant, $m_\pi \simeq 135$ MeV is the neutral pion mass, and m_u and m_d denote the mass of the u and d quarks. The ratio of m_u and m_d is given by $z \equiv m_u/m_d \simeq 0.48$ from the average of the lattice results [81, 82, 83]. Then the axion mass is given by

$$m_{\phi,0} = \frac{\sqrt{z}}{1+z}\frac{f_\pi m_\pi}{f_\phi} \tag{2.11}$$

$$\simeq 5.7\mu\mathrm{eV}\left(\frac{10^{12}\ \mathrm{GeV}}{f_\phi}\right), \tag{2.12}$$

where, in the second line, we take the NNLO result in chiral perturbation theory [80].

The important ingredient for the non-thermal production of axion DM is the potential and mass at temperature around or higher than $\Lambda_{\rm QCD}$. However, the above chiral perturbation theory is no longer applicable to such high temperature region, because of the

asymptotic freedom, that is, the system should be described by the quark-gluon plasma rather than hadrons. We should rely on alternative methods, such as the dilute instanton gas approximation [84] or the lattice simulation [85, 86, 87, 88, 89]. The result of the former method provides the temperature-dependent potential of the axion, [90]

$$V_{\rm DIGA}(\phi, T) = (m_\phi^{\rm (DIGA)}(T))^2 f_\phi^2 \left(1 - \cos\frac{\phi}{f_\phi}\right) \tag{2.13}$$

with $m_\phi^{\rm (DIGA)}(T) \propto T^{-4}$ for the 3-flavor model.

On the other hand, lattice simulations are also useful. In Fig. 2.1, we show the latest lattice result [86] which covers the temperature region of 100 MeV $< T <$ 3 GeV. The lattice result does not reach the region of temperatures higher than 3 GeV, but the result from 1 GeV to 3 GeV is consistent with the dilute instanton gas approximation which is applicable at such high temperatures. In fact, we fit the lattice result from 1 GeV to 3 GeV to obtain the temperature dependence of the axion mass,

$$m_\phi(T) \simeq m_{\phi,0} \left(\frac{T}{\Lambda_{\rm QCD}}\right)^{-b} \tag{2.14}$$

with $b = 3.92$ and $\Lambda_{\rm QCD} \equiv 0.15$ GeV. The fitting function is shown by the black dashed line in Fig. 2.1, and its dependence on the temperature is consistent with dilute instanton gas approximation. We note that this function can be continuously connected with the zero-temperature mass (2.12) at $T = \Lambda_{\rm QCD}$. Thus we assume in this thesis that the potential form at high temperature is described by

$$V_{\rm QCD}(\phi, T) = m_\phi^2(T) f_\phi^2 \left(1 - \cos\frac{\phi}{f_\phi}\right). \tag{2.15}$$

Note that the axion mass around 1 GeV is most relevant for the estimate of the axion dynamics, and that the precise axion mass above 3 GeV does not significantly change our results as long as it decreases smoothly with increasing temperature.

Before going to the next discussion, let us comment on the shape of the potential at the lower temperature. While the dilute instanton gas approximation predicts the cosine-shape potential (2.15), the chiral perturbation theory gives the potential (2.10) with somewhat spiky top. Though we assume the former potential even in the region of low temperature, the difference does not alter our results presented in subsequent chapters, which in fact, we confirmed numerically.

2.4 Axion dark matter

In the PQ mechanism, the axion dynamically washes out the strong CP violation, which has interesting cosmological implications. Here we will see that when the axion starts to oscillate around the potential minimum, the axion behaves like matter whose abundance can explain that of DM (Sec. 2.4.1). Also, we will discuss a measurable quantity for the existence of the quantum fluctuation of axion during inflation in Sec. 2.4.2. Note that when the PQ symmetry is spontaneously broken before or during inflation and not restored afterwards, the axionic fluctuation has an impact on density perturbation. This is called the pre-inflationary scenario that we focus on throughout this thesis. On the contrary, if the PQ symmetry is broken after inflation, topological defects such as cosmic string and domain wall are produced. This is called the post-inflationary scenario.

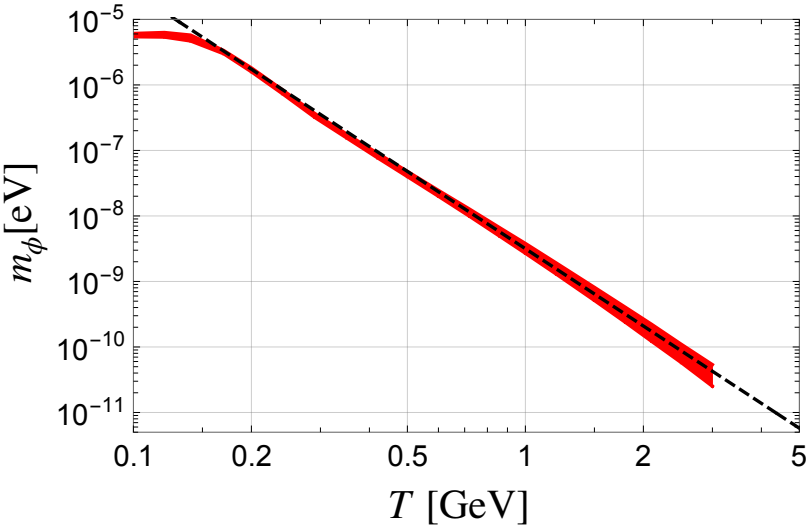

Figure 2.1: The temperature dependence of $m_\phi(T)$ obtained by the lattice result (red line) [86] for $f_\phi = 10^{12}$ GeV. The width of the red line represents the statistical and systematic errors. The black dashed line is the numerical fit obtained from the lattice result between $T = 1$ GeV and 3 GeV assuming the power-law function (2.14).

2.4.1 Misalignment mechanism

The axion dynamics on the potential is important for understanding its cosmological implications. At first, let us begin with taking a rough look at the cosmic history before the QCD transition. See Fig. 2.2 for the schematic picture. When the PQ symmetry is spontaneously broken, the axion degree of freedom appears as a Nambu-Goldstone boson. At this moment, the axion is positioned somewhere ($\phi = \phi_{\rm ini}$) according to uniform distribution. The Hubble patch at the spontaneous breakdown of the PQ symmetry (yellow shaded region), within which things were causally correlated with each other and all the axion fields have the same position $\phi_{\rm ini}$ plus small fluctuations, stretches out by the inflationary expansion. After the end of inflation, both the uniform region of $\phi_{\rm ini}$ (yellow shaded region) and the causal region continue expanding. In this way, the uniform region of $\phi_{\rm ini}$ contains the whole of the currently observed universe (blue circle), and we can find only the axions with the same initial field value, leading to the spatially homogeneous axion density up to the density fluctuation which will be discussed in the next subsection. Note that the initial position $\phi_{\rm ini}$ is chosen arbitrarily, and so, it is a free parameter. In the following, the initial misalignment angle is defined as $\theta_{\rm ini} \equiv \phi_{\rm ini}/f_\phi$.

To this time, the axion is massless and stays at the initial position. When the universe undergoes the QCD phase transition at $T \sim \Lambda_{\rm QCD}$, the axion acquires the potential and starts to oscillate around the potential minimum. While the axion dynamics solves the Strong CP problem because the minimum of the potential conserves CP symmetry, the oscillating axion becomes a non-relativistic matter component which contributes to the DM. Such a production mechanism of the axion cold DM (CDM) is called misalignment mechanism [22, 23, 21], whose schematic picture is shown in Fig. 2.3.

Let us analyze the dynamics described above quantitatively. Assuming the minimal coupling to gravity, we obtain the equation of motion for the spatially homogeneous axion

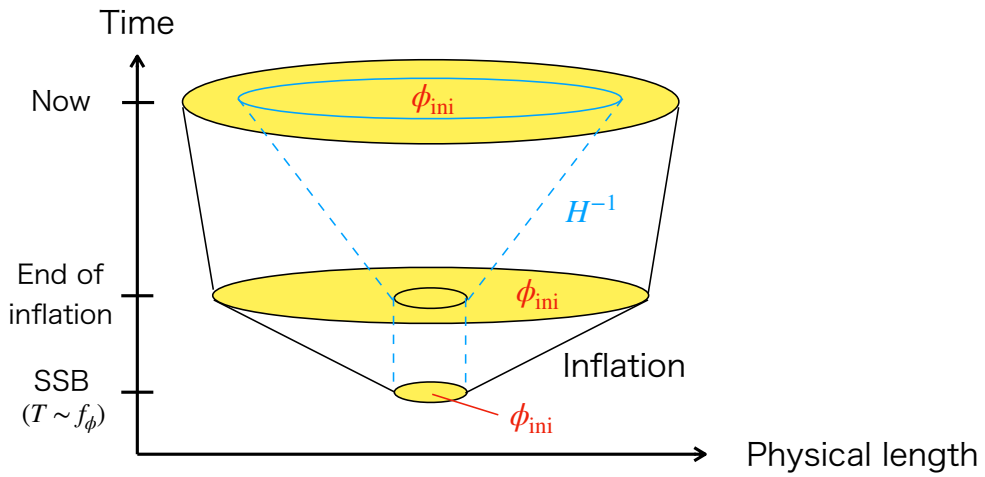

Figure 2.2: The schematic picture for the evolution of $\phi_{\rm ini}$-distribution (yellow shaded region) in the pre-inflationary scenario. The blue dashed line is the Hubble horizon. The blue circle represents the currently observed region.

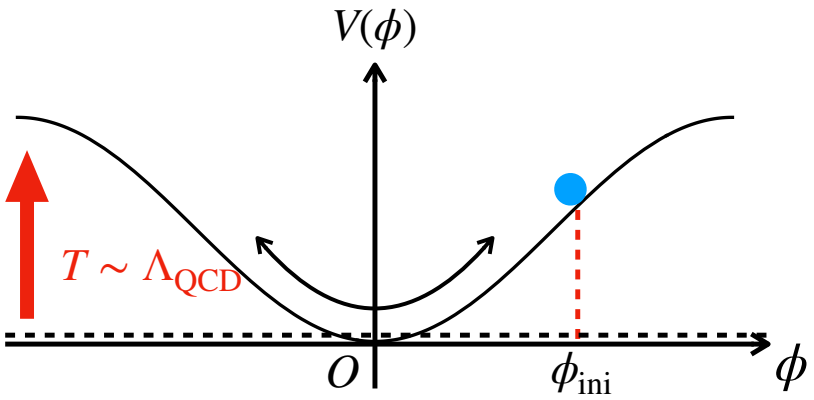

Figure 2.3: The schematic picture of the misalignment mechanism. The blue circle represents the axion field. At $T \sim \Lambda_{\rm QCD}$, the QCD potential grows and the axion starts to oscillate.

field,

$$\ddot{\phi} + 3H\dot{\phi} + V'(\phi) = 0, \tag{2.16}$$

where $H \equiv \dot{a}/a$ is the Hubble parameter with $a(t)$ the scale factor, and the prime and the dot represent the derivatives with respect to axion field ϕ and time t, respectively. We can solve this equation for the initial conditions of position and velocity $(\phi_{\rm ini}, \dot{\phi}_{\rm ini})$ to follow the evolution.[3] In this thesis, we choose the zero initial velocity. The second term works as a friction effect so that the axion sticks to the initial position before the QCD phase transition. Assuming the axion is initially near the potential minimum so that the potential can be approximated to be quadratic, when the Hubble parameter becomes

[3]In Appendix C, the dimensionless equation of motion is shown for the numerical computation. Our numerical results were estimated by solving it.

comparable to the axion mass, the axion is driven by the potential toward the minimum. The temperature at the onset of oscillations is given by

$$T_{\rm osc}^{(\rm conv)} \simeq 1.1\ {\rm GeV} \left(\frac{g_*}{80}\right)^{-0.084} \left(\frac{f_\phi}{10^{12}\ {\rm GeV}}\right)^{-0.17}. \tag{2.17}$$

which satisfies $m_\phi(T_{\rm osc}^{(\rm conv)}) = 1.67H(T_{\rm osc}^{(\rm conv)})$, and the superscript (conv) represents the case when there is no extra potential.[4] Here we use the mass relations (2.12) and (2.14). Henceforth, we assume the radiation-dominated universe until the matter-radiation equality, and using (A.1) and (A.4), the Hubble parameter is given by

$$H^2 = \frac{\pi^2}{90 M_{\rm Pl}^2} g_*(T) T^4, \tag{2.18}$$

where $g_*(T)$ is defined as the effective relativistic degrees of freedom for energy density, and $M_{\rm Pl}$ is the reduced Planck mass.

When the axion oscillates around the potential minimum, the number density is conserved in the fixed comoving volume, and so, n_ϕ/s is a conserved quantity because $sa^3 = $ const., where $s(T)$ is the entropy density. The basic strategy to estimate the QCD axion energy density is to follow the time evolution of n_ϕ/s and multiply the zero temperature mass after the increase of the mass stops. The present ratio is given by

$$\frac{n_\phi(T_0)}{s_0} \simeq \frac{n_\phi(T_{\rm osc}^{(\rm conv)})}{s(T_{\rm osc}^{(\rm conv)})} = \frac{45}{4\pi^2 g_{*s}(T_{\rm osc}^{(\rm conv)})} \frac{m_\phi(T_{\rm osc}^{(\rm conv)})\phi_{\rm ini}^2}{(T_{\rm osc}^{(\rm conv)})^3}, \tag{2.19}$$

where the subscript '0' denotes the present value, and g_{*s} is the effective relativistic degrees of freedom for entropy density. The density parameter is given by

$$\Omega_\phi^{(\rm conv)} h^2 = \frac{\rho_\phi(T_0)}{\rho_{\rm crit} h^{-2}} = \frac{m_{\phi,0} n_\phi(T_0)}{\rho_{\rm crit} h^{-2}}. \tag{2.20}$$

In the above estimate, we assume that the potential can be approximated to be quadratic, but when a broader parameter region of $\theta_{\rm ini}$, the abundance is altered by the anharmonic parts of potential. When the initial position is close to the potential maximum, the abundance increases logarithmically. This is known as the anharmonic effect. Including the anharmonic effect, we obtain the axion abundance [91],

$$\Omega_\phi^{(\rm conv)} h^2 \simeq 0.14 F^{(\rm conv)}(\theta_{\rm ini}) \theta_{\rm ini}^2 \left(\frac{f_\phi}{10^{12}\ {\rm GeV}}\right)^{1.17}, \tag{2.21}$$

where $\theta_{\rm ini} \equiv \phi_{\rm ini}/f_\phi$ is defined as the dimensionless initial angle. The coefficient $F^{(\rm conv)}(\theta_{\rm ini})$ represents the anharmonic effect, and is given by [33, 35, 36]

$$F^{(\rm conv)}(\theta_{\rm ini}) = \left[\ln\left(\frac{e}{1-\theta_{\rm ini}^2/\pi^2}\right)\right]^{1.17}. \tag{2.22}$$

[4] The numerical coefficient is determined by comparing with the numerical calculations of the axion abundance.

We can understand the anharmonic effect as follows. In the hilltop limit, the axion finds the potential so flat that it does not feel strong dragging due to the potential. Thus the onset of the axion oscillation is delayed significantly, resulting in the less suppression of abundance due to the cosmic expansion. This is how the anharmonicity causes the enhancement of the axion abundance.

In order to explain the total DM density $\Omega_{\rm DM}h^2 \simeq 0.12$, the decay constant should be $\sim 10^{12}$ GeV for $\theta_{\rm ini} \sim 1$. For smaller f_ϕ, the abundance is inadequate. In this case, the anharmonic effect can enhance the abundance, but there is another problem. The anharmonic effect also enhances the isocurvature perturbation which will be discussed in the next subsection. Although the post-inflationary scenario is not the main theme in this thesis, topological defects possibly complement the abundance in this scenario [92, 93]. On the other hand, for larger f_ϕ, the axion is overproduced. A simple solution is to tune $\theta_{\rm ini}$ small. In the pre-inflationary scenario, $\theta_{\rm ini}$ is randomly chosen, but for instance, by considering the competition between the effect of quantum fluctuation and the classical axion dynamics during inflation, $\theta_{\rm ini}$ can be naturally small [40, 41] (cf. [42, 43] for ALP DM). Anyway, it is nontrivial and important to investigate whether the axion can totally explain dark matter for both smaller and larger f_ϕ, which motivates our works presented in this thesis.

2.4.2 Isocurvature perturbation

To explain the isocurvature perturbation, let us begin with briefly discussing density perturbations. Hereafter, only when we discuss the cosmological perturbation, we define quantities X_i (e.g. n_i, ρ_i, P_i, etc) as $X_i = \bar{X}_i(t) + \delta X_i(t, \mathbf{x})$, where $\bar{X}_i$ and $\delta X_i (\ll \bar{X}_i)$ denote the homogeneous part and the perturbation of X_i, and the subscripts 'i' represents particle species, like radiation, CDM, etc.

The present universe contains complicated structures such as stars and galaxies, but what their seeds are is an open question. Now it is broadly believed that a light scalar field, inflaton is responsible for its origin. The inflaton acquires quantum fluctuations during inflation [94]. When the inflation ends, the inflaton decays into various particles. The SM particles of the decay products are promptly thermalized to each other. At the moment, the perturbation of the inflaton is converted to that of them. Since the origin is the same, the ratio of number density between two components is expected to be spatially homogeneous, which is written by

$$\frac{\delta n_i}{\bar{n}_i} = \frac{\delta n_j}{\bar{n}_j}, \tag{2.23}$$

in the superhorizon scale. The homogeneous energy density $\bar{\rho}_i$ obeys the energy conservation Eq. (A.3), and we obtain $\bar{\rho}_i \propto a^{-3(1+w_i)}$. Noting $\bar{n}_i \propto a^{-3}$, the above equation can be rewritten as

$$\frac{\delta \rho_i}{\bar{\rho}_i + \bar{P}_i} = \frac{\delta \rho_j}{\bar{\rho}_j + \bar{P}_j}, \tag{2.24}$$

where P_i denotes the pressure. We can further rewrite it as $\zeta_i = \zeta_j$ by using the gauge invariant combination of perturbations

$$\zeta_i \equiv -\psi - \frac{\delta \rho_i}{3(\bar{\rho}_i + \bar{P}_i)}, \tag{2.25}$$

where ψ is defined as the curvature perturbation, i.e. the perturbation of expansion rate. This is a conserved perturbation on superhorizon scale [95, 96]. All the observed perturbations exit the horizon during inflation and is conserved until the horizon re-entry, and (2.25) is the initial condition for their evolution.

The definition of ζ_i (2.25) indicates that if the energy density of one component is dense, so is that of the other. This is called adiabatic perturbation. All the current observations are consistent with the adiabatic perturbation, and there is only narrow room for deviations from it. Nevertheless, the existence of non-adiabatic perturbation is not completely excluded, and next we consider the axion-induced one.

Since an axion is almost massless during inflation, it acquires quantum fluctuations like inflaton. The axion exists as a spectator during inflation, and the axionic fluctuation is independent of the inflaton one. Thus the axionic fluctuation can induce a non-adiabatic perturbation, which provides nonzero perturbations of the relative number density in contrast to an adiabatic perturbation. The relevant perturbation is defined as

$$S(\boldsymbol{x}) \equiv 3(\zeta_{\rm CDM} - \zeta_{\rm rad}). \tag{2.26}$$

This non-adiabatic perturbation obeys the initial condition that both the curvature perturbation and the perturbation of the total energy density are zero well before the horizon re-entry, and such an initial condition is called isocurvature perturbation [97, 98]. The axion density perturbation produced just after the QCD phase transition obeys this initial condition. It is converted to the curvature perturbation through the entropy perturbation and thus leaves a distinctive imprint on observables.

In Fig. 2.4, we show the schematic picture for the initial conditions of density perturbations as a function of spatial coordinates (only one direction is depicted for simplicity). The left and right panel respectively denotes the adiabatic and isocurvature perturbation. The lower black line denotes the energy density of CDM, and the upper one does the total density, $\rho_{\rm rad} + \rho_{\rm CDM}$. In the case of the adiabatic perturbation, both radiation and CDM fluctuates with the similar spatial dependence. On the other hand, the isocurvature perturbation fluctuates so that the total density is zero. Such a difference generates the difference of observed perturbations. For instance, distinct signatures appear in the spectrum for CMB temperature anisotropy. The evolution equations of density perturbations around the recombination can be written by wave equations which possess two types of solution. The periodicity of these solutions differs by half a period, and thus, the isocurvature mode has a distinct peak at different scale from the adiabatic mode.

The statistical information on perturbations can be extracted by correlation functions. The important calculable quantity is the power spectrum which is defined by

$$\langle S(\boldsymbol{k}) S(\boldsymbol{k}') \rangle \equiv (2\pi)^3 \mathcal{P}_S(\boldsymbol{k}) \delta^{(3)}(\boldsymbol{k} + \boldsymbol{k}') \tag{2.27}$$

$$\Delta_S^2 \equiv \frac{k^3}{2\pi^2} \mathcal{P}_S(\boldsymbol{k}), \tag{2.28}$$

where $S(\boldsymbol{k})$ with $k \equiv |\boldsymbol{k}|$ is the Fourier transformation of $S(\boldsymbol{x})$, and $\langle \cdot \rangle$ represents a spatially averaged value. The second equation is the definition of the dimensionless power spectrum, which is compared to observational results. Higher order correlation functions can be calculated as non-Gaussianity.

The recent Planck data of the CMB anisotropy constrains the scale-invariant and

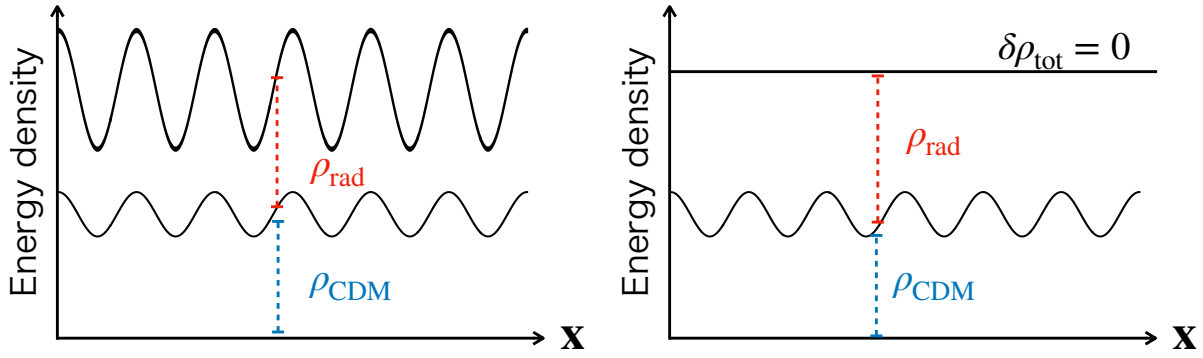

Figure 2.4: The schematic picture for the initial conditions for density perturbation as a function of spacial coordinates (only one direction is depicted for simplicity): the adiabatic mode (left) and the isocurvature mode (right).

uncorrelated isocurvature perturbation as [99]:

$$\beta_{\rm iso}(k_0) < 0.038 \quad (95\%{\rm CL}), \tag{2.29}$$

where $k_0 = 0.05\ {\rm Mpc}^{-1}$ is the pivot scale and $\beta_{\rm iso}$ is defined as the ratio between the power spectrum of the adiabatic perturbation $\mathcal{P}_\zeta$ and the isocurvature one $\mathcal{P}_S$, i.e. $\beta_{\rm iso} \equiv \mathcal{P}_S/\mathcal{P}_\zeta$. Thus the current upper bound on the isocurvature power spectrum reads

$$\Delta_S^2 < 8.3 \times 10^{-11}. \tag{2.30}$$

For instance, let us here consider the QCD axion with the potential approximated to be quadratic. When the universe is highly dominated by radiations, the QCD axion becomes DM, and $\delta\rho_{\rm rad}/\bar{\rho}_{\rm rad} \ll \delta\rho_{\rm CDM}/\bar{\rho}_{\rm CDM}$. Noting $\rho_\phi \propto \phi_{\rm ini}^2$, we obtain

$$S(\boldsymbol{x}) \simeq -\frac{\delta\rho_{\rm CDM}}{\bar{\rho}_{\rm CDM}} = -\frac{\Omega_\phi}{\Omega_{\rm DM}}\frac{\delta\rho_\phi}{\bar{\rho}_\phi} \simeq -\frac{\Omega_\phi}{\Omega_{\rm DM}}\frac{2\delta\phi_*}{\phi_*}, \tag{2.31}$$

where $\delta\phi_*(t, \boldsymbol{x})$ is defined as the perturbation of the axion field at the horizon exit. In the second equality, we assume that other CDM components than the axion have no isocurvature perturbation. The power spectrum of the isocurvature perturbation is given by

$$\mathcal{P}_S(\mathbf{k}) = \left(\frac{\Omega_\phi}{\Omega_{\rm CDM}}\frac{H_{\rm inf}}{\pi\theta_{\rm ini}f_\phi}\right)^2\frac{2\pi^2}{k^3}, \tag{2.32}$$

$$\Delta_S^2 \simeq \left(R_\phi\frac{H_{\rm inf}}{\pi\theta_{\rm ini}f_\phi}\right)^2 \equiv (R_\phi\Delta_\phi)^2, \tag{2.33}$$

where $R_\phi \equiv \Omega_\phi/\Omega_{\rm CDM}$, $H_{\rm inf}$ is the Hubble parameter during inflation, and we use the power spectrum of the axion field perturbation, $\mathcal{P}_{\delta\phi_*}(\vec{k}) \simeq H_{\rm inf}^2/2k^3$. The point is that the isocurvature bound provides the upper bound on the inflation scale. According to the observational esults (2.30), the bound on $H_{\rm inf}$ is given by

$$H_{\rm inf} \lesssim 3 \cdot 10^7\ {\rm GeV}\theta_{\rm ini}\left(\frac{f_\phi}{10^{12}\ {\rm GeV}}\right), \tag{2.34}$$

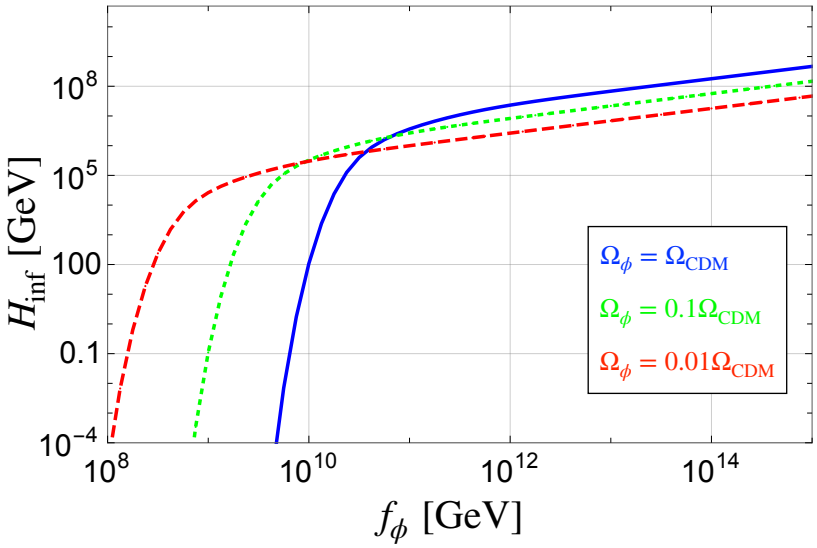

Figure 2.5: The isocurvature bound on $H_{\rm inf}$ as a function of f_ϕ. We set the axion abundance, $R_\phi = 1$ (blue solid), 0.1 (green dotted), 0.01 (red dashed).

where we assume $R_\phi = 1$. For smaller decay constant, the bound is tighter and the universe requires low-scale inflation.

The above estimate is limited to the quadratic potential. To study the anharmonic effect, we can use more precise analytic formula [100],

$$\Delta_S^2 \simeq \left(R_\phi \frac{\partial \ln \Omega_\phi}{\partial \theta_{\rm ini}} \frac{H_{\rm inf}}{2\pi f_\phi} \right)^2 . \tag{2.35}$$

The formula is derived in Sec. D.2. Including the anharmonic effect, the bound becomes much severe, because the abundance becomes very sensitive to the initial position of the axion when it is close to the potential maximum. To see it explicitly, we show the upper bound on $H_{\rm inf}$ in Fig. 2.5. The axion abundance is set to be $R_\phi = 1$ (blue solid), 0.1 (green dotted), 0.01 (red dashed). Note that $\theta_{\rm ini}$ is fixed by the abundance of the axion (2.21). Looking at the blue solid line, one can see that the bound becomes intensely severe for $f_\phi \lesssim 10^{11}$ GeV, because the initial position $\theta_{\rm ini}$ has to be close to the top of the potential to saturate the DM density.

2.5 Axion detection

Axions can weakly but surely couple to the SM sector, and experiments and observations for the axion detection have been carried out and planned energetically. Here we summarize the axion detection experiments, particularly related to our research. There are mainly three types of experiment: Haloscope, Helioscope, and astrophysical arguments in terms of e.g. supernovae or neutron star.

Before going on to the discussion about each experiment, let us present the definition of the axion coupling to the SM particles. First, we consider only the axion-photon coupling. Taking account of the non-conservation of the axial current associated with the

PQ symmetry, the axion effective Lagrangian includes

$$\mathcal{L}_{\rm axion} = -\mathcal{N}\frac{g_s^2}{16\pi^2}\frac{\phi}{v_\phi}G^a_{\mu\nu}\tilde{G}^{a\mu\nu} - \mathcal{E}\frac{e^2}{16\pi^2}\frac{\phi}{v_\phi}F_{\mu\nu}F^{\mu\nu}, \tag{2.36}$$

where $\mathcal{N}$ and $\mathcal{E}$ denote the anomaly coefficient for QCD and electromagnetism, respectively, e is an electric charge, and v_ϕ is the vacuum expectation value of the additional Higgs field which spontaneously breaks the PQ symmetry. When the decay constant is defined as $f_\phi \equiv v_\phi/2\mathcal{N}$, the Lagrangian is rewritten as

$$\begin{aligned}\mathcal{L}_{\rm axion} &= -\frac{g_s^2}{32\pi^2}\frac{\phi}{f_\phi}G^a_{\mu\nu}\tilde{G}^{a\mu\nu} - \frac{\mathcal{E}}{\mathcal{N}}\frac{e^2}{32\pi^2}\frac{\phi}{f_\phi}F_{\mu\nu}\tilde{F}^{\mu\nu} \\ &= -\frac{g_s^2}{32\pi^2}\frac{\phi}{f_\phi}G^a_{\mu\nu}\tilde{G}^{a\mu\nu} - \frac{g^0_{\phi\gamma}}{4}\phi F_{\mu\nu}\tilde{F}^{\mu\nu}.\end{aligned} \tag{2.37}$$

Here we define $g^0_{\phi\gamma} \equiv (\alpha_{\rm EM}/2\pi f_\phi)\cdot(\mathcal{E}/\mathcal{N})$ as the dimensionful, model-dependent coupling that is determined by UV physics.

We impose the field-dependent chiral rotation to doublet quarks, $q \to e^{-i\gamma_5\frac{\phi}{2f_\phi}Q_\phi}q$, where $q^T = (u,d)$ denotes the doublet quark field and Q_ϕ represents a matrix acting on the doublet quark field which is specified in the process of the chiral effective theory. The chiral anomaly is induced on both terms. Taking ${\rm Tr}[Q_\phi] = 1$ to vanish the $G\tilde{G}$ term, we obtain the Lagrangian for the axion-photon coupling, $\mathcal{L}_{a\gamma} = -\frac{g_{\phi\gamma}}{4}\phi F_{\mu\nu}\tilde{F}^{\mu\nu}$ with the coupling

$$g_{\phi\gamma} = g^0_{\phi\gamma} - \frac{\alpha_{\rm EM}}{2\pi f_\phi}\left(\frac{3}{2}{\rm Tr}[Q_\phi Q^2]\right) = \frac{\alpha_{\rm EM}}{2\pi f_\phi}\left(\frac{\mathcal{E}}{\mathcal{N}} - \frac{2}{3}\frac{4m_d+m_u}{m_u+m_d}\right), \tag{2.38}$$

where, in the second equality, we use the specific matrix $Q_\phi = M_q^{-1}/{\rm Tr}M_q^{-1}$ so that the axion-pion mass mixing disappears, which enables us to estimate the axion-photon coupling simply from $\phi F\tilde{F}$ term. Though the second term in the last equation is estimated about -2, more precisely, we can obtain the NLO result from the chiral perturbation theory [101],

$$g^{\rm NLO}_{\phi\gamma} = \frac{\alpha_{\rm EM}}{2\pi f_\phi}\left(\frac{\mathcal{E}}{\mathcal{N}} - 1.92\right). \tag{2.39}$$

The orange shaded region in Fig. 2.6 shows the coupling strength of QCD axion to photon, whose uncertainty is attributed to the model-dependence of $\mathcal{E}/\mathcal{N}$.

In addition to the photon coupling, the axion have the coupling to nucleon. According to the chiral effective theory [101], these Lagrangian terms are written by

$$\mathcal{L}_{\rm axion} \supset C_{\phi N}\frac{\partial_\mu\phi}{2f_\phi}\bar{N}\gamma^\mu\gamma_5 N, \tag{2.40}$$

where the model-dependent coefficient $C_{\phi N} = {\rm diag}(C_{\phi p}, C_{\phi n})$ is given at the leading order in the chiral expansion (see [101], for the values).

Below, each detection strategy is listed up. In particular, we show the parameter regions of the axion-photon coupling $(m_{\phi,0}, |g_{\phi\gamma}|)$ in Fig. 2.6 which is taken from the website [102]. While the already excluded region is depicted in the upper panel, the future sensitivity is shown in the lower panel.

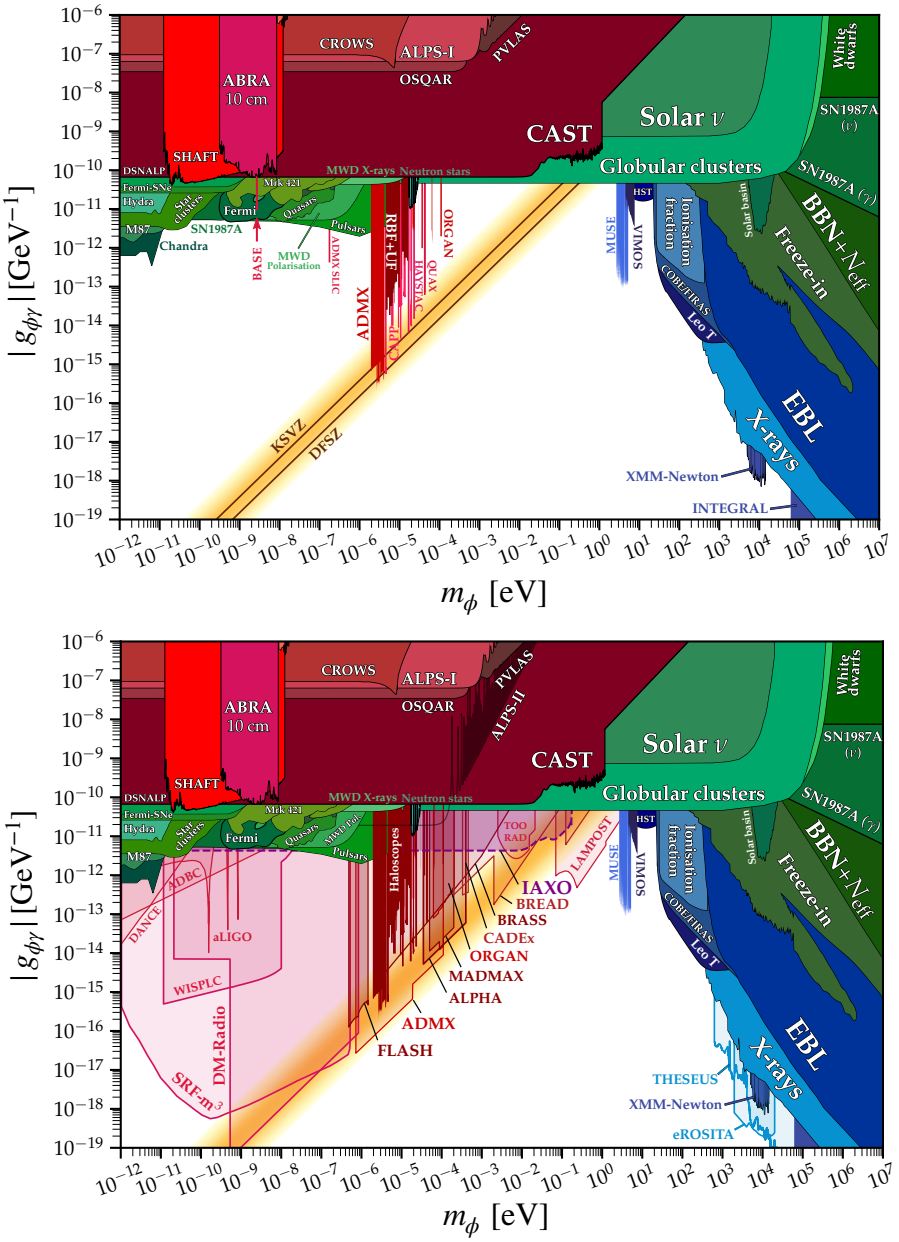

Figure 2.6: The axion-photon coupling $|g_{\phi\gamma}|$ as a function of the axion mass m_ϕ. These figures are taken from [102]. The upper panel shows the excluded region by current experiments and observations. In the lower panel, the future sensitivities are also depicted.

■ **Astrophysics** In the laboratory experiments, the axion properties can be probed as will be explained later, but the use of astrophysical objects is a good way to constrain it. Since the axion couples to photon and nucleon, it can be thermally produced in some high temperature environment, such as supernova core and neutron star, but it runs away with energy due to its large free-streaming scale. The cooling process of such astrophysical objects is understood for each object, and so, the energy loss rate by the axion provides an upper bound on the strength of the axion coupling.

According to the stellar cooling arguments of supernovae [24, 25, 26, 27, 28] and

neutron star [29, 30, 31, 32], the lower bound on f_ϕ is about 10^8 GeV. In addition of the upper bound from the axion abundance assuming $\theta_{\rm ini} \sim 1$, the bound becomes close and is called axion window,

$$10^8 \text{ GeV} \lesssim f_\phi \lesssim 10^{12} \text{ GeV}. \tag{2.41}$$

■ **Haloscope** Around us, dark matter is expected to exist. The local energy density is fixed as $\rho_{\rm DM}^{\rm (local)} \simeq 0.45$ GeV/cm^3, so we can detect DM particle on the Earth. If the axion is really dark matter, we are surrounded by a greater number of axion particle compared to the case of the other heavier candidates, because the axion is very light. Thus the ground-based experiments look a good idea for axion detection.

Haloscope is an experimental set where the axion in dark matter halo is detected. The principle is based on the axion-photon conversion in strong external magnetic field. For instance, when the axion enters into the container (resonant cavity) applying magnetic field and is converted to photon, we can extract the information about the axion mass and coupling strength by detecting the produced photons. Now haloscope experiments have been carried out and planned, e.g. ADMX [103], MADMAX [104], ABRACADABRA [105] (see Fig. 2.6).

■ **Helioscope** It is possible that the axion not only lives with us but also comes to fly from outside (but it may not be dark matter). The main source is the Sun. The axion can be produced by axion-photon conversion due to the external electric field around ions in the Sun, which is called the Primakoff effect, and propagates to the Earth. We can search for the sign of axion by using the axion-photon conversion again in laboratory. The sensitivity is less than haloscope, but a broader mass region can be probed. For instance, helioscope experiments include CAST [106], IAXO [107, 108]

Chapter 3

Extra Peccei-Quinn symmetry breaking and trapping effect

In the previous chapter, it has been clearly shown that the minimal extension of the SM introducing the QCD axion successfully conserves the CP symmetry in QCD sector. It must require single PQ symmetry breaking by the QCD anomaly. Still, there can be a vast room for the extra PQ breaking in a UV completed theory, and the strong CP phase can be deviated from the origin. This is called quality problem of the PQ symmetry, which will be discussed in Sec. 3.1. There, we will see how much the PQ breaking effect should be suppressed using a concrete example. In Sec. 3.2, the Witten effect of hidden monopoles will be explained as an example for time-dependent extra potential. The above extra PQ breaking potentials must be significantly suppressed to satisfy the nEDM bound. However, the QCD potential is negligibly small in the early universe, and the axion dynamics can be altered. In Sec. 3.3, we will study the case that the axion is initially trapped by the extra potential. We will classify the axion dynamics by the adiabaticity and evaluate the abundance of axion analytically.

3.1 Quality problem of PQ symmetry

The global symmetry $\mathrm{U}(1)_{\mathrm{PQ}}$ is the building block of the PQ mechanism. To resolve the Strong CP problem, any other explicit PQ breaking must be so suppressed that the potential minimum satisfies the nEDM bound. However, in quantum gravity theory, it is strongly believed that any global symmetry is explicitly broken [44, 45, 46, 47, 48]. An example is the absorption process of black hole. When a black hole eats particles with some global charges, it becomes impossible to observe it. Such a quantum gravity effect and other effects may induce extra potentials for axion in the low energy effective field theory. The, the effective strong CP phase might be largely altered, and the PQ mechanism could be spoiled. This is known as the quality problem of PQ symmetry. For instance, non-renormalizable operators induce explicit breaking of the PQ symmetry.[1]

[1] Actually, even some renormalizable operators can break down the PQ symmetry, but it is usually assumed to be protected as an accidental symmetry by e.g. discrete symmetry.

Let us consider a d-dimensional Planck suppressed operator,

$$\mathcal{L}_{\not PQ} \supset \frac{c|\Phi|^{2m}\Phi^n}{M_{\rm Pl}^{d-4}} e^{-i\delta} + \text{h.c.}, \tag{3.1}$$

where Φ denotes the PQ scalar whose phase corresponds to the axion, $d = 2m + n$, and c and δ are a real constant. Parametrizing the PQ scalar field as $\Phi = (v_\phi/\sqrt{2})e^{i\phi/v_\phi}$ (dropping the radial component), we obtain the PQ breaking potential for axion as

$$V_{\not PQ} = -\frac{v_\phi^4 c}{2}\left(\frac{v_\phi}{M_{\rm Pl}}\right)^{d-4} \cos\left(n\frac{\phi}{v_\phi} - \delta\right). \tag{3.2}$$

One can see that δ represents the shift from the origin, and the suppression factor $v_\phi/M_{\rm Pl}$ and the dimension d determines its size.

The axion mass from this potential is given as an expansion coefficient of the second order, $m_{\not PQ}^2 = (cn^2 v_\phi^2/2)\cdot(v_\phi/M_{\rm Pl})^{d-4}$. Both the QCD potential and the Planck suppressed potential are approximated as quadratic one, and we can obtain the effective strong CP phase,

$$\langle\theta\rangle \simeq \frac{m_{\not PQ}^2 \tan\delta}{n(m_{\phi 0}^2 + m_{\not PQ}^2)}. \tag{3.3}$$

To solve the strong CP problem, we require $|\langle\theta\rangle| \lesssim 10^{-10}$. This result gives a nontrivial constraint on UV theory. Taking c and $\tan\delta$ to be of the order unity and setting the power n to unity, the dimension has to be $d \gtrsim 8,\ 12,\ 28$ for $v_\phi = 10^8,\ 10^{12},\ 10^{16}$ GeV, respectively. For this estimate, we use the mass relation (2.12) assuming the unit domain wall number, i.e. $v_\phi = f_\phi$. The suppression of all lower dimension operators than the required dimension must be explained by some additional symmetry, like a Z_N symmetry with large N.

In this thesis, we are interested in how such ubiquitous PQ breaking effects change the axion properties. If the potential is modified, then so is the axion dynamics, leading to the nontrivial cosmological implications, such as the axion abundance and the isocurvature fluctuations.

To estimate the impact of the extra PQ breaking on the axion dynamics, let us first evaluate which parts in the parameter region are allowed by the nEDM bound (2.6). In addition to the QCD potential (2.15), we consider an additional PQ breaking term in the form of

$$V_{\not PQ}(\phi) = \Lambda_H^4\left[1 - \cos\left(N\left(\frac{\phi}{f_\phi} - \theta_H\right)\right)\right], \tag{3.4}$$

which is parametrized by the potential height Λ_H, a rational number N, and a phase θ_H. We assume $\theta_H > 0$ without loss of generality. Here Λ_H is take to be a constant, but it can be time-dependent. A time-dependent potential can also violate the PQ symmetry, but it is less problematic as far as diluted enough with time. The potential term via the Witten effect will be discussed in the next section. Thus, the total potential is

$$\begin{aligned} V(\phi, T) &= V_{\rm QCD}(\phi, T) + V_{\not PQ}(\phi) \\ &= m_\phi^2(T) f_\phi^2\left(1 - \cos\frac{\phi}{f_\phi}\right) + \Lambda_H^4\left[1 - \cos\left(N\left(\frac{\phi}{f_\phi} - \theta_H\right)\right)\right]. \end{aligned} \tag{3.5}$$

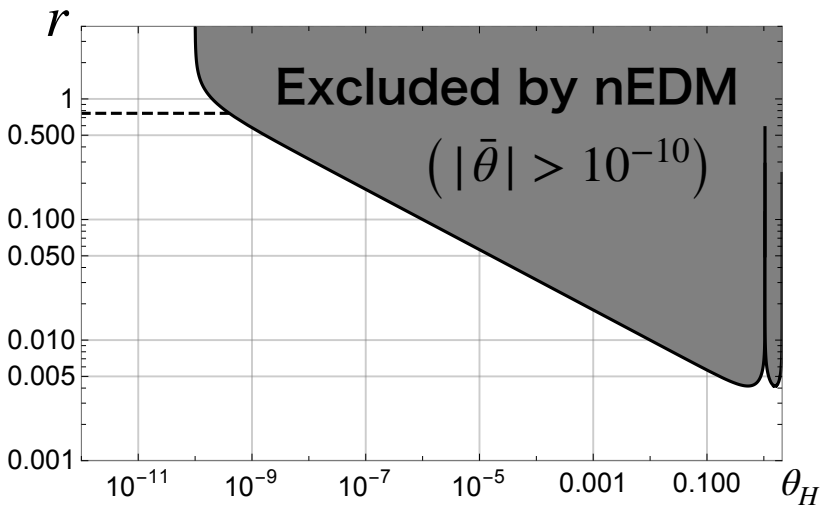

Figure 3.1: The nEDM constraint (3.6) for $N = 3$. The gray shaded region is excluded. The axion remains trapped at a false minimum in the case of $r \gtrsim N^{-1/4}$ denoted by the black dashed line, leading to a too much contribution to $\bar{\theta}$.

The neutron EDM bound (2.6) can be converted to the limits on Λ_H and θ_H. One can solve the equation $V'(\phi) = 0$ to evaluate the effective strong CP phase $\bar{\theta}$ modified by the extra PQ breaking term. For convenience, let us define r as the relative size of $V_{\not{\rm PQ}}$ with respect to $V_{\rm QCD}$ at $T \ll \Lambda_{\rm QCD}$, and the limit is expressed as

$$r \equiv \frac{\Lambda_H}{\sqrt{m_{\phi,0} f_\phi}} \lesssim \left| \frac{10^{-10}}{N \sin(N(10^{-10} - \theta_H))} \right|^{1/4} . \tag{3.6}$$

The excluded parameter region for $N = 3$ is shown by the gray shaded region in Fig. 3.1. While it is trivial for the upper bound to disappear at $\theta_H < 10^{-10}$, the upper bound is coincidently relaxed at particular values of $\theta_H = \pi/N$ where the minimum of $V_{\not{\rm PQ}}$ is aligned with that of $V_{\rm QCD}$. If $Nr^4 \gtrsim 1$ (shown by the black dashed line), there are multiple false vacua even in the low energy, and the axion would be trapped at one of them if $|\theta_{\rm ini} - \theta_H| \gtrsim \pi/N$. Then, it would give a too large contribution to $\bar{\theta}$ unless the axion escapes from the wrong minimum by tunneling.

We note that a relatively large extra potential can avoid the constraint from the nEDM, if some mild tuning of θ_H is allowed. In the previous literature [109, 110, 111, 112, 113], assuming $\theta_H \sim \mathcal{O}(\pi/N)$, the axion quality problem was estimated. However, the quantum gravity effect necessarily induces the explicit breaking of PQ symmetry, and it is important to investigate a broader parameter region. In Chapter 4, the dynamics, abundance, and isocurvature in this setup will be studied in detail.

3.2 Witten effect on axion potential

We found in the previous section that the axion acquires additional potentials from other explicit PQ breaking effects, which leads to the necessity of high quality PQ symmetry. Of these additional potentials, there is a type of potential that does not to spoil the PQ

mechanism. It is the case when the extra PQ breaking potential is time-dependent and decreases with time. For example, the Hubble-induced mass originating from the coupling to the Ricci curvature [114], and the Witten effect [50]. Here and in Chapter 5, we discuss the latter case and its implications about the axion dark matter.

The Witten effect is a phenomenon related to magnetic monopole. The electromagnetic monopole are tightly constrained by experiments [115]. Still, there is a room for inducing sizable effects in nature if the monopole is in hidden sectors. Throughout this thesis, we consider the hidden monopole as the 't Hooft-Polyakov monopole [52, 53]. The monopole is a solution of the $\mathrm{SU}(2)_H$ gauge theory which is spontaneously broken to the hidden Abelian gauge group.

First let us begin with a hidden $\mathrm{U}(1)_\mathrm{H}$ gauge theory in the presence of a 't Hooft-Polyakov monopole [52, 53]. Including the Chern-Simons term associated with hidden gauge group, the Lagrangian in the gauge sector is given by

$$\mathcal{L} \supset -\frac{1}{4}X_{\mu\nu}X^{\mu\nu} - \frac{e_H^2\Theta_H}{32\pi^2}X_{\mu\nu}\tilde{X}^{\mu\nu}, \tag{3.7}$$

where e_H is the gauge coupling, Θ_H is a constant parameter, and $X_{\mu\nu}$ and $\tilde{X}^{\mu\nu} \equiv \epsilon^{\mu\nu\alpha\beta}X_{\alpha\beta}/2$ represent the field strength of the hidden gauge field and its dual, respectively. While the Chern-Simons term has no effects perturbatively because it is a total derivative, a non-trivial effect exists in the presence of magnetic monopole. From the Lagrangian, we can derive the equation of motion,

$$\partial_\mu\left(X^{\mu\nu} + \frac{e_H^2\Theta_H}{8\pi}\tilde{X}^{\mu\nu}\right) = 0, \tag{3.8}$$

which corresponds to the Maxwell equation for hidden gauge theory modified by the Chern-Simons term. Using the hidden electric field $\boldsymbol{E}$ and magnetic field $\boldsymbol{B}$, the modified Gauss's law is given by

$$\nabla\cdot\boldsymbol{E} = -\frac{e_H^2}{8\pi^2}\nabla\cdot(\Theta_H\boldsymbol{B}), \tag{3.9}$$

where $E_i \equiv X_{0i}$ and $B_i \equiv -\epsilon_{ijk}X^{jk}/2$. In the presence of hidden monopole, the magnetic flux becomes nonzero since the magnetic monopole possesses a point-like magnetic charge density, $g_H(n_{M+}-n_{M-})$ where $g_H = 4\pi/e_H$ is a magnetic charge, and n_{M+} (n_{M-}) denotes the number density of the (anti-)monopole. Thus the Θ_H-term shifts the hidden electric charge by $Q_E/e_H = -\Theta_H/2\pi$, that is, the magnetic monopole becomes dyon. This is called the Witten effect [50].

The next step is to introduce the QCD axion coupled to the $\mathrm{U}(1)_\mathrm{H}$ such as

$$\mathcal{L}_\phi = \frac{1}{2}\partial_\mu\phi\partial^\mu\phi - V_\mathrm{QCD}(\phi) - \frac{e_H^2}{32\pi^2}\left(\Theta_H + \frac{\phi}{f_H}\right)X_{\mu\nu}\tilde{X}^{\mu\nu}, \tag{3.10}$$

where f_H is the axion decay constant associated with the hidden sector. When the anomaly coefficient of color and hidden $\mathrm{U}(1)_H$ are respectively given by N (see Eq. (2.36)) and E_H, it is defined by

$$f_H = \frac{N}{E_H}f_\phi \equiv \frac{N_\mathrm{DW}}{N_H}f_\phi. \tag{3.11}$$

In the last equality, we redefine the anomaly coefficients as the domain wall numbers for each group. By imposing shift transformation of the axion so that the θ-term in QCD disappears, the axion is coupled to the hidden gauge field instead of the parameter Θ_H,

$$\mathcal{L}_\phi \supset -\frac{e_H^2}{32\pi^2}\frac{(\phi-\phi_*)}{f_H}X_{\mu\nu}\tilde{X}^{\mu\nu}, \tag{3.12}$$

where ϕ_* is given as a free parameter. Note that Θ_H generally differs from $\bar{\theta}$ in QCD, so ϕ_* has a nonzero value. In the presence of the axion, we can rewrite the relation for the electric charge of dyon as

$$\frac{Q_E}{e_H} = -\frac{(\phi-\phi_*)}{2\pi f_H}. \tag{3.13}$$

Therefore, as the axion field value changes, the electric charge of the dyon changes. At $\phi \neq \phi_*$, the monopole has an electric charge so that the coupling to hidden electric fields induces the axion effective potential whose minimum is determined by $\phi = \phi_*$.

To see the effective potential explicitly, the axion-dependent contribution to the electromagnetic energy of a single monopole is estimated as [51]

$$V_M \sim \beta f_H \frac{(\phi-\phi_*)^2}{f_H^2}, \tag{3.14}$$

$$\beta = \frac{\alpha_H}{32\pi^2}\frac{1}{r_c f_H}, \tag{3.15}$$

where $\alpha_H \equiv e_H^2/4\pi$, and r_c is the radius of the monopole core. In the case of the 't Hooft-Polyakov monopole, r_c is the inverse of the heavy gauge boson mass, m_W, which is about α_H times the monopole mass. Taking a spatial average over the whole space, we obtain the energy density of the axion ground state in the plasma with monopoles and anti-monopoles as $U = n_M V_M$, where $n_M = n_{M+} + n_{M-}$. Thus, the homogeneous mode of the axion effectively obtains a potential

$$V_M(\phi) = \frac{1}{2}m_{\phi,M}^2(\phi-\phi_*)^2, \tag{3.16}$$

where the mass $m_{\phi,M}$ is given by

$$m_{\phi,M}^2(T) = 2\beta\frac{n_M(T)}{f_H} \tag{3.17}$$

$$= \frac{\alpha_H^2}{16\pi^2}\frac{\rho_M(T)}{f_H^2}. \tag{3.18}$$

The mass (3.18) decreases in time due to the cosmic expansion, so that this does not spoil the Peccei-Quinn mechanism to solve the strong CP problem. The Chapter 5 will be devoted to the detailed analysis in this situation.

Lastly we comment on an upper bound on the coupling constant α_H. The $\mathrm{SU(2)_H}$ instanton effect gives another effective mass to the axion, which is proportional to $e^{-\pi/\alpha_H}$ [116, 117, 118] and does not decrease in time in the low energy. The effective mass squared from this contribution should be smaller by a factor of 10^{-10} than that from the QCD effect, otherwise the PQ mechanism would be spoiled. This requires

$$\alpha_H \lesssim 0.07. \tag{3.19}$$

In the following, we assume that this condition is satisfied.

3.3 Trapping effect

So far, we saw that the QCD axion can acquire an additional potential from the other PQ symmetry breaking. Although a time-independent potential is constrained by the experiments of nEDM, there is still a broad parameter region where the potential can alter the axion dynamics. Since an effective potential from the Witten effect becomes stronger in the earlier universe, the dynamics can be significantly modified. If the axion is temporarily trapped by such an additional potential, we expect that the dynamics becomes completely different. We call such an effect the trapping effect.

Here we will study the trapping effect on the axion dynamics by the extra PQ breaking potential. We do not assume any specific extra potential. Categorizing the dynamics neatly and analyzing the abundance and the isocurvature perturbation, we will present the importance of the trapping effect on the axion DM.

We consider the potential,

$$V(\phi, T) = V_{\rm QCD} + V_{\not{\rm PQ}}^{\rm (G)}, \tag{3.20}$$

where the second term denotes the potential from the extra PQ breaking which induces the trapping effect. We perform a general analysis of the axion dynamics without specifying the form of the PQ breaking potential, and the superscript '(G)' of the second term indicates the generality. The temperature dependence of the PQ breaking potential does not matter. The given consequences will be applied to the specific potentials in the subsequent two chapters.

Here let us categorize the axion dynamics into two regimes, and calculate the abundance for each regime. At first, let us explain the dynamics (see the schematic picture in Fig. 3.2). We are interested in the case when the PQ breaking potential drives the axion oscillations before the QCD phase transition, $T_{\rm osc} \gg \Lambda_{\rm QCD}$, where $T_{\rm osc}$ is the temperature at the onset of oscillation. In the following, the subscript 'osc' implies that the variable is evaluated at $T = T_{\rm osc}$. Also, we define the position of potential minimum at $T = T_{\rm osc}$ as $\phi_{\rm min}$. If the trapping effect is small enough compared to the QCD potential, and $T_{\rm osc} \lesssim \Lambda_{\rm QCD}$, then the dynamics would not differ from that of the conventional case. After the axion oscillates about the minimum of PQ breaking potential ($\phi = \phi_{\rm min}$), the QCD potential becomes dominant over the PQ breaking potential, and the structure of potential minima is deformed. All the minima, except for the origin, disappear, and the axion is eventually stabilized at the CP conserving minimum to solve the Strong CP problem.[2] Note that we assume that the potential satisfies the nEDM bound (2.6), and the size of $V_{\not{\rm PQ}}^{\rm (G)}$ in Fig. 3.2 is exaggerated for illustration purpose..

The temperature of onset of oscillation is determined by the ratio of the Hubble parameter to the effective mass of $V_{\not{\rm PQ}}^{\rm (G)}$. The effective mass is given by the potential curvature near the minimum ($\phi = \phi_{\rm min}$), i.e. $m_{\not{\rm PQ}}^2 \equiv |(V_{\not{\rm PQ}}^{\rm (G)})''(\phi_{\rm min})|$. We define $T_{\rm osc}$ by $H(T_{\rm osc}) = m_{\not{\rm PQ}}(T_{\rm osc})$. Note that the anharmonic effect can delay the onset of oscillation, but the contribution is introduced by multiplying the anharmonic factor (e.g. Eq. (2.22)) to the abundance. In the following, we focus on the case of $T_{\rm osc} \gtrsim T_{\rm osc}^{\rm (conv)}$ where $T_{\rm osc}^{\rm (conv)}$

[2]Here we do not consider the case that the axion remains trapped at a wrong minimum even after the QCD phase transition. The situation can be realized if the trapping effect is very strong and time-independent. Such a quasi-eternal trapping was considered in [119].

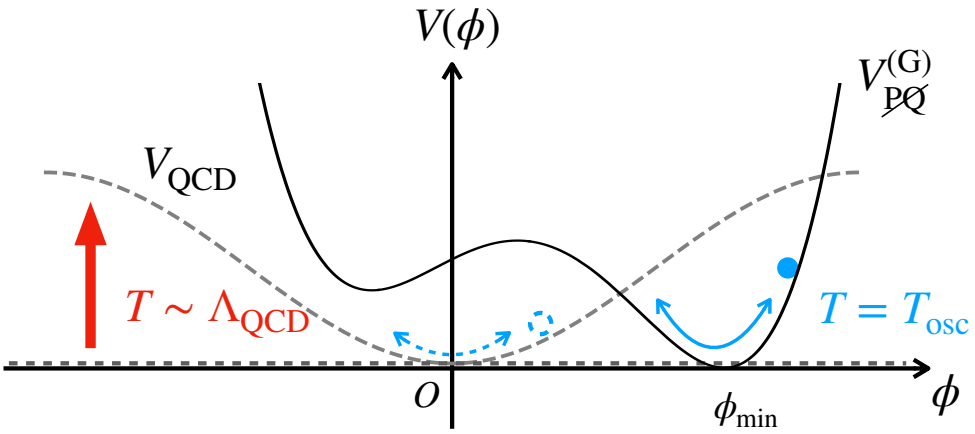

Figure 3.2: The schematic picture of the potential $V(\phi)$: the extra PQ breaking potential $V^{(\mathrm{G})}_{\not{\mathrm{PQ}}}$ (the black solid line) plus the QCD potential V_{QCD} (the gray dashed lines). The size of $V^{(\mathrm{G})}_{\not{\mathrm{PQ}}}$ is exaggerated for illustration purpose. Before the QCD phase transition $T \gg \Lambda_{\mathrm{QCD}}$, the position of potential minimum is determined only by $V^{(\mathrm{G})}_{\not{\mathrm{PQ}}}$, and the PQ breaking potential drives the axion oscillation at $T = T_{\mathrm{osc}}$. At $T \sim \Lambda_{\mathrm{QCD}}$, the vacuum structure starts to be deformed, and finally, there remains only the CP conserving minimum (the origin).

is the oscillation temperature without any extra potential (see Eq. (2.17)). It means that the axion starts to oscillate around the minimum of $V_{\not{\mathrm{PQ}}}$ before the QCD phase transition. The oscillating axion generically acquires an additional oscillation amplitude because of the deformation of entire potential shape. Naively speaking, there are two contributions to the axion abundance,

$$\Omega_\phi \simeq \Omega^{(1)}_\phi + \Omega^{(2)}_\phi. \tag{3.21}$$

Here, the first and second term denote the contributions of the primary oscillation by the PQ breaking potential and the secondary oscillation induced by the deformation of potential, respectively. The temperature at the onset of deformation (defined as T_{def}) is determined by $m_\phi(T_{\mathrm{def}}) = m_{\not{\mathrm{PQ}}}(T_{\mathrm{def}})$. The temperature at the onset of the secondary oscillation (defined as T_{osc2}) is roughly given by the same temperature, $T_{\mathrm{osc2}} \sim T_{\mathrm{def}}$, but more precisely, we require model-dependent analysis. Hereafter, the subscript 'osc2' ('def') implies that the variable is evaluated at $T = T_{\mathrm{osc2}}$ (T_{def}).

In fact, it is not possible to separate the axion abundance into such two parts completely, because the primary oscillations are mixed with the secondary ones when the potential deformation occurs, $T \sim T_{\mathrm{def}}$. Thus we need numerical calculations to obtain the accurate abundance. Nevertheless, by considering special situations, the abundance can be approximately saturated only by either contribution, which decomposes the axion dynamics into two regimes. One case corresponds to the regime where the axion is always trapped around the same minimum due to the strong PQ breaking potential. In this regime, the additional amplitude is almost not induced, and the abundance is fixed only by the primary oscillation, $\Omega_\phi \simeq \Omega^{(1)}_\phi$. The primary oscillations are protected adiabatically by the trapping effect of extra potential, and we refer to this regime as the adiabatic regime. In the other case, a sizable amplitude is generated, and the secondary

oscillation dominates over the primary one, $\Omega_\phi \simeq \Omega_\phi^{(2)}$. In this regime, the strong trapping effect induces the primary oscillation at $T \gg T_{\rm osc}^{(\rm conv)}$, but the primary oscillations are not protected adiabatically due to model-dependent factors that we will see later. This case is referred to as the non-adiabatic regime. Note that the primary oscillations have to start well before the conventional onset of oscillation, $T_{\rm osc} \gg T_{\rm osc}^{(\rm conv)}$, in the non-adiabatic regime. If the onset of primary oscillation is earlier than but comparable to that of the conventional one, the primary amplitude is non-negligible at the timing of deformation. As a result, the primary oscillations can also contribute to the abundance, and thus, if the trapping effect is not so strong in the non-adiabatic regime, the above naive classification is spoiled. In this case, we need numerical calculations which will be shown in the subsequent chapters.

Adiabaticity

The axion dynamics can be categorized into the two regimes described above. What is important is whether the primary oscillations are protected adiabatically or not. We can call this property the adiabaticity in the system. Before beginning the analysis of each regime, let us clarify the condition that the adiabaticity is broken. To this end, we introduce a parameter that describes the violation of adiabaticity, $\epsilon(t)$, defined by

$$\epsilon(t) \equiv \left| \frac{1}{m_{\rm eff}^2(\phi)} \frac{dm_{\rm eff}(\phi)}{dt} \right| , \tag{3.22}$$

where the effective mass is defined by $m_{\rm eff}^2 \equiv |V''(\phi)|$ for the temporal position ϕ of the axion field. If $\epsilon \ll 1$, the effective mass changes adiabatically, which implies that the system also evolves adiabatically. The axion field tracks the temporal minimum, as long as the effective mass is larger than the Hubble parameter. On the contrary, if $\epsilon \sim 1$, the axion cannot follow the deformation of potential minima, and it acquires an additional amplitude which induces the secondary oscillation. In particular, we are interested in the value at $T = T_{\rm def}$, because the violation of adiabaticity is expected to become the largest when the potential minima start to be deformed. Importantly, this parameter will be also useful for estimating the dependence of the abundance on the strength of the trapping effect, which will be demonstrated in a toy model soon later.

Using the violation of adiabaticity at $T = T_{\rm def}$, we can summarize the categorization of axion dynamics:

(i) *Adiabatic regime* : $\epsilon(t_{\rm def}) \ll 1$ $(\Omega_\phi \simeq \Omega_\phi^{(1)})$

(ii) *Non-adiabatic regime* : $\epsilon(t_{\rm def}) \sim 1$ $(\Omega_\phi \simeq \Omega_\phi^{(2)})$

Below, the axion abundance in each regime is calculated analytically, and in Chapter 4 and 5, we will use specific extra PQ breaking potentials to study the axion dynamics both analytically and numerically.

Adiabatic regime

In this regime where $\epsilon(t_{\rm def}) \ll 1$, the axion field follows the temporal minimum, and any extra oscillation is almost not generated. When the potential minimum smoothly shifts

from a wrong vacuum to the true (CP conserving) vacuum, the abundance is fixed only by the primary oscillations, $\Omega_\phi \simeq \Omega_\phi^{(1)}$. As with the standard misalignment mechanism, the number density in the comoving volume remains conserved after the oscillation, and we obtain the ratio of the number density to the entropy density,

$$\frac{n_{\phi,0}}{s_0} = \frac{n_{\phi,\mathrm{osc}}}{s_{\mathrm{osc}}} = \frac{45 m_{\not{\mathrm{PQ}}}(T_{\mathrm{osc}})(\phi_{\mathrm{ini}} - \phi_{\mathrm{min}})^2}{4\pi^2 g_{*s}(T_{\mathrm{osc}}) T_{\mathrm{osc}}^3}, \tag{3.23}$$

or equivalently,

$$\Omega_\phi h^2 \simeq \frac{m_{\phi,0} m_{\not{\mathrm{PQ}}}(\phi_{\mathrm{ini}} - \phi_{\mathrm{min}})^2}{2\rho_{\mathrm{crit}} h^{-2}} \frac{g_{*s0}}{g_{*s}(T_{\mathrm{osc}})} \left(\frac{T_0}{T_{\mathrm{osc}}}\right)^3 \cdot F^{(\mathrm{AD})}(\theta_{\mathrm{ini}}). \tag{3.24}$$

The coefficient $F^{(\mathrm{AD})}(\theta_{\mathrm{ini}})$ is defined as the anharmonic factor, written by

$$F^{(\mathrm{AD})}(\theta_{\mathrm{ini}}) = \left[\ln\left(\frac{e}{1 - (\theta_{\mathrm{ini}} - \theta_{\mathrm{min}})^2/\theta_d^2}\right)\right]^k. \tag{3.25}$$

The exponent k is model-dependent and determined in the way suggested by Refs. [33, 36], and θ_d represents the distance between the minimum and the maximum of extra PQ breaking potential. Estimating the oscillation temperature T_{osc} and the mass $m_{\not{\mathrm{PQ}}}$ by PQ breaking potential, and fixing the form of the anharmonic factor $F^{(\mathrm{AD})}(\theta_{\mathrm{ini}})$, this result is applicable to any PQ breaking potential, as long as $\epsilon(t_{\mathrm{def}}) \ll 1$. In general, the abundance is suppressed compared to the conventional case, because of the earlier oscillation.

In the above estimate, we assume no secondary oscillations, but precisely speaking, how much the secondary oscillation is suppressed depends on the strength of trapping effect by the extra PQ breaking potential. It is known that the contribution of secondary oscillations is exponentially suppressed due to the strong trapping effect. This is why this phenomena in the adiabatic regime is called adiabatic suppression mechanism [56, 57, 120, 54, 55].

Let us see explicitly the adiabatic suppression mechanism on the basis of the simplest setup [56].[3] Suppose that a massive scalar field acquires an effective mass that is proportional to the Hubble parameter such as

$$V(\chi) = \frac{1}{2} m_\chi^2 \chi^2 + \frac{1}{2} C^2 H^2 (\chi - \chi_{\mathrm{min}})^2 \,, \tag{3.26}$$

where C (≥ 0) is a constant that represents the size of the Hubble-induced mass term, χ_{min} is its minimum, and m_χ is the scalar mass at low energy when the Hubble-induced mass is negligible. In the radiation dominated era, the Hubble parameter decreases as $H \propto T^2$, and the potential minimum changes with time; at high temperatures the minimum is at $\chi \simeq \chi_{\mathrm{min}}$, while at low temperatures it is at $\chi \simeq 0$. In the case of $0 \leq C \lesssim 1$, the scalar field is not strongly trapped by the Hubble-induced mass term, and it begins to oscillate around $\chi = 0$ when $H \sim m_\chi$. The result is the same with the case of no Hubble induced mass. In the case of $C \gg 1$, on the other hand, the scalar field is trapped so strongly

[3] The adiabatic suppression mechanism originally studied in a context of the Polonyi/moduli problem, which was recently applied to the axion dynamics in Refs. [54, 55].

that it begins to track the potential minimum adiabatically when $H(T_{\rm def}) \sim m_\chi/C$. The abundance of the scalar field is exponentially smaller than the case with $0 \leq C \lesssim 1$. This is the adiabatic suppression mechanism.

The amount of suppression can be evaluated by solving the equation of motion for the homogeneous scalar field:

$$\ddot{\chi} + 3H\dot{\chi} + V'(\chi) = 0\,. \tag{3.27}$$

An analytic result for the suppression factor can be obtained from (3.27) with the initial condition $(\chi, \dot{\chi}) = (\chi_{\rm min}, 0)$ at $H \gg m_\chi$ as [56]

$$\frac{\Omega_\chi(C \gg 1)}{\Omega_\chi(C=1)} \propto C^{5/2} \exp\left(-C\pi/2\right). \tag{3.28}$$

One can see that the amplitude of the scalar field is exponentially suppressed for $C \gg 1$. This is the important feature of the adiabatic suppression.

The exponent in (3.28) can be understood by using the adiabatic parameter ϵ. In this case, it is given by

$$\epsilon(t) = \frac{2C^2H^3}{(m_\chi^2 + C^2H^2)^{3/2}}. \tag{3.29}$$

At $T = T_{\rm def}$ when $m_\chi \simeq CH$, $\epsilon(t_{\rm def}) = 1/\sqrt{2}C$. We can see that the exponent of the suppression factor is given by $\epsilon^{-1}(t_{\rm def})$ up to some coefficients. Thus, $\epsilon(t_{\rm def}) \ll 1$ is the reasonable condition for the adiabatic regime. Using this result, we can also see that if the extra PQ breaking potential can be approximated to be quadratic, and the trapping is strong enough, then the adiabatic suppression works well.

Non-adiabatic regime

In the region where $\epsilon(t_{\rm def}) \sim 1$, the axion cannot follow the deformation of potential shape, and an additional amplitude is induced. Defining the axion position at the onset of secondary oscillations $T = T_{\rm osc2}$ as $\theta_{\rm osc2} \equiv \theta(T_{\rm osc2})$, the oscillation amplitude is given by $|\theta_{\rm osc2} - \bar{\theta}_{\rm eff}| \simeq \theta_{\rm osc2}$ where $\bar{\theta}_{\rm eff}$ is the eventual minimum and contributes to the nEDM. Thus, assuming $T_{\rm osc} \gg T_{\rm osc}^{\rm (conv)}$, the abundance is estimated as

$$\Omega_\phi h^2 \simeq \Omega_\phi^{(2)} h^2 \simeq \frac{m_{\phi,0} m_\phi(T_{\rm osc2}) f_\phi^2 \theta_{\rm osc2}^2}{2\rho_{\rm crit} h^{-2}} \frac{g_{*s0}}{g_{*s}(T_{\rm osc2})} \left(\frac{T_0}{T_{\rm osc2}}\right)^3 \cdot F^{\rm (NAD)}(\theta_{\rm osc2}). \tag{3.30}$$

The anharmonic factor is given by

$$F^{\rm (NAD)}(\theta_{\rm osc2}) = \left[\ln\left(\frac{e}{1 - \theta_{\rm osc2}^2/\theta_d^2}\right)\right]^k. \tag{3.31}$$

$T_{\rm osc2}$ and $\theta_{\rm osc2}$ are model-dependent parameters. Importantly, the abundance is independent of the initial position of the axion field $\theta_{\rm ini}$.

Lastly, it is worth mentioning that it is nontrivial to realize the non-adiabatic regime or to satisfy the conditions, $T_{\rm osc} \gtrsim T_{\rm osc}^{\rm (conv)}$ and $\epsilon(t_{\rm def}) \sim 1$, simultaneously. According to

the discussion of adiabatic regime, the violation of the adiabatic condition requires the weak trapping effect, but the condition $T_{\rm osc} \gtrsim T_{\rm osc}^{(\rm conv)}$ requires the strong trapping effect. One might wonder it is inconsistent. However, it is possible that the adiabaticity is broken by some factor independent of the strength of the trapping effect. We need the analysis of specific models to understand the factors violating the adiabaticity. In Chapter 4 and 5, we will consider concrete extra PQ breaking potentials and estimate the violation of the adiabaticity. We also need model-dependent analysis for estimating the isocurvature perturbations and identifying a viable region where the axion can explain DM.

Chapter 4

Trapping effect on axion dark matter

The PQ symmetry plays an essential role in addressing the Strong CP problem, but it must be of high quality and all the breaking terms be significantly suppressed as a result of the severe constraints on the nEDM. Such a tiny correction to the axion potential would not seem to leave any imprint on the predicted axion nature. However, we saw in Sec. 3.1 that there is still room to investigate the possibility of its nontrivial effects by small breaking terms, since the potential from nonperturbative effects of QCD is almost negligible in the very early universe ($T \gg \Lambda_{\rm QCD}$).

While we studied the general features of the trapping effect on the axion in the previous chapter, we focus on a time-independent, concrete potential $V_{\not{\rm PQ}}$, based on the paper [49]. After introducing our setup and classifying the axion dynamics by taking account of the adiabaticity, the axion abundance and isocurvature power spectrum will be evaluated numerically in Sec. 4.2 and 4.3. We will find that the abundance and the isocurvature power spectrum can be altered depending on the initial position of the axion.

4.1 Axion potential

We consider the same setup with the last discussion in Sec. 3.1 where the axion acquires a potential with multiple minima from explicit PQ breaking in addition to the nonperturbative effect of QCD,

$$\begin{aligned} V(\phi, T) &= V_{\rm QCD}(\phi, T) + V_{\not{\rm PQ}}(\phi) \\ &= m_\phi^2(T) f_\phi^2 \left(1 - \cos\frac{\phi}{f_\phi}\right) + \Lambda_H^4 \left[1 - \cos\left(N\left(\frac{\phi}{f_\phi} - \theta_H\right)\right)\right]. \end{aligned} \tag{4.1}$$

The schematic picture of the potential is shown in Fig. 4.1 for $N = 3$ and a negligibly small θ_H that is assumed to be positive. $V_{\rm QCD}(\phi, T)$ and $V_{\not{\rm PQ}}(\phi)$ are denoted by the gray dotted and red dashed line, respectively. In the very early universe $T \gg \Lambda_{\rm QCD}$, the potential is dominated only by $V_{\not{\rm PQ}}$. When the temperature becomes close to the QCD scale, the QCD potential deforms the entire form of the potential and eventually becomes dominant over the extra PQ breaking potential, denoted by the blue solid line.

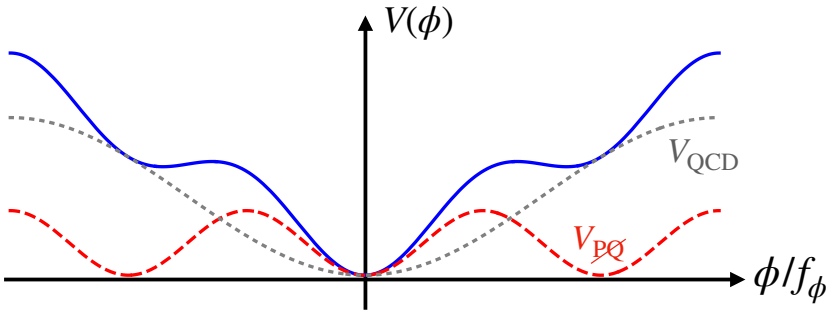

Figure 4.1: The schematic picture of the total potential $V(\phi)$ at the zero temperature (solid blue line) for $N = 3$ and a negligibly small θ_H. $V_{\rm QCD}(\phi)$ and $V_{\not{\rm PQ}}(\phi)$ are denoted by the gray dotted and red dashed line, respectively. The size of $V_{\not{\rm PQ}}$ is exaggerated for illustration purpose.

Here let us remember the definition of the dimensionless, relative height of the potential compared to the QCD potential,

$$r \equiv \frac{\Lambda_H}{\sqrt{m_{\phi,0} f_\phi}}. \tag{4.2}$$

It is an important parameter in the following discussion.

4.2 Axion abundance

In this section, the abundance of axion will be studied analytically and numerically, when the extra PQ symmetry breaking satisfies the constraints (3.6) from the nEDM experiment. The previous literature focused only on the vicinity of $\theta_H \sim \mathcal{O}(\pi/N)$, or equivalently $r \lesssim \mathcal{O}(10^{-3})$, and the impact on the abundance was neglected [109, 110, 111, 112, 113]. We investigate the whole of allowed space in Fig. 3.1 comprehensively. As explained in Chapter 3, the results are systematically classified into two regimes, and the trapping effect due to the extra PQ breaking potential has a nontrivial impact on the dynamics of the axion in both regimes.

4.2.1 Dynamics and analytical estimate

First let us begin with estimating the dynamics of the axion on the basis of the consequences given in Chapter 3. The effective mass which is evaluated around the potential minimum is approximately given by $m_{\not{\rm PQ}} = Nr^2 m_{\phi,0}$. Then the temperature at the onset of oscillations is given by

$$T_{\rm osc} \simeq 0.91\ {\rm GeV} \left(\frac{g_*(T_{\rm osc})}{80}\right)^{-1/4} \left(\frac{Nr^2}{3\times 10^{-4}}\right)^{1/2} \left(\frac{f_\phi}{10^{12}\ {\rm GeV}}\right)^{-1/2}, \tag{4.3}$$

where we have used $Nr^2 m_{\phi,0} = 1.67 H(T_{\rm osc})$. We focus on the case of $T_{\rm osc} \gtrsim T_{\rm osc}^{\rm (conv)}$, or equivalently,

$$Nr^2 \gtrsim 3.0\times 10^{-4} \left(\frac{g_*(T_{\rm osc})}{80}\right)^{0.33} \left(\frac{f_\phi}{10^{12}\ {\rm GeV}}\right)^{0.66}. \tag{4.4}$$

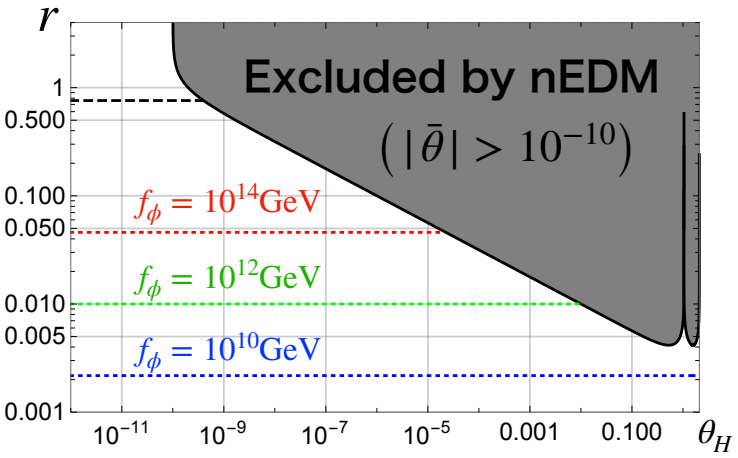

Figure 4.2: The region of our interest with the nEDM constraint (3.6) for $N = 3$ (cf. Fig. 3.1). The red, green, and blue dotted lines show the condition $T_{\rm osc} \gtrsim T_{\rm osc}^{(\rm conv)}$ for $f_\phi = 10^{14}, 10^{12}$, and 10^{10} GeV, respectively. In the region above each dotted line, the extra PQ breaking potential drives the axion oscillation, which is our interest.

The lower bound on f_ϕ is set by the stellar cooling arguments (see Eq. (2.41)), and for the boundary point, r is also bounded from below as $Nr^2 \gtrsim 6.7 \times 10^{-7}$. Note that for $f_\phi \gtrsim 10^{11}$ GeV, some tuning of θ_H is required for a sizable effect on the axion dynamics, while the effect can be important for smaller f_ϕ without tuning of θ_H. The lower bound on r for different f_ϕ is shown as colored dotted lines in Fig. 4.2.

The axion dynamics can be categorized into two regimes according to the adiabaticity, $\epsilon(t_{\rm def})$. In this case, the value of initial position $\theta_{\rm ini}$ is the criterion:

(i) Adiabatic regime : $|\theta_{\rm ini} - \theta_H| < \pi/N \quad (\leftrightarrow \ \epsilon(t_{\rm def}) \ll 1)$

(ii) Non-adiabatic regime : $|\theta_{\rm ini} - \theta_H| > \pi/N \quad (\leftrightarrow \ \epsilon(t_{\rm def}) \sim 1)$.

The schematic picture of the axion dynamics is shown in Fig. 4.3 for $N = 3$ and $\theta_H \ll 1$.

In the adiabatic regime, the minimum of the extra PQ breaking term ($\theta = \theta_H$) where the axion first starts to oscillate is continuously deformed to the eventual minimum where $\bar{\theta}$ vanishes. In this case, the adiabaticity is obviously tiny, $\epsilon \ll 1$, because the axion always feels only the quadratic potential as with the analysis of a toy model [56]. Thus, the minimum smoothly shifts to the origin as $V_{\rm QCD}$ becomes dominant, which is nothing but the adiabatic suppression mechanism.

In the non-adiabatic regime, the axion initially starts to oscillate in a wrong vacuum, and gets trapped there for a while until the wrong minimum disappears. It is not necessary to calculate it to know that the adiabaticity is broken, because the axion cannot move until the potential wall is completely gone and gains extra amplitudes. We will see the axion abundance is enhanced in contrast to the adiabatic regime. If $r \gtrsim N^{-1/4}$, i.e. the region above the black dashed line in Fig. 4.2, the axion cannot escape from a wrong minimum. In this case, the tunneling process is required for solving the Strong CP problem, and such a trapping was discussed in [119].

Below, let us analytically estimate the axion abundance in each regime.

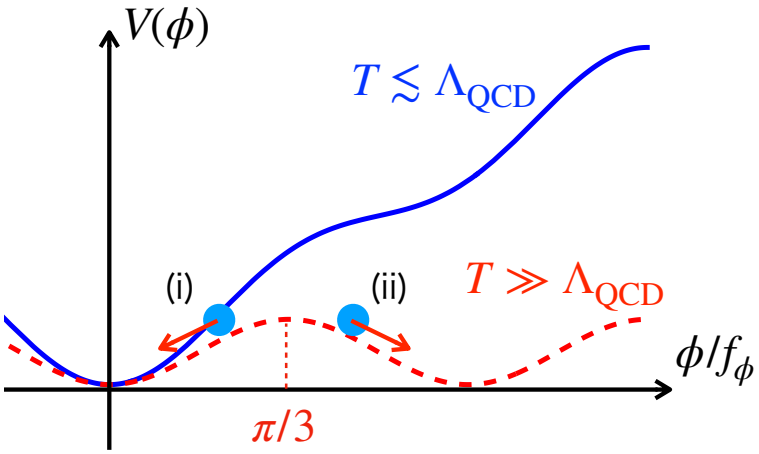

Figure 4.3: The schematic picture for the dynamics of the axion denoted by blue circles for $N = 3$ and $\theta_H \ll 1$. The blue solid and red dashed line represent the total potential after the QCD phase transition and the explicit PQ breaking potential, respectively.

■ **Adiabatic regime** In the adiabatic regime, i.e. $|\theta_{\rm ini} - \theta_H| < \pi/N$, the axion oscillation starts around the closest minimum to the origin. When $V_{\rm QCD}$ becomes relevant, the minimum smoothly shifts to the origin. Thus the oscillating axion adiabatically follows the temporal minimum without extra particle production, as long as the effective mass by the extra PQ breaking potential is much larger than the Hubble parameter. As a result, the axion abundance is significantly suppressed. According to the analytic formula (3.24), the axion abundance is determined by the primary oscillation with the initial amplitude $|\theta_{\rm ini} - \theta_H|$. Thus we obtain the axion abundance as

$$\Omega_\phi h^2 \simeq 5.0 \times 10^{-3} F_1(\theta_{\rm ini}) \left(\frac{g_*(T_{\rm osc})}{80}\right)^{-\frac{1}{4}} (\theta_{\rm ini} - \theta_H)^2 \left(\frac{Nr^2}{3\times 10^{-2}}\right)^{-\frac{1}{2}} \left(\frac{f_\phi}{10^{12}\ {\rm GeV}}\right)^{\frac{3}{2}}, \tag{4.5}$$

where we assume $g_*(T_{\rm osc}) \simeq g_{*s}(T_{\rm osc})$. Here the coefficient $F_1(\theta_{\rm ini})$ represents the contribution of the anharmonic effect for the extra PQ breaking term,

$$F_1(\theta_{\rm ini}) = \left[\ln\left(\frac{e}{1-(\theta_{\rm ini}-\theta_H)^2/(\pi/N)^2}\right)\right]^{3/2}, \tag{4.6}$$

which is obtained following the way suggested by Refs. [33, 36] under the assumption that the extra term has no temperature dependence. For larger r, the abundance is more suppressed, because the axion starts to oscillate earlier than the conventional case, with no additional oscillation. We also note that (4.5) is expected to become consistent with (2.21) in the conventional case as r decreases and the condition (4.4) is violated, or $T_{\rm osc} \lesssim T_{\rm osc}^{\rm (conv)}$.

■ **Non-adiabatic regime** Next, let us consider the non-adiabatic regime with $|\theta_{\rm ini} - \theta_H| \gtrsim \pi/N$, where the axion is temporarily trapped in a wrong minimum at $|\theta - \theta_H| = 2\pi k/N$ with $k = 1, 2, ..., N-1$. As long as the extra breaking term is subdominant

compared to $V_{\rm QCD}$ at low temperatures, i.e. $Nr^4 \lesssim 1$, all the $N-1$ local minima disappears at a certain point, and the axion begins to oscillate around the true minimum at $\theta \simeq 0$. As discussed in Chapter 3, the axion abundance can be roughly divided into two parts: the primary oscillations around a wrong vacuum, and the secondary oscillations around the true vacuum. However, as long as $T_{\rm osc} \gg T_{\rm soc}^{(\rm conv)}$, the contribution of the primary oscillations is washed out by the second oscillations.[1] Thus the final axion abundance is determined mainly by the difference between the disappearing local minimum and the true minimum, and thus it is not sensitive to the initial position $\theta_{\rm ini}$. Such a temporal trapping of the axion in a wrong vacuum was studied in Refs. [121, 122, 123], and the final axion abundance can be enhanced compared to the conventional case.

The axion starts to fall into the true minimum when the wrong vacuum disappears, i.e., $V'(\phi_{\rm osc2}) = 0$ and $V''(\phi_{\rm osc2}) = 0$. The temperature and the oscillation amplitude satisfy the following equations,

$$N \tan\theta_{\rm osc2} = \tan[N(\theta_{\rm osc2} - \theta_H)], \tag{4.7}$$

$$\frac{T_{\rm osc2}}{\Lambda_{\rm QCD}} \simeq (Nr^4)^{-0.13} \left[1 + \left(\frac{1}{N^2} - 1\right) \cos^2\theta_{\rm osc2}\right]^{0.064}. \tag{4.8}$$

Note that the first equation has N solutions. One solution is the minimum closest to $\theta = 0$ which corresponds to the adiabatic regime. The other $N-1$ solutions correspond to this regime. If the axion is trapped in the k-th wrong vacuum, the oscillation amplitude will be about $\theta_{\rm osc2} \sim (2k-1)\pi/N$. Note that $\theta_{\rm osc2}$ is mainly determined only by N and θ_H but is independent of f_ϕ or r. Barring cancellation in the parenthesis in (4.8), or equivalently unless focusing on $N \gg 1$, the temperature $T_{\rm osc2}$ is approximated by

$$T_{\rm osc2} \sim 0.4\ {\rm GeV} \left(\frac{Nr^4}{3\times 10^{-4}}\right)^{-0.13}. \tag{4.9}$$

Using the analytic formula (3.30), we can obtain the axion abundance as

$$\Omega_\phi h^2 \simeq 0.25\theta_{\rm osc2}^2 \left(\frac{g_*(T_{\rm osc2})}{60}\right)^{-1} \left(\frac{Nr^4}{10^{-6}}\right)^{0.88}. \tag{4.10}$$

Interestingly, the axion abundance does not depend on the decay constant because it is determined only by the potential height at $T_{\rm osc2}$. We note that this relation is valid when the trapping effect by the PQ breaking term is strong enough, or equivalently, $T_{\rm osc} \gg T_{\rm osc}^{(\rm conv)}$, because we have neglected the contribution from the primary oscillations. We will see numerically in the next subsection that, as the trapping effect becomes smaller, the abundance becomes dependent on f_ϕ and then converges to the conventional one. The dependence of the abundance on f_ϕ also mildly appears even in the region of high r, which will be explicitly shown in Fig. 4.7.

4.2.2 Numerical calculations

Here let us present results of our numerical calculations of the axion abundance in the presence of the extra PQ breaking. By following the axion dynamics numerically, we can estimate the axion abundance. The useful description for the equation of motion in Appendix C can be also used in this setup.

[1] We will see in Sec. 4.3 that the primary oscillations actually give the dominant contribution to the isocurvature perturbations.

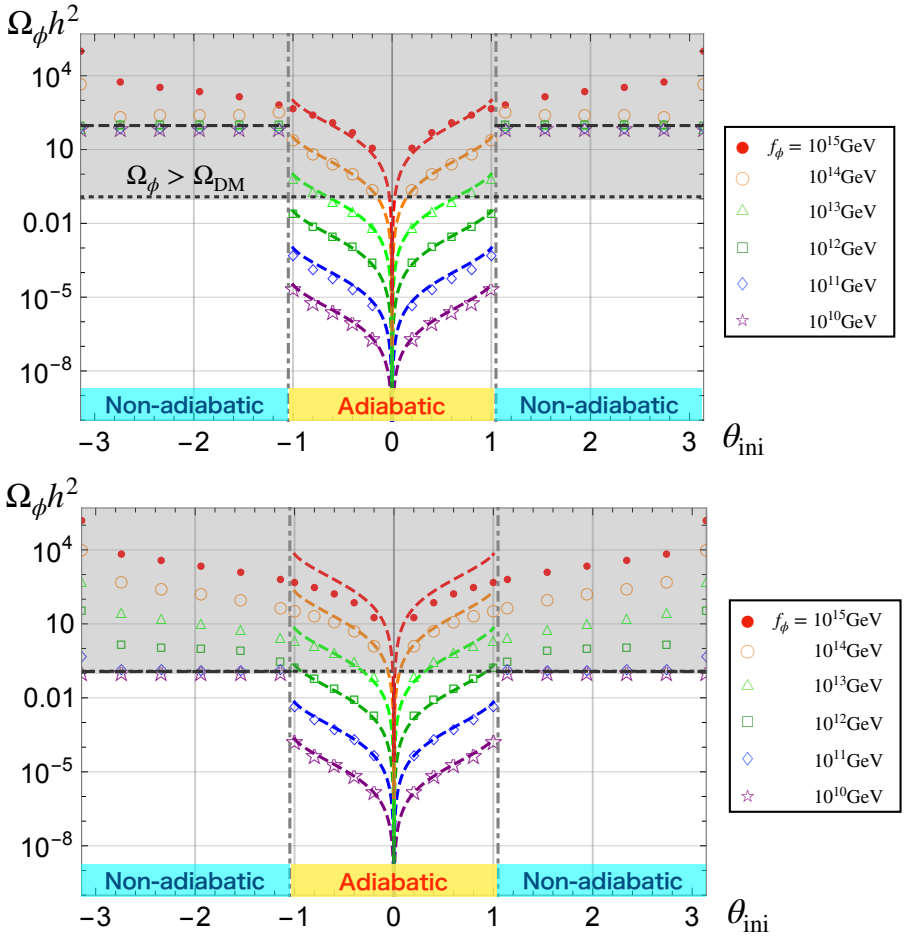

Figure 4.4: The numerical results of the axion abundance $\Omega_\phi h^2$ as a function of $\theta_{\rm ini}$ for $f_\phi = 10^{15}$ GeV (red $\bullet$), 10^{14} GeV (orange $\circ$), 10^{13} GeV (green $\triangle$), 10^{12} GeV (dark green $\square$), 10^{11} GeV (blue $\diamondsuit$), and 10^{10} GeV (purple $\star$). In the upper panel, we take $N = 3$, $r = 0.1$, and $\theta_H = 10^{-7}$, and in the lower panel, we take $N = 3$, $r = 0.015$, and $\theta_H = 10^{-7}$. The colored dashed lines represent the analytical solutions (4.5) and the black one denotes (4.10). The gray shaded region above the black dotted line indicates the overproduction of the DM axion $\Omega_\phi > \Omega_{\rm DM}$. The vertical gray dot-dashed lines denote the local maxima of the PQ breaking term $|\theta_{\rm ini} - \theta_H| = \pi/3$.

First we show in Fig. 4.4 how the axion abundance depends on the initial angle $\theta_{\rm ini}$ for various values of the decay constant f_ϕ. Here we take $N = 3$, $\theta_H = 10^{-7}$, and $r = 0.1$ (0.015) in the upper (lower) panel. Note that although we have adopted a nonzero θ_H, the result is not sensitive to θ_H unless it is of the order of unity, or for $f_\phi \gtrsim 10^{11}$ GeV as shown in Fig. 4.2. The red ($\bullet$), orange ($\circ$), green ($\triangle$), dark green ($\square$), blue ($\diamondsuit$), and purple ($\star$) points denote the case of $f_\phi = 10^{15}, 10^{14}, 10^{13}, 10^{12}, 10^{11}$, and 10^{10} GeV, respectively, and each colored dashed line and the black dashed line are the analytic solutions (4.5) and (4.10). The gray shaded region above the black dotted line represents the overproduction of the DM axion, $\Omega_\phi > \Omega_{\rm DM}$. The vertical gray dot-dashed lines denote the position of the local maxima of the PQ breaking term, $\theta_{\rm ini} = \pm\pi/3$, which separates the two regimes.

In the adiabatic regime, the axion abundance increases in proportion to $(\theta_{\rm ini} - \theta_H)^2$ in good agreement with the analytical estimate (4.5). By comparing both panels, one can also see that the axion abundance is more suppressed for larger r. Note that the abundance near the top of the PQ breaking term denoted by the gray dot-dashed lines is enhanced by the anharmonic effect.

In the non-adiabatic regime, the axion abundance becomes independent of the initial position, and can be analytically explained well by Eq. (4.10). For $r \lesssim 0.02$, it becomes possible to explain DM in the non-adiabatic regime (see the lower panel). Note also that the results for $f_\phi \gtrsim 10^{15}$ GeV in the upper panel or for $f_\phi \gtrsim 10^{13}$ GeV in the lower panel deviate from the analytical expectations in both regimes. This is because the PQ breaking term becomes relatively ineffective or $T_{\rm osc} < T_{\rm osc}^{\rm (conv)}$, which should reproduce the results for the conventional QCD axion.

Next we discuss how the axion abundance depends on r. In Figs. 4.5 and 4.6, we show the contour plots of the axion abundance on the (θ_H, r) plane in the adiabatic regime and the non-adiabatic regime, respectively. In both regimes we take $N = 3$. In Fig. 4.5 for the adiabatic regime, we set $\theta_{\rm ini} = 1$ $(< \pi/3)$, and $f_\phi = 10^{12}$ GeV (left) and 10^{13} GeV (right). The gray shaded region denotes the nEDM bound. One can see that the abundance decreases with r in the region where $T_{\rm osc}^{\rm (conv)} \lesssim T_{\rm osc}$ or Eq. (4.4) is satisfied. On the other hand, there is a plateau in the complementary region of (4.4), because the axion starts to oscillate around $\theta = 0$ due to $V_{\rm QCD}$, leading to the same results for the conventional case.

In Fig. 4.6 for the non-adiabatic regime, we set $\theta_{\rm ini} = 3/2$ $(> \pi/3)$, and $f_\phi = 10^{11}$ GeV (left) and 10^{10} GeV (right). The horizontal part of the gray region represents the condition, $Nr^4 \gtrsim 1$, where the axion remains trapped a wrong vacuum, giving a too large contribution to the strong CP phase. The axion abundance increases with r because the axion is trapped for a longer time, and the potential height at $T_{\rm osc2}$ becomes higher. Such r-dependence should be contrasted to the adiabatic regime. As with the adiabatic regime, there is a plateau in the region of small r which gives the conventional results.

Finally it is worth mentioning the dependence of Ω_ϕ on f_ϕ in the non-adiabatic regime since the strength of the extra PQ breaking effect differs for different decay constants. In other words, the trapping starts later for larger f_ϕ, and the effect of the PQ breaking should become relevant at larger values of r for larger f_ϕ. In Fig. 4.7 we show the numerical results of $\Omega_\phi h^2$ as a function of $N^{1/4} r$, where we set $N = 3$, $\theta_H = 10^{-7}$, and $\theta_{\rm ini} = 3/2$ $(> \pi/3)$. The red $(\bullet)$, green $(\circ)$, and blue $(\square)$ denote the abundance for $f_\phi = 10^{12}$ GeV, 10^{11} GeV, and 10^{10} GeV, from top to bottom. The purple star on each line represents a point that satisfies $T_{\rm osc} = T_{\rm osc}^{\rm (conv)}$, and to the right of it, $T_{\rm osc} > T_{\rm osc}^{\rm (conv)}$. The black dashed line denotes the analytic estimate (4.10). The horizontal black dotted line represents the observed DM abundance, $\Omega_{\rm DM} h^2 \simeq 0.12$. The gray shaded region represents the nEDM bound. On the right of each star, it is consistent with the analytic solution (4.10), because the axion oscillation begins before the barrier at $\theta \sim \pi/N + \theta_H$ disappears. On the other hand, on the left of it, the dynamics of axion and its abundance are similar to the usual scenario. Note that there is a small deviation among the results for different f_ϕ even in the deep non-adiabatic regime. In particular, the abundance is slightly larger for larger f_ϕ. This is because, when the false vacuum disappears, it takes a bit longer for the axion to start oscillating for larger f_ϕ due to smaller hierarchy between the curvature of the potential and the Hubble parameter. The delay of the onset of the secondary oscillations results in a slight enhancement of the axion abundance.

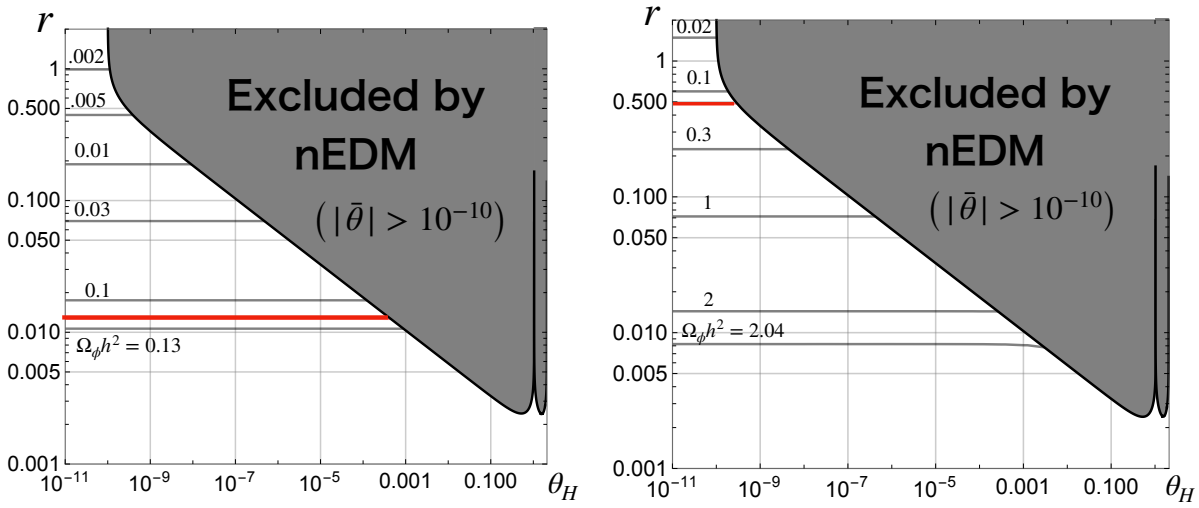

Figure 4.5: Contours of the axion abundance $\Omega_\phi h^2$ in the adiabatic regime as a function of (θ_H, r) for $N = 3$, and $\theta_{\rm ini} = 1$. We set $f_\phi = 10^{12}$ GeV (left) and $f_\phi = 10^{13}$ GeV (right). The red horizontal line represents $\Omega_\phi h^2 = \Omega_{\rm DM} h^2 = 0.12$. The axion abundance is almost constant when r is sufficiently small, but gradually decreases with respect to r, because of the early oscillations and the adiabatic suppression.

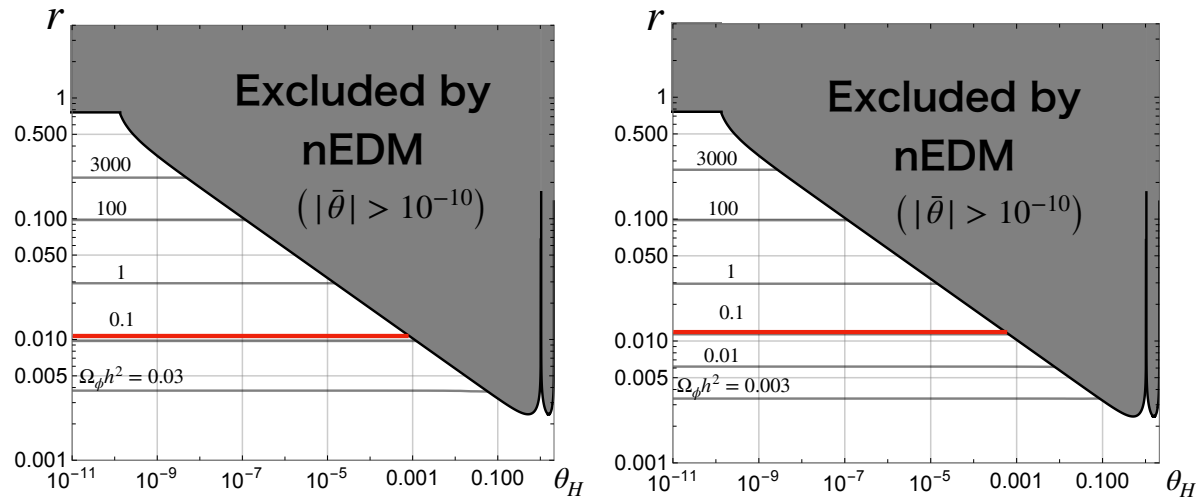

Figure 4.6: Contours of the axion abundance $\Omega_\phi h^2$ in the non-adiabatic regime as a function of (θ_H, r) for $N = 3$, and $\theta_{\rm ini} = 3/2$. We set $f_\phi = 10^{11}$ GeV (left) and $f_\phi = 10^{10}$ GeV (right). The red horizontal line represents $\Omega_\phi h^2 = \Omega_{\rm DM} h^2 = 0.12$. The horizontal part of the gray region at small θ_H denotes the condition that the axion remains trapped in the CP violating minimum, i.e., $Nr^4 \gtrsim 1$. The abundance increases with respect to r, and becomes independent of f_ϕ, because of the trapping effect.

Let us briefly summarize the parameter region where it is possible to explain DM by axion with the explicit PQ breaking. First, in the adiabatic regime, we can explain DM completely even for $f_\phi \gtrsim 10^{12}$ GeV due to the adiabatic suppression mechanism if r is relatively large. However, such a large value of r is severely constrained by nEDM, and

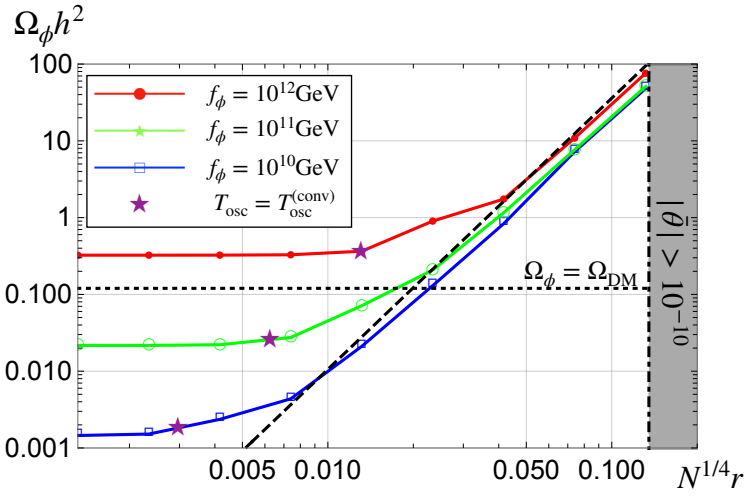

Figure 4.7: The axion abundance in the non-adiabatic regime as a function of $N^{1/4}r$ for $f_\phi = 10^{12}$ GeV (red •), 10^{11} GeV (green ∘) and 10^{10} GeV (blue □). The purple stars denote the points satisfying $T_{\rm osc} = T_{\rm osc}^{\rm (conv)}$. We take $N = 3$, $\theta_H = 10^{-7}$, and $\theta_{\rm ini} = 3/2$. The black dashed line denotes the analytical estimate (4.10), which is consistent with the numerical ones at $T_{\rm osc} \gtrsim T_{\rm osc}^{\rm (conv)}$, i.e., (4.4). The black dotted line denotes the observed DM abundance. The gray shaded region represents the nEDM bound. The right DM abundance can be explained at $N^{1/4}r \sim 0.02$ for any $f_\phi \lesssim 10^{11}$ GeV.

we need some tuning of θ_H, e.g. $\theta_H \lesssim 10^{-6}$ for $r \simeq 0.1$. In addition, even if the tuning of θ_H is allowed, we also need a tuning of $\theta_{\rm ini}$ for $f_\phi \gtrsim 10^{14}$ GeV. We show the allowed parameter region satisfying $\Omega_\phi = \Omega_{\rm DM}$ as a function of (f_ϕ, θ_H) in Fig. 4.8, where we take $N = 3$ and $\theta_H = 0$. The red bullets, green circles, and purple stars denote the numerical results for $N^{1/2}r = 0.01$, 0.1, and 0.5, respectively. The red solid line represents the case of the conventional QCD axion (2.21). The blue dashed line is the bound obtained by using (4.4) and (4.5), above which the PQ breaking term is important. The gray shaded region indicates the non-adiabatic regime. From this figure, one can explicitly see that DM can be explained for $f_\phi \gtrsim 10^{12}$ GeV without tuning of $\theta_{\rm ini}$. At larger f_ϕ, some tuning of $\theta_{\rm ini}$ is required, but it is still milder compared with the conventional case. Secondly, one can explain DM for arbitrary small f_ϕ in the non-adiabatic regime, which is very interesting. As one can see in Fig. 4.7, if $N^{1/4}r \simeq 0.015$, the DM abundance can be totally explained for any $f_\phi \lesssim 10^{11}$ GeV, almost independent of f_ϕ. This size of the PQ breaking requires a tuning of $\theta_H \lesssim 10^{-3}$, described in Fig. 4.2. Here, the quality problem of the PQ symmetry appears as some tuning of $\theta_{\rm ini}$, and this will be discussed in Sec. 4.4.

4.3 Isocurvature perturbation

In the presence of the extra PQ breaking potential, the QCD axion has a nonzero but tiny mass compared to the Hubble scale during inflation, and it generates almost scale-independent perturbations. In Sec. 2.4.2, we estimated the power spectrum in the standard setup analytically, but we need numerical calculations for more complicated setup. Here we compute the isocurvature power spectrum analytically and numerically in the

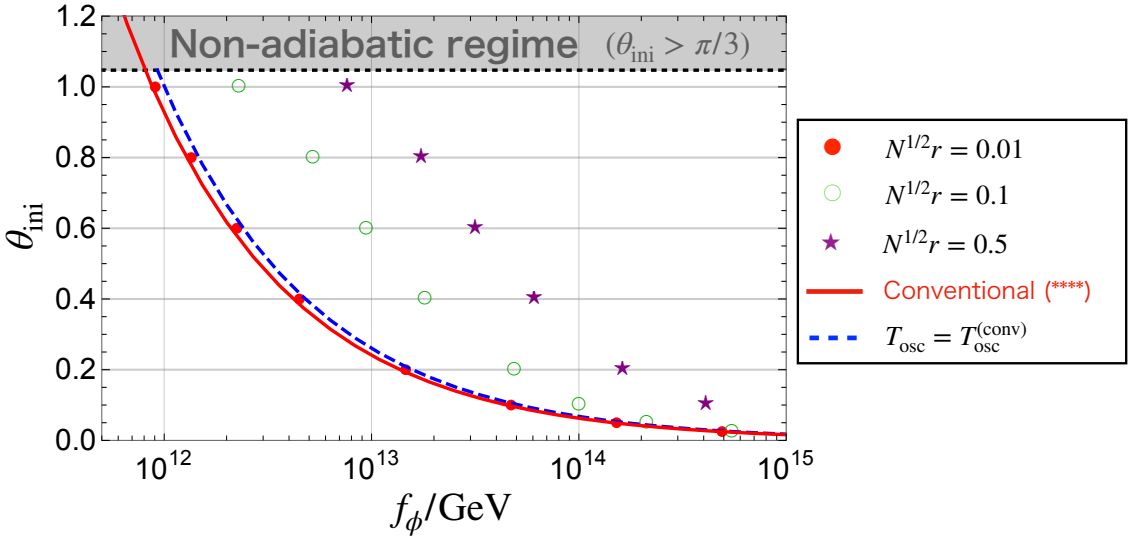

Figure 4.8: The allowed parameter region for explaining the DM density ($\Omega_\phi = \Omega_{\rm DM}$) as a function of $(f_\phi, \theta_{\rm ini})$ in the adiabatic regime where we take $N = 3$ and $\theta_H = 0$. The red bullets, green circles, and purple stars denote the numerical results for $N^{1/2}r = 0.01$, 0.1, and 0.5, respectively. The red solid and blue dashed lines represent the conventional QCD axion case (2.21) and the lower bound for our interest which is analytically estimated by using (4.4) and (4.5). The gray shaded region indicates the non-adiabatic regime.

presence of the extra PQ breaking potential, and the upper bounds on the inflation scale $H_{\rm inf}$ are presented.

4.3.1 Analytical evaluation

First let us estimate the power spectrum of the isocurvature perturbation analytically. In the adiabatic regime, we can use the formula (2.35) straightforwardly to estimate the power spectrum,

$$\Delta_S^2 \equiv (R_\phi \Delta_\phi)^2 \simeq \left(R_\phi \frac{H_{\rm inf}}{\pi f_\phi (\theta_{\rm ini} - \theta_H)} \right)^2 . \tag{4.11}$$

Although the parameter dependence is similar to the conventional case, we can expect the looser isocurvature bounds than those of the conventional case, since the suppression of the axion abundance due to the adiabatic suppression allows the tuning of $\theta_{\rm ini}$ to be relaxed, which will be explicitly shown in the next subsection together with numerical results.

In contrast to the adiabatic regime, we need more careful estimate in the non-adiabatic regime. This is because the axion abundance is almost determined by the amplitude $\theta_{\rm osc2}$ of the secondary oscillations and thus apparently does not depend on the initial position $\theta_{\rm ini}$. However, we note that the axion fluctuation $\delta\phi_*$ is diluted in proportion to $a^{-3/2}(t)$ because of the cosmic expansion, as long as the axion oscillates around the quadratic potential. We obtain the fluctuation at $T_{\rm osc2}$ as $\delta\phi_{\rm osc2} \simeq (T_{\rm osc2}/T_{\rm osc})^{3/2}\delta\phi_{\rm ini}$. Thus, in the

non-adiabatic regime, the isocurvature power spectrum is given by

$$\Delta_S^2 \simeq \left(R_\phi \frac{\partial \ln \Omega_\phi}{\partial \theta_{\rm osc2}} \left(\frac{T_{\rm osc2}}{T_{\rm osc}} \right)^{\frac{3}{2}} \frac{H_{\rm inf}}{2\pi f_\phi} \right)^2 . \tag{4.12}$$

Using (4.3) and (4.9), the suppression factor is given by

$$\begin{aligned} \left(\frac{T_{\rm osc2}}{T_{\rm osc}} \right)^{\frac{3}{2}} &= \left(\frac{(1.67)^2 \pi^2 g_*(T_{\rm osc}) \Lambda_{\rm QCD}^4}{90 N M_{\rm Pl}^2 m_{\phi,0}^2} \right)^{\frac{3}{8}} \cdot (N^{\frac{1}{4}} r)^{-\frac{2}{b}-1} \\ &\simeq 1.5 \times 10^{-2} N^{-\frac{3}{8}} \left(\frac{N r^4}{3 \times 10^{-4}} \right)^{-0.57} \left(\frac{f_\phi}{10^{12}\ {\rm GeV}} \right)^{\frac{3}{4}} . \end{aligned} \tag{4.13}$$

The suppression becomes stronger for larger r and smaller f_ϕ. Note that the above estimate does not take account of the anharmonic effect of the oscillations around the false vacuum, nor the axion dynamics when the false vacuum disappears and the trapping ends. In fact it is not possible to completely separate the trapped epoch from the subsequent oscillations, and the above analytical estimate should be considered as a rough order evaluation. Further refinements require taking account of the effects of the velocity of the axion field and the evolution of the axion fluctuation in a time-dependent potential that deviates significantly from the quadratic one toward the end of the trapping. As we shall see shortly, however, the above analytical estimate gives an overall good fit to the numerical results, and the dependence on $\theta_{\rm ini}$ is relatively mild.

4.3.2 Numerical results

Here let us present our numerical results of the axionic isocurvature power spectrum. We explain how to estimate it numerically in Appendix D.2.

In the left panel of Fig. 4.9, we show the results of the isocurvature power spectrum as a function of $\theta_{\rm ini}$, with the abundance in the non-adiabatic regime put in the right panel to see the comparison to Δ_ϕ^2. We set $N = 3$, $r = 0.1$, $\theta_H = 10^{-7}$, $f_\phi = 10^{12}$ GeV, and $H_{\rm inf} = 5 \times 10^7$ GeV. The red and blue bullets denote the numerical values of Δ_ϕ^2 and $\Omega_\phi h^2$. The black dashed lines are the analytical results, (4.11) and (4.12). Let us comment that we can basically choose an arbitrary value of $H_{\rm inf}$. However, $\delta\theta_{\rm ini}/\theta_{\rm ini} \simeq H_{\rm inf}/2\pi f_\phi \theta_{\rm ini} \ll 1$ is required for the linear approximation with good accuracy in $\delta\mathcal{N}$ expansion (see Appendix D.2).

In the adiabatic regime, the numerical results are consistent with the analytical one, and the anharmonic effect starts to be effective and enhances the isocurvature perturbation at $|\theta_{\rm ini}| \gtrsim \pi/6$, or at the place higher than the inflection points of $V_{\not PQ}$.

In the non-adiabatic regime, the isocurvature perturbation is significantly suppressed because the axion fluctuation is damped due to the cosmic expansion until the end of the trapping. Note that the time derivative of the axion field at $T \sim T_{\rm osc2}$ makes the $\theta_{\rm ini}$-dependence complicated. Just before the potential barrier disappears at $T \sim T_{\rm osc2}$, the axion generically has a (non-negligible) small velocity which depends on the evolution during the oscillations in the false vacuum as well as the anharmonicity of the PQ breaking term. If the axion has a velocity in the opposite direction with the shift of the potential minimum, then its abundance is slightly enhanced because the onset of oscillations is

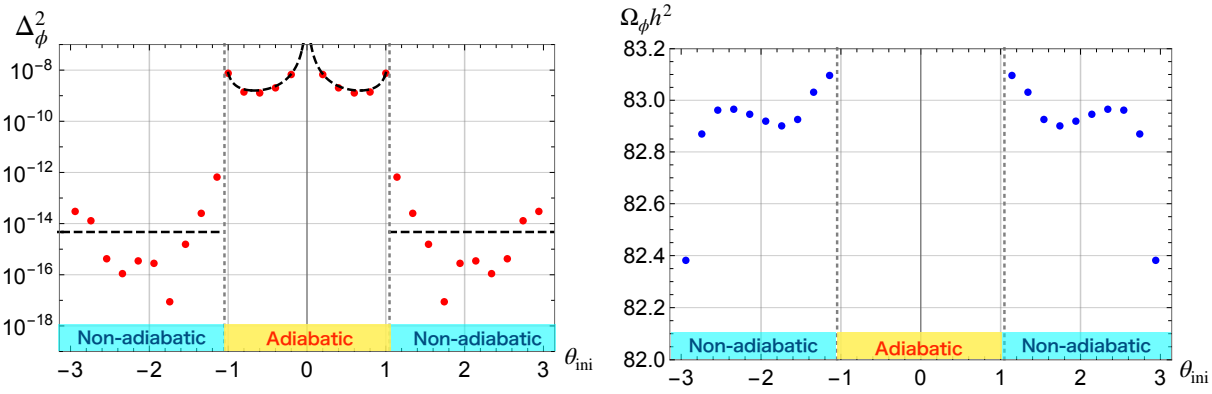

Figure 4.9: The isocurvature power spectrum (left) and the axion abundance (right) as a function of the initial position. We set $N = 3$, $r = 0.1$, $\theta_H = 10^{-7}$, $f_\phi = 10^{12}$ GeV, and $H_{\rm inf} = 5\times10^7$ GeV. The red (blue) bullets denote the numerical results of the isocurvature power spectrum (abundance), and the black dashed line is the analytical formula (4.11) and (4.12). The gray dotted lines represent the maxima of the PQ breaking term.

delayed. In the opposite case, the abundance is suppressed for similar reason. As a result, complicated wiggles appear in the behavior of the axion abundance as well as the isocurvature power spectrum. Our analytical formula (4.12) cannot explain such a complicated dependence. When it comes to the dependence of the axion abundance on $\theta_{\rm ini}$, we find that it has a local minimum and maximum at $|\theta_{\rm ini}| \approx 1.7$ and 2.4. At these points, $\partial\Omega_\phi/\partial\theta_{\rm ini}$ vanishes, which means that the corresponding isocurvature fluctuations disappear in the linear approximation.

Next, let us show the dependence of Δ^2_ϕ on r for the non-adiabatic regime in Fig. 4.10, although the power spectrum in the adiabatic regime is not sensitive to r. We take $N = 3$, $\theta_H = 0$, $\theta_{\rm ini} = 3/2$, $f_\phi = 10^{12}$ GeV, and $H_{\rm inf} = 5 \times 10^7$ GeV. The adopted parameters are same as in Fig. 4.9, from which one can see that the analytical and numerical results agree with each other at $\theta_{\rm ini} = 3/2$. This value of $\theta_{\rm ini}$ was chosen in order to check numerically the r-dependence of the analytical solution of the isocurvature fluctuation. The red bullets denote the numerical results, and the blue dotted line denotes the analytic solution (4.12) combined with the conventional one. At $r \gtrsim 0.01$ where (4.4) is satisfied, one can see that the isocurvature perturbation is more suppressed for higher r. This is because the axion is trapped at a wrong vacuum for a longer time for higher r, i.e. $T_{\rm osc} \gg T_{\rm osc2}$, and the axionic fluctuations are suppressed due to the cosmic expansion. Thus, the dependence of the isocurvature perturbation on r is well explained by the analytical estimate. However, we note that the overall agreement is partly due to our special choice of $\theta_{\rm ini}$, as described above.

Lastly let us present the isocurvature bound on the axion DM in our scenario. Using the observational bound (2.30), we obtain Fig. 4.11, which shows the upper bound on the Hubble parameter $H_{\rm inf}$ during inflation as a function of f_ϕ for the adiabatic regime. We set $N = 3$, $\theta_H = 0$, and $\Omega_\phi = \Omega_{\rm DM}$ that fixes $\theta_{\rm ini}$. The red bullet ($\bullet$), green circle ($\circ$), and blue diamond ($\diamondsuit$) denote the numerical results for $N^{1/2}r = 0.01, 0.1$, and 0.5, respectively. In each case, numerical results correspond to the result for $\theta_{\rm ini} = 1, 0.8, 0.6, 0.4, 0.2, 0.1, 0.05, 0.025$ in the order from the left point. The green dashed and blue solid line represent the analytical results for $N^{1/2}r = 0.1$ and 0.5, respectively. The

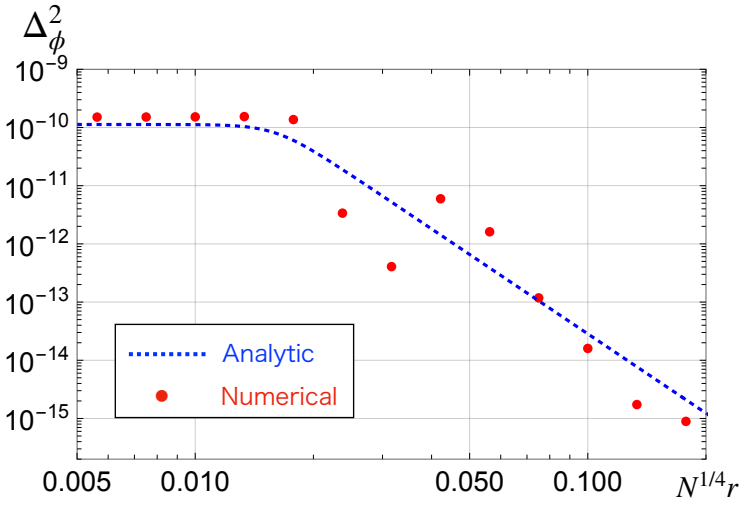

Figure 4.10: The isocurvature power spectrum as a function of r for $f_\phi = 10^{12}$ GeV, $N = 3$, $\theta_H = 0$, $\theta_{\rm ini} = 3/2$, and $H_{\rm inf} = 5 \times 10^7$ GeV. The red bullets denote the numerical results. The blue dotted line denotes the analytic formula (4.11) with the quadratic approximation.

purple dotted line denotes the analytical result for the conventional QCD axion. Here we have taken into account the anharmonic effect. One can see that the isocurvature bound on $H_{\rm inf}$ is relaxed compared to the conventional case, and we have $H_{\rm inf} \lesssim 10^8 - 10^9$ GeV for $f_\phi \gtrsim 10^{13}$ GeV. This is because the axion abundance is suppressed due to the adiabatic suppression mechanism and the early oscillations, and $\theta_{\rm ini}$ increases in order for the axion to explain DM abundance. For $f_\phi \lesssim 10^{12}$ GeV, the isocurvature bound becomes tighter than the usual case because of the anharmonic effect of the extra PQ breaking potential, because we need to put the initial position of the axion near top of the PQ breaking term to explain DM. For $f_\phi \gtrsim 10^{14}$ GeV and $N^{1/2}r = 0.1$, the numerical results start to deviate from the analytical results and approach asymptotically to the conventional case. This is because the trapping effect becomes less effective for higher f_ϕ.

We show in Fig. 4.12 the isocurvature bound on $H_{\rm inf}$ for the non-adiabatic regime. We take $N = 3$, $\theta_H = 0$, and $\Omega_\phi = \Omega_{\rm DM}$ which sets $N^{1/4}r$ (~ 0.02). The red bullet ($\bullet$), green diamond ($\diamondsuit$), and blue circle ($\circ$) denote the numerical results for $\theta_{\rm ini} = 5/4, 3/2$, and $7/4$, respectively. The blue solid line represents the analytical result (4.12). The purple star ($\star$) and the purple dotted line denote the numerical and analytical results for the conventional case, respectively. Interestingly, the isocurvature bound is much more relaxed than the conventional result especially for small $f_\phi \lesssim \mathcal{O}(10^{10})$ GeV. This is because of the suppression of the axionic fluctuation by the cosmic expansion. As expected, the analytical results agree reasonably well with the numerical ones, but do not completely fit to the dependence on f_ϕ and $\theta_{\rm ini}$.

4.4 Discussions

We have so far focused on the case of $N = 3$ in our numerical calculations. In the case of $N = 2$, when the axion is trapped around a wrong vacuum $\theta = \pi$ in the non-adiabatic

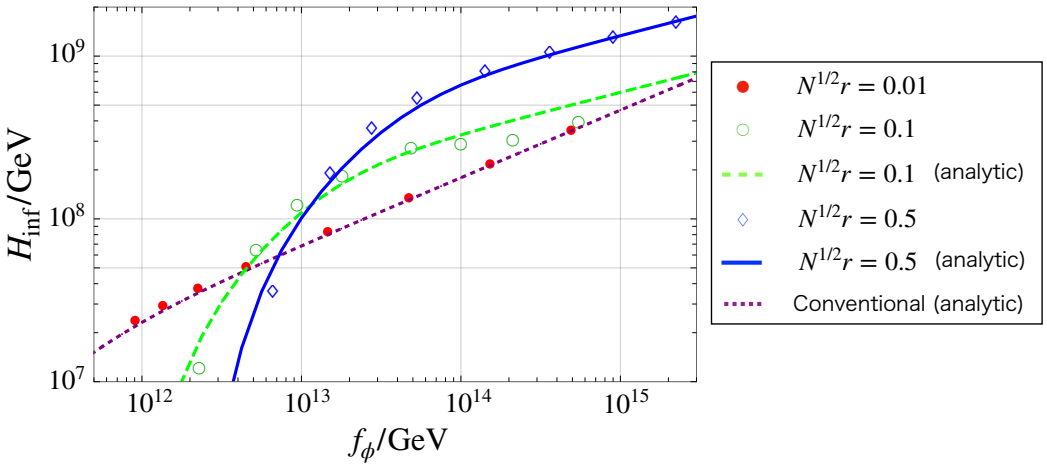

Figure 4.11: The upper bound on the Hubble parameter $H_{\rm inf}$ during inflation as a function of f_ϕ for the adiabatic regime. We take $N = 3$, $\theta_H = 0$, and $\Omega_\phi = \Omega_{\rm DM}$. The red bullet, green circle, and blue diamond denote the numerical results for $N^{1/2}r = 0.01, 0.1$, and 0.5. The green dashed and blue solid line denote the analytical results for $N^{1/2}r = 0.1$ and 0.5, respectively. The purple dotted line represents the analytical result for the conventional QCD axion.

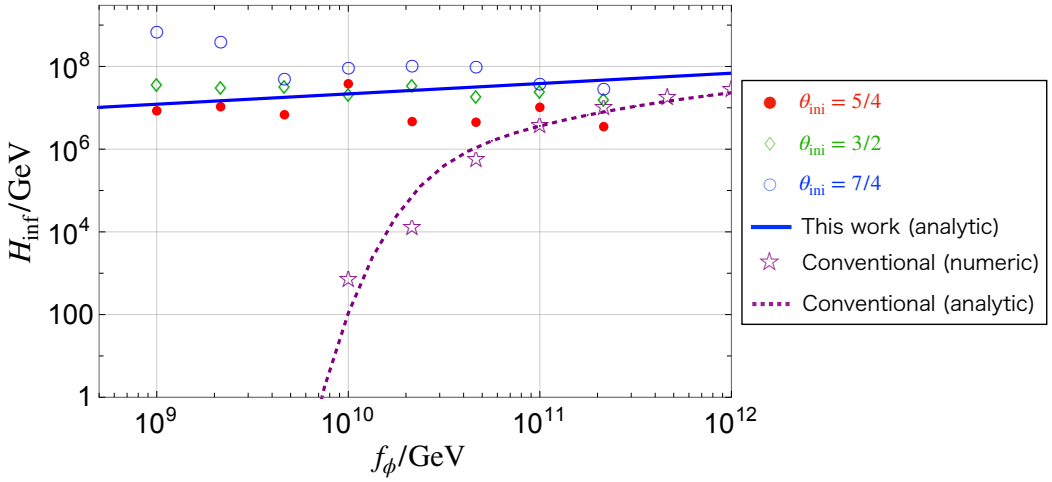

Figure 4.12: The upper bound on the Hubble parameter $H_{\rm inf}$ during inflation as a function of f_ϕ for the non-adiabatic regime. We take $N = 3$, $\theta_H = 0$, and $\Omega_\phi = \Omega_{\rm DM}$. The red bullet ($\bullet$), green diamond ($\diamond$), and blue circle ($\circ$) denote the numerical results for $\theta_{\rm ini} = 5/4, 3/2$, and $7/4$, respectively. The blue solid line represents the analytical result (4.12). The purple star ($\star$) and the purple dotted line denote the numerical and analytical results for the conventional case, respectively. The gray shaded region is the lower bound on f_ϕ from astrophysical facts.

regime, the final abundance can be strongly enhanced due to the anharmonic effect in addition to the trapping effect, because the minimum turns into a potential maximum at $T \lesssim T_{\rm osc2}$. In the case of even integer N, the situation is similar, and one of the vacua is located near $\theta = \pi$, if $|\theta_H| \ll 1$. On the other hand, the usual enhancement of the

isocurvature perturbations due to the anharmonic effect is expected to be milder because of the earlier oscillations.

Let us briefly comment on the quality problem of the PQ symmetry. Our work has opened up a new parameter region allowed for the axion DM. In particular, the axion abundance can be significantly enhanced in the non-adiabatic regime due to the extra PQ breaking, and its abundance is independent of f_ϕ. As a result, if we assume the anthropic bound on the axion DM is close to the observed DM abundance, the size of the PQ breaking should satisfy $r \lesssim 0.02$. Thus, the quality problem is equivalent to fine-tuning the relative phase as $|\theta_{\rm H}| \lesssim 10^{-3}$ (see Fig. 4.6). One of the important implications we have obtained is that the quality problem of the PQ symmetry becomes closely related to the anthropic argument on the axion DM abundance when there is extra breaking of the PQ symmetry.

The parameter region for DM axion is extended by the extra PQ breaking effect, and a vast parameter region can be searched for by various experiments (see Fig. 2.6). In the non-adiabatic regime, the DM abundance can be explained independently of f_ϕ if $r \sim 0.02$. In particular, it is very attractive that the axion with $f_\phi \lesssim 10^{11}$ GeV is allowed. Such a relatively heavy axion coupled to photon can be searched for by DM axion search experiments, such as ADMX [103], MADMAX [104], ORGAN [124], and TOORAD [125, 126]. Moreover, a new way to detect DM axion with $f_\phi \sim 10^{10} - 10^{11}$ GeV using a correlation with "condensed matter axion" has been proposed recently [127]. We have also shown that, in the adiabatic regime, the axion abundance is suppressed, and so one can relax the fine-tuning of $\theta_{\rm ini}$ to have the right DM abundance by axions for $f_\phi \gtrsim 10^{13}$ GeV. Such relatively light axions can be searched for by ABRACADABRA [105] or DMRadio [128], and KLASH [129]. In addition, if θ_H is near the upper limit of the nEDM experiments, it could be probed through nEDM in the near future. For instance, $|d_n| < 10^{-27} e$ cm for nEDM collaboration [130], n2EDM collaboration [131], and PanEDM[132].

Chapter 5

QCD axion with the Witten effect

In contrast to Chapter 4, we consider a time-dependent extra PQ breaking potential from the Witten effect in a broader region of $\theta_{\rm ini}$. The basic consequences of the axion abundance are roughly consistent with the results presented in Chapter 3, but the deviations from the analytic solution have to be estimated numerically. Also, the important and distinct feature lies in when the adiabatic condition $\epsilon(t_{\rm def}) \ll 1$ is satisfied or violated. In the case of time-independent extra potential, we saw in Chapter 4 that the adiabaticity is broken due to the tapping effect around a wrong minimum. In the time-dependent case, the key to this question is the anharmonicity of the potential induced from the QCD nonperturbative effect. The discussion here is mainly based on [58].

First let us introduce the setup including the Witten effect and clarify the motivation of this research in Sec. 5.1. We will review the case that the QCD potential can be approximated by the quadratic potential (corresponding to the adiabatic regime) in Sec. 5.2. After that, we will begin with discussing the adiabatic parameter $\epsilon(t_{\rm def})$ to understand how the violation of adiabaticity can be caused by the anharmonicity of the QCD potential, and then estimate the abundance for the non-adiabatic regime (Sec. 5.3). Next let us present the numerical results of the abundance of the axion (Sec. 5.4).

5.1 Setup and motivation

Let us consider an $\mathrm{SU}(2)_{\rm H}$ group in hidden sector in addition to the visible sector. As explained in Sec. 3.2, the spontaneous breakdown into $\mathrm{U}(1)_{\rm H}$ leaves a magnetic monopole, and if the axion couples to the $\mathrm{U}(1)_{\rm H}$ gauge boson, it acquires an effective potential from the plasma in the hidden sector. The total potential is given by

$$\begin{aligned} V(\phi) &= V_{\rm QCD}(\phi, T) + V_M(\phi, T) \\ &= m_\phi^2(T) f_\phi^2 \left(1 - \cos\frac{\phi}{f_\phi}\right) + \frac{1}{2} m_{\phi,M}^2(T)(\phi - \phi_*)^2. \end{aligned} \tag{5.1}$$

The mass term originating from the Witten effect has the minimum at $\phi = \phi_*$, which is generically deviated from the low-energy minimum at $\phi = 0$ where the strong CP phase vanishes. We focus on a pre-inflationary scenario where the PQ symmetry is spontaneously broken during inflation, and assume that hidden monopoles are generated sometime after inflation when the phase transition takes place in the hidden sector. We also assume that, the second term dominates over the first one in the early universe, that is, $T_{\rm osc} \gtrsim T_{\rm osc}^{\rm (conv)}$,

and the temporal minimum of the potential is located at $\phi \simeq \phi_*$ where the axion starts to oscillate. Eventually the axion is expected to oscillate around $\phi = 0$.

On the assumption that $V_{\rm QCD}$ is approximated to be quadratic, the abundance of the axion was studied [54, 55] which will be reviewed in the next section, and it showed that if the trapping effect of $V_{\not{\rm PQ}}$ is strong enough, the axion abundance is adiabatically suppressed. Such an assumption is valid for a generic potential only if $|\phi_*/f_\phi| \ll 1$. However, it is worth investigating the adiabatic suppression mechanism for a more general position of ϕ_*, since ϕ_* is an arbitrary parameter ($-\pi < \phi_*/f_\phi \leq \pi$). In particular, in the vicinity of the top of $V_{\rm QCD}$ ($\phi_* \simeq \pi$), the axion cannot follow the temporal minimum at the timing of the deformation of the potential because of the anharmonicity of $V_{\rm QCD}$. Thus we can expect the anharmonicity breaks down the adiabaticity. In the subsequent sections, we will evaluate the violation of the adiabaticity $\epsilon(t_{\rm def})$ to see the above expectation explicitly, and we will analyze the abundance and isocurvature power spectrum on the basis of the results in Chapter 3 or numerically.

5.2 Dynamics of axion

Let us begin with describing the dynamics of the axion that acquires a time-dependent potential from the Witten effect, and evaluate important physical quantities such as the temperature at the onset of oscillations and the axion abundance for qualitative understanding. Note that the discussion here is limited only to the case that $V_{\rm QCD}$ is approximately quadratic, in other words, the system adiabatically evolves [54, 55, 120].

First, we define ω that is useful to parametrize the strength of the Witten effect:

$$\omega \equiv \alpha_H^2 \left(\frac{N_H}{N_{\rm DW}}\right)^2 \Omega_M h^2, \tag{5.2}$$

$$\simeq 5.9 \times 10^{-4} \left(\frac{\alpha_H}{0.07}\right)^2 \left(\frac{N_H}{N_{\rm DW}}\right)^2 \left(\frac{\Omega_M h^2}{0.12}\right), \tag{5.3}$$

where $\Omega_M \equiv \rho_M/\rho_{\rm crit}$ represents the monopole density parameter. Using this definition, the mass can be rephrased as

$$\begin{aligned} m_{\phi,M}^2(T) &= \frac{\alpha_H^2}{16\pi^2}\frac{\rho_M(T)}{f_H^2}. \\ &= \frac{\omega \rho_{\rm crit} h^{-2}}{16\pi^2 f_\phi^2}\frac{s(T)}{s_0}. \end{aligned} \tag{5.4}$$

In addition, the sum of the axion and the monopole abundance should not be larger than the dark matter abundance, i.e.,

$$\Omega_\phi h^2 + \Omega_M h^2 \lesssim \Omega_{\rm DM} h^2 \simeq 0.12\,, \tag{5.5}$$

since the monopole is stable and behave like matter. Thus ω is smaller than 5.9×10^{-4} unless $N_H > N_{\rm DW}$.

The axion starts to oscillate around the temporal minimum of the potential, $\phi = \phi_*$, when the Hubble parameter becomes comparable to the mass due to the Witten effect,

$H(T_{\rm osc}) \simeq m_{\phi,M}(T_{\rm osc})$. Here $T_{\rm osc}$ is the temperature at the onset of oscillations, and it is given by [54, 55]

$$T_{\rm osc} \simeq 64\ {\rm GeV} \left(\frac{\omega}{0.12}\right) \left(\frac{f_\phi}{10^{12}\ {\rm GeV}}\right)^{-2} . \tag{5.6}$$

Remembering that when the potentials are quadratic, the system is adiabatic (see the analysis of a toy model in Chapter 3), and using the formula (3.24), the axion abundance is determined by the first oscillation as

$$\Omega_\phi h^2 \simeq 3 \times 10^{-4} \left(\theta_{\rm ini} - \theta_*\right)^2 \left(\frac{\omega}{0.12}\right)^{-1} \left(\frac{f_\phi}{10^{12}\ {\rm GeV}}\right)^{3} . \tag{5.7}$$

where $\theta_* \equiv \phi_*/f_\phi$. Here we assume $0 \leq \theta_* < \pi$ without loss of generality, and $\theta_{\rm ini}$ and θ_* satisfy $|\theta_{\rm ini} - \theta_*| \leq \pi(N_{\rm DW}/N_H)$. The abundance is adiabatically more suppressed by the stronger trapping effect from the Witten effect.

Let us estimate the temperature $T_{\rm def}$ when the temporal minimum starts to move toward $\phi = 0$. As the temperature goes down, the potential from the Witten effect becomes comparable to that from non-perturbative QCD effects. Solving $m^2_{\phi,M}(T_{\rm def}) \simeq m^2_\phi(T_{\rm def})$, we obtain the temperature at this time,

$$T_{\rm def} \simeq 0.8\ {\rm GeV} \left(\frac{g_{*s}(T)}{80}\right)^{-1/(3+2b)} \left(\frac{\omega}{0.12}\right)^{-1/(3+2b)} , \tag{5.8}$$

where we assume $T_{\rm osc} > T_{\rm def}$, i.e.,

$$\left(\frac{\omega}{0.12}\right)^{q} \left(\frac{f_\phi}{10^{12}\ {\rm GeV}}\right)^{-2} \left(\frac{g_*(T)}{80}\right)^{1/(3+2b)} \gtrsim 0.01 \tag{5.9}$$

with $q \equiv (2b+4)/(2b+3)$. This gives the lower bound on the parameter ω for a given f_ϕ. This condition is equivalent to $T_{\rm osc} \gtrsim T_{\rm osc}^{\rm (conv)}$.

If the potentials can be approximated by quadratic ones, then the production of extra axion oscillations are exponentially suppressed in this process. However, when the potential $V_{\rm QCD}$ has a more generic form, it is nontrivial whether the adiabatic suppression really works because of the anharmonic effect. In the following, we will study under what condition the adiabatic suppression does not work.

5.3 Violation of adiabaticity

To see the condition that the adiabaticity is broken, we calculate the parameter $\epsilon(t_{\rm def})$ defined by Eq. (3.22). Let us focus on the potential around the temporal minimum $\phi_{\rm min}^{\rm temp}$, which can be written as

$$V(\phi) = \frac{1}{2}\left(m^2_{\phi,M}(T) - m^2_\phi(T)\right)\left(\phi - \phi_{\rm min}^{\rm temp}\right)^2 + \frac{1}{24}\frac{m^2_\phi(T)}{f^2_\phi}\phi^4 + \dots , \tag{5.10}$$

where the dots represent higher-order terms in terms of ϕ/f_ϕ and we define the temporal minimum as

$$\phi_{\rm min}^{\rm temp} \equiv \frac{m^2_{\phi,M}(T)}{m^2_{\phi,M}(T) - m^2_\phi(T)}\phi_* . \tag{5.11}$$

Note here that we expand the potential around $\phi = \phi_{\rm min}^{\rm temp}$ after transforming as $\phi \to \phi + \pi f_\phi$ for simplicity, so the final result is given by re-transformation $\phi \to \phi - \pi f_\phi$. The effective mass squared at a field value ϕ is given by

$$m_{\rm eff}^2(\phi) = m_{\phi,M}^2(T) - m_\phi^2(T) + \frac{1}{2}\frac{m_\phi^2(T)}{f_\phi^2}\phi^2 \,. \tag{5.12}$$

As T approaches $T_{\rm def}$, the first and second term becomes canceled and the third term becomes relevant. If we take $\phi = \phi_{\rm min}^{\rm temp}$, the threshold of the temperature $T_{\rm th}$ ($\approx T_{\rm def}$) below which the third term becomes relevant is given by

$$m_{\phi,M}^2(T_{\rm th}) - m_\phi^2(T_{\rm th}) = \left(\frac{1}{2}\frac{m_\phi^2(T_{\rm th})}{f_\phi^2} m_{\phi,M}^4(T_{\rm th})\phi_*^2\right)^{1/3} . \tag{5.13}$$

Now we shall calculate the parameter for the violation of adiabaticity ϵ, assuming that it is sufficiently small. From this assumption, we expect that ϕ follows its temporal minimum, $\phi_{\rm min}^{\rm temp}$, until $T = T_{\rm th}$. Then it is calculated as

$$\epsilon(T) \simeq \left|\frac{1}{|m_{\rm eff}|^3}\frac{1}{2t}\left(-3m_{\phi,M}^2(T) - 2bm_\phi^2(T)\right)\right| , \tag{5.14}$$

for $T \gtrsim T_{\rm th}$. At $T = T_{\rm def} (\approx T_{\rm th})$, it is given by

$$\begin{aligned} \epsilon(T_{\rm def}) &\simeq \frac{(3+2b)\, f_\phi}{\sqrt{2}t_{\rm th} m_\phi(T_{\rm th})\phi_*} \\ &\propto T_{\rm def}^{1/2}\omega^{-1/2}\left|\theta_* - \pi\right|^{-1} \\ &\propto \omega^{-q/2}\left|\theta_* - \pi\right|^{-1} , \end{aligned} \tag{5.15}$$

where we use Eq. (5.13) and $\phi_*/f_\phi \to |\theta_* - \pi|$ which means the distance from the top of $V_{\rm QCD}$ ($\phi = \pi f_\phi$). The last line comes from Eq. (5.8). When $\epsilon \ll 1$, the resulting abundance is exponentially suppressed by a factor of $e^{-\mathcal{O}(1)/\epsilon}$. Thus, even if the trapping effect is so strong, the adiabatic condition is not necessarily satisfied due to the anharmonic effect.

If $\epsilon(t_{\rm def}) \sim 1$, i.e. in the non-adiabatic regime, the delayed start of the axion field gives rise to additional amplitudes whose oscillation dominates over the primary oscillation. To estimate the abundance, we can use the formula of the non-adiabatic regime (3.30), but considering the situation, we can more easily estimate it. The timing of the deformation almost corresponds to the conventional onset of oscillation, $T_{\rm def} \approx T_{\rm osc}^{\rm (conv)}$, because the QCD potential increases more intensely than the Hubble parameter and the potential induced from the Witten effect. Now we consider the vicinity of the top of $V_{\rm QCD}$, so the practical oscillation timing is later than $T_{\rm osc}^{\rm (conv)}$. Thus we can use the conventional formula of the abundance with the anharmonic effect (2.21). Noting that the oscillation amplitude is roughly given by $\theta_{\rm osc2} \simeq \theta_*$, we obtain the abundance,

$$\Omega_\phi h^2 \simeq 0.14 F_{\rm NAD}(\theta_*)\theta_*^2 \left(\frac{f_\phi}{10^{12}\ {\rm GeV}}\right)^{1.17} , \tag{5.16}$$

where the anharmonic factor is given by

$$F^{\rm (NAD)} = \left[\ln\left(\frac{e}{1-\theta_*^2/\pi^2}\right)\right]^{1.17} . \tag{5.17}$$

In the non-adiabatic regime of this model, the abundance depends on the decay constant, instead of the case of time-independent potential with multiple minima described in Chapter 4. Not depending on f_ϕ comes from the trapping effect at a wrong minimum. Note that this analytic solution is roughly estimated, and actually the abundance should slightly depend on ω. Numerical calculations are required for the correct behavior.

5.4 Numerical estimate of abundance

Here we solve the equation of motion for the axion taking account of the Witten effect, to see if the adiabatic suppression works and to find a parameter space in which we can explain the observed dark matter density.

Substituting (3.5) to (C.4), we obtain the following equation of motion,

$$F^2(\tau)\frac{d^2\theta}{d\tau^2} + F(\tau)\left\{\frac{dF(\tau)}{d\tau} + \sqrt{g_*(\tau)}\tau^{-2}\right\}\frac{d\theta}{d\tau} + \frac{10M_{\rm Pl}^2}{\pi^2 T_n^4}m_\phi^2(\tau)\sin\theta + \kappa\omega g_{*s}(\tau)\tau^{-3}(\theta-\theta_*) = 0, \tag{5.18}$$

and

$$\kappa \equiv \frac{M_{\rm Pl}^2\rho_{\rm crit}h^{-2}}{36\pi^2 T_n f_\phi^2 s_0} \tag{5.19}$$

The time variable $\tau \equiv T_n/T$ is defined, where in this work, the normalization factor is chosen as

$$T_n = \sqrt{m_{\phi,0}M_{\rm Pl}}. \tag{5.20}$$

In order to see if the adiabatic suppression mechanism works, we plot the ratio between the density parameter with a given nonzero $\Omega_M h^2$ and the one without it (i.e., with $\Omega_M h^2 = 0$) in Fig. 5.1. We take $\theta_{\rm ini} = \theta_*$ and $\partial_\tau\theta_{\rm ini} = 0$ for the initial condition. In this case, the contribution from the first oscillation, Eq. (5.7), is negligible because the initial field value is close to the temporal minimum of the potential.

Fig. 5.1 shows our results as a function of ω for $f_\phi = 10^{12}$ and 10^{11} GeV, where the lines with $\bullet, \circ, \triangle, \square, \times, \star$ correspond to $|\theta_* - \pi| = 0.01, 0.05, 0.1, 0.5, 1, \pi/2$, respectively. As one can see from the left figure, the abundance is not strongly suppressed for $f_\phi = 10^{12}$ GeV. This is because the potential from the Witten effect is weaker for a larger f_ϕ and the trapping effect is smaller. In both figures, the abundance is more suppressed for a larger ω. This is because the axion is trapped by the Witten effect more strongly for a larger ω and the adiabatic suppression mechanism works more efficiently.

Next, we evaluate the density parameter for the axion $\Omega_\phi h^2$ to determine a realistic parameter space where both the axion and the monopole can explain dark matter. The results for $N_H = N_{\rm DW}$ and $\alpha_H = 0.07$ are shown in Fig. 5.2 for $f_\phi = 10^{10}$ GeV (left panel) and $f_\phi = 10^{11}$ GeV (right panel), where the lines with $\bullet, \circ, \triangle, \square, \star$ correspond to the cases with $|\theta_* - \pi| = 0.5, 1, \pi/2, \pi - 1, \pi - 0.1$, respectively. Each solid line represents the solution for $\theta_{\rm ini} = \theta_* + (N_{\rm DW}/N_H)$ $(= \theta_* + 1)$, and each dashed line represents the one for $\theta_{\rm ini} = \theta_*$. In the former case, an oscillation is induced at $T = T_{\rm osc}$ and Eq. (5.7) may not be negligible. In the latter case, the contribution from the first oscillation, Eq. (5.7), is

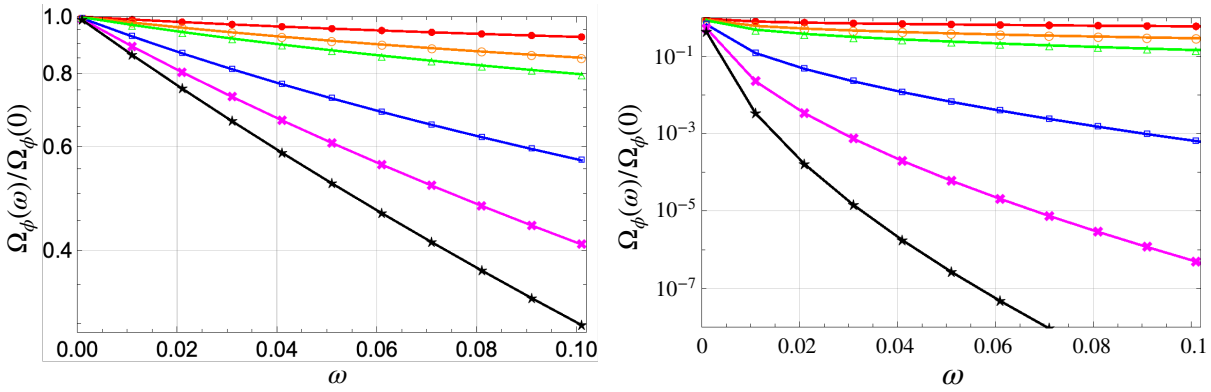

Figure 5.1: The axion abundance normalized by the case without the Witten effect as a function of ω for various initial conditions, $|\theta_* - \pi| = 0.01$ (red $\bullet$), 0.05 (orange $\circ$), 0.1 (green $\triangle$), 0.5 (blue $\square$), 1 (magenta $\times$), and $\pi/2$ (black $\star$) from top to bottom. We take $f_\phi = 10^{12}$ (left panel) and 10^{11} GeV (right panel).

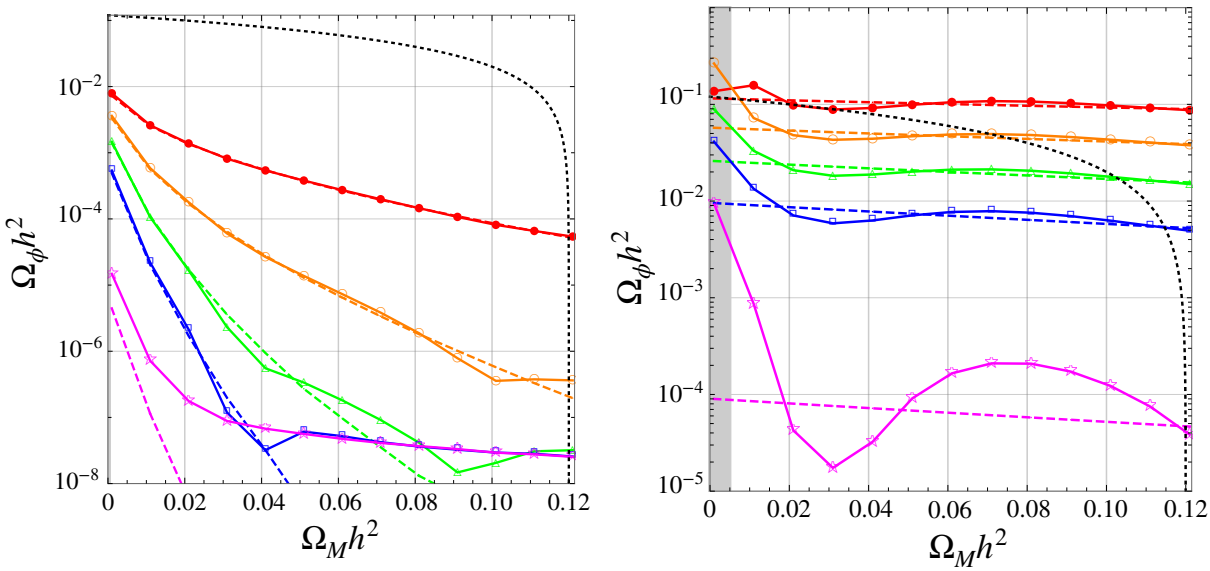

Figure 5.2: The axion abundance $\Omega_\phi h^2$ as a function of $\Omega_M h^2$ for $|\theta_* - \pi| = 0.5$ (red $\bullet$), 1 (orange $\circ$), $\pi/2$ (green $\triangle$), $\pi - 1$ (blue $\square$), and $\pi - 0.1$ (magenta $\star$) from top to bottom. We set $\alpha_H = 0.07$ and $f_\phi = 10^{10}$ GeV (left panel) and for $f_\phi = 10^{11}$ GeV (right panel). Each solid line represents the numerical result for the initial condition with $\theta_{\rm ini} = \theta_* + (N_{\rm DW}/N_H)\,(= \theta_* + 1)$, and each dashed line represents the one with $\theta_{\rm ini} = \theta_*$. The black dotted line denotes $\Omega_\phi h^2 + \Omega_M h^2 = 0.12$. We are not interested in the gray shaded region where $T_{\rm osc} \lesssim T_{\rm def}$.

negligible because the initial field value is close to the temporal minimum of the potential. The black dotted line represents the upper bound Eq. (5.5).

The left panel of Fig. 5.2 for $f_\phi = 10^{10}$ GeV shows that the axion abundance is more suppressed for a larger fraction of monopole, and the axion is only a subdominant component of dark matter. In particular, for $\Omega_\phi h^2 \sim 10^{-(8\text{-}6)}$, (i.e., for small θ_* and large $\Omega_M h^2$), the solid lines are deviated from the dashed lines. This is because the contribution

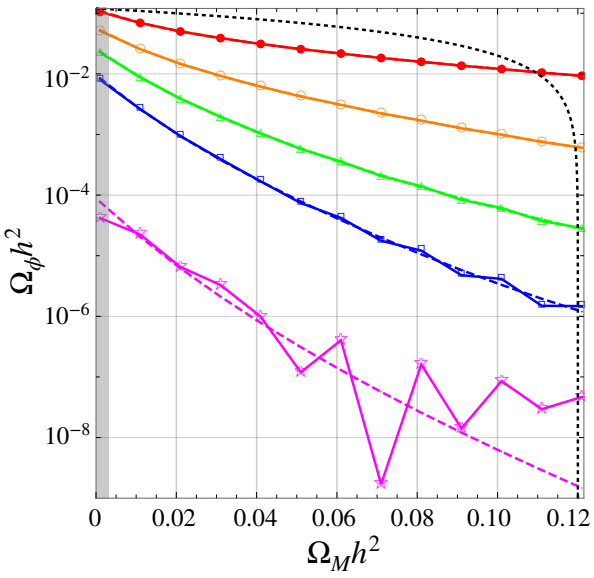

Figure 5.3: Same as the right panel of Fig. 5.2 (i.e., $f_\phi = 10^{11}$ GeV, $\alpha_H = 0.07$, and $|\theta_* - \pi| = 0.5, 1, \pi/2, \pi - 1, \pi - 0.1$) but with $N_H/N_{\rm DW} = 5$.

from the first oscillation becomes important for the case of $\theta_{\rm ini} = \theta_* + 1$ in that parameter space. Substituting $\theta_{\rm ini} = \theta_* + 1$ into Eq. (5.7), we obtain $\Omega_\phi h^2 \simeq 6 \times 10^{-8} (\Omega_M h^2/0.12)^{-1}$ for $f_\phi = 10^{10}$ GeV. This is also independent of $|\theta_* - \pi|$. These can be actually observed in the left panel of Fig. 5.2, where the magenta and blue lines are overlapped and satisfy $\Omega_\phi h^2 \sim 6 \times 10^{-8} (\Omega_M h^2/0.12)^{-1}$ for $\Omega_M h^2 \gtrsim 0.05$. One can also see that the green line becomes overlapped for $\Omega_M h^2 \gtrsim 0.1$. This means that the first oscillation around the potential by the Witten effect is dominant in this parameter space, while the second oscillation around the QCD potential is dominant in the other parameter space. In the region of $|\theta_* - \pi| \lesssim 1$ (the red and orange line), the adiabatic suppression only has a weak effect so that the solid line corresponds to the dashed one. This is the non-adiabatic regime, and it means that the anharmonicity breaks the adiabatic condition. In the case of weak trapping effect ($\Omega_M h^2 \lesssim 0.01$), the abundance is consistent with the analytical result (5.16).

In the right panel, the solid lines are deviated from the dashed lines at a small $\Omega_M h^2$. This is because the adiabatic suppression mechanism is not efficient as f_ϕ is larger than in the left panel. For a small $\Omega_M h^2$, the condition Eq. (5.9) is barely satisfied and the dynamics of the axion depends non-trivially on the initial condition. In the gray-shaded region, the condition Eq. (5.9) is violated and we cannot distinguish between the timing of oscillation by the Witten effect and the QCD effect.

Comparing the two panels in Fig. 5.2, we can see that the axion abundance becomes larger as f_ϕ increases because the Witten effect is more suppressed. In the right panel, the axion abundance can be comparable to or even larger than the monopole abundance. On the other hand, the axion of $f_\phi \gtrsim 10^{11}$ GeV can be adiabatically suppressed if we take $N_H > N_{\rm DW}$. This can be seen from Fig. 5.3, which shows the axion abundance in the case of $N_H/N_{\rm DW} = 5$ and $f_\phi = 10^{11}$ GeV. The initial condition is taken to be $\theta_{\rm ini} = \theta_*$ for each solid line and $\theta_{\rm ini} = \theta_* + (N_{\rm DW}/N_H)$ for each dashed line.

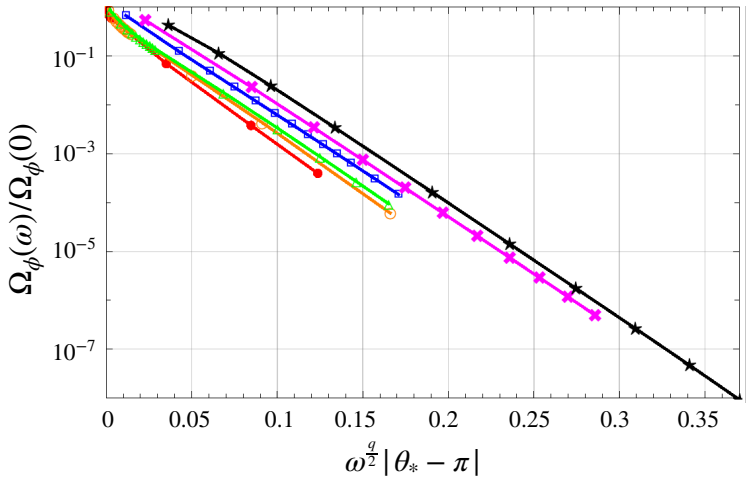

Figure 5.4: Same as the right panel of Fig. 5.1 (i.e., $f_\phi = 10^{11}$ GeV and $|\theta_* - \pi| = 0.01, 0.05, 0.1, 0.5, 1, \pi/2$) but the horizontal axis is given by the inverse of the parameter for the violation of adiabaticity, $\omega^{q/2}|\theta_* - \pi|$.

The reason why the solid lines are deviated from the dashed lines in Fig. 5.3 is the same as the one in the left panel in Fig. 5.2. Namely, the contribution Eq. (5.7) becomes important for a very small $\Omega_\phi h^2$. However, one can see an oscillating behavior in Fig. 5.3. The deviation appears when the temporal minimum starts to shift around the time when the axion oscillates due to the Witten effect, namely for the case of $T_{\rm osc} \sim T_{\rm def}$. In this case, the oscillation amplitude at $T = T_{\rm def}$ has a non-negligible effect on the axion dynamics when the temporal minimum is moving. If the axion moves toward the same (opposite) direction as the temporal minimum, the abundance gets suppressed (enhanced). The result hence depends on the axion field value at $T = T_{\rm def}$, which non-trivially depends on $\Omega_M h^2$.

To summarize the above argument, the adiabatic suppression mechanism works for $f_\phi \lesssim 10^{11}$ GeV and large $\omega, |\theta_* - \pi|$. For a qualitative understanding of the suppression factor in this case, we plot the ratio of the density parameter with and without the Witten effect as a function of $\omega^{q/2}|\theta_* - \pi|$ in Fig. 5.4. We can fit the result by an exponential function such as

$$\log\left[\frac{\Omega_\phi(\omega)}{\Omega_\phi(0)}\right] \propto -\omega^{q/2}|\theta_* - \pi|\,, \tag{5.21}$$

which is consistent with the analytical estimate of the adiabatic parameter $\epsilon^{-1}(t_{\rm def})$ (see Eq. (5.15)). Note that, while the lines in the figure are not completely overlapped, all of them exhibit the same exponential dependence like Eq. (5.21). Their differences are only $\mathcal{O}(1)$ factors and hence the exponential dependence of Eq. (5.21) is robust.

5.5 Discussions

We have considered the QCD axion DM scenario with an extra potential from the Witten effect in the presence of hidden monopoles. We have clarified the condition for the adiabatic suppression mechanism to work in the vicinity of the top of the potential. The

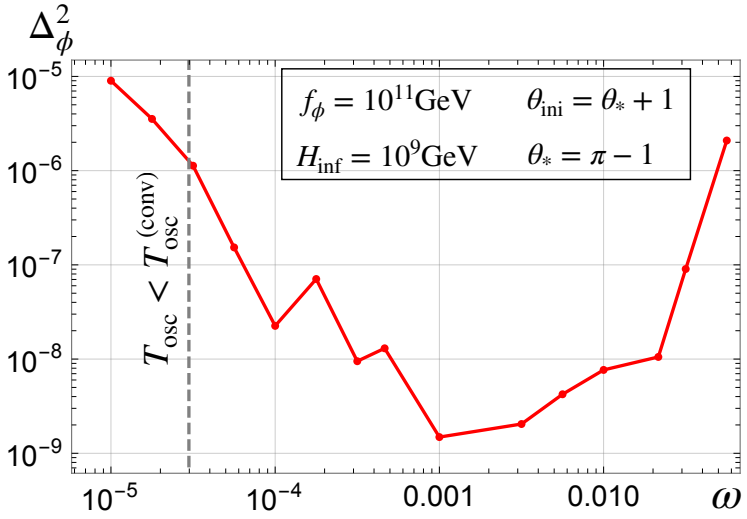

Figure 5.5: The isocurvature power spectrum as a function of ω. We set $\theta_{\rm ini} = \theta_* + 1$, $\theta_* = \pi - 1$, $f_\phi = 10^{11}$ GeV, and $H_{\rm inf} = 10^9$ GeV.

condition can be understood by the violation of the adiabaticity $\epsilon(t_{\rm def})$. We need much stronger trapping effect for the efficient adiabatic suppression near the potential top. It looks difficult to realize the adiabatic suppression for $f_\phi \gtrsim 10^{11}$ GeV. However, the Witten effect can be stronger if the monopole abundance is larger than the observed DM abundance. This scenario is consistent with observations if the monopole can disappear before the BBN. Another possibility is to consider the case of $N_H \gg N_{\rm DW}$, which can be realized in the clockwork QCD axion model [133, 121].

Let us comment on the isocurvature perturbations. In the adiabatic regime, the isocurvature perturbation can be produced as with the case of quadratic potential (see Eq. (2.33)). When the adiabatic suppression works well, the axion is a subdominant DM component, and the power spectrum is expected to be significantly suppressed. In the non-adiabatic regime, it is difficult to estimate the power spectrum analytically, as in the previous chapter, but we can guess from the results of the previous chapter that it is suppressed. We show the numerical results of the power spectrum as a function of ω in Fig. 5.5. We set $\theta_{\rm ini} = \theta_* + 1$, $\theta_* = \pi - 1$, $f_\phi = 10^{11}$ GeV, and $H_{\rm inf} = 10^9$ GeV. The red points represent the numerical results, and the gray dashed line is the lower bound on ω of our interest, $T_{\rm osc} < T_{\rm osc}^{\rm (conv)}$. As the trapping effect becomes strong, the power spectrum decreases. At the intermediate strength, the anharmonic effect breaks the adiabaticity, but $T_{\rm osc} < T_{\rm osc}^{\rm (conv)}$ is satisfied, i.e. this corresponds to the non-adiabatic regime. The isocurvature power spectrum is suppressed as we expected. For stronger trapping, the power spectrum becomes larger, because it enters the adiabatic regime and the isocuravture perturbation is almost the same with the case of quadratic potential. Thus we shortly conclude that the isocurvature perturbation is suppressed in both the adiabatic and the non-adiabatic regime. In particular, the axion can explain a (sizable) fraction of DM in the non-adiabatic regime with the isocurvature bounds highly relaxed. Such axions with small f_ϕ are motivated by experiments for axion detection.

Lastly, we discuss the implications for an axion-like particle (ALP) in the presence of the Witten effect of hidden monopoles. ALP is a pseudo-scalar field with a periodic

potential, which is predicted e.g. in string theory [20]. If an ALP has a shallow potential ($m_\phi \lesssim 10^{-28}$ eV) in addition to the potential from the Witten effect, it remains trapped by the Witten effect until sometime in the late-time universe. In Ref. [134], this idea was applied to a mechanism that the ALP inducing cosmic birefringence. Cosmic birefringence is a phenomenon which rotates the CMB photon polarization when the axion field starts to oscillate after the recombination [135, 136, 137, 138, 139]. Without the Witten effect, the ALP mass must be limited in the region of 10^{-33} eV $\lesssim m_\phi \lesssim 10^{-28}$ eV [140], which leads to one question why the mass is so small, or coincidence problem. However, by stabilizing the ALP due to the Witten effect until the recombination, we only require the upper bound on the mass $m_\phi \lesssim 10^{-28}$ eV for reasonable parameters, $\alpha_H \sim \alpha$ and $f_\phi \sim M_{\rm GUT}$, if dark matter can be totally explained by the hidden monopole [134].

Chapter 6

Conclusions

The existence of DM is the most crucial mystery in particle physics and cosmology. Of various candidates, QCD axion can nicely explain both DM and the Strong CP problem, and it looks a promising candidate for DM and new physics. In fact, various types of experiments for axion detection have been carried out and planned, and we can expect to obtain some signatures in the near future. DM axion can be non-thermally produced via the misalignment mechanism, where the axion dynamics in the early universe is an essential ingredient. Since the axion potential can be altered by interactions with other particles, it is important to reveal what properties the axion has (e.g. mass, decay constant) under various situations.

In this thesis, we have discussed the trapping effect on QCD axion by extra PQ breaking potentials. We have focused on a scenario where the axion is initially trapped by the potential and starts to oscillate around the minimum. Then, after the QCD phase transition, the total potential form is deformed with time, and finally the axion is stabilized around the origin where the Strong CP problem is solved. What is important is how the axion moves at the timing of the deformation. We found in Chapter 3 that the dynamics can be categorized in terms of the parameter $\epsilon(t_{\rm def})$ which describes the violation of adiabaticity. For $\epsilon(t_{\rm def}) \ll 1$ (adiabatic regime), the axion adiabatically follows the temporal minimum, which does not induce any additional amplitude. The type of this dynamics corresponds to the case that the adiabatic suppression mechanism works well. On the contrary, for $\epsilon(t_{\rm def}) \sim 1$ (non-adiabatic regime), the temporal minimum leaves the axion near the initial minimum, and after a little while, it starts to oscillate again. The delay of commencement of oscillation enhances the axion abundance. By categorizing as such, we obtained the analytical formula of the abundance for both regimes. We note that the analysis is applicable to a broad class of extra potential.

In Chapter 4, we considered a time-independent extra potential and estimated the abundance and isocurvature power spectrum analytically and numerically. We have opened up a new parameter region for DM axion. In the adiabatic regime, $|\theta_{\rm ini} - \theta_H| \lesssim \pi/N$, the axion with $f_\phi \gtrsim 10^{12}$ GeV can explain DM with a milder tuning of $\theta_{\rm ini}$ than the conventional case, thanks to the adiabatic suppression. In the non-adiabatic regime, $|\theta_{\rm ini} - \theta_H| \gtrsim \pi/N$, if $r \simeq 0.02$ and $f_\phi \lesssim 10^{11}$ GeV, the axion explains all DM, almost independent of f_ϕ. Both cases have important implications for the current or projected axion search experiments, e.g. ABRACADABRA for $f_\phi \sim 10^{14}$, ADMX for $f_\phi \sim 10^{11-13}$. Also, in both regimes, the isocurvature perturbation can be suppressed compared to the

conventional QCD axion without PQ breaking potentials. The upper bound on $H_{\rm inf}$ is given by $\sim 10^8 - 10^9$ GeV in the adiabatic regime and $\sim 10^7 - 10^8$ GeV in the non-adiabatic regime. We emphasize that in the non-adiabatic regime, since the isocurvature perturbation is suppressed without the enhancement due to the anharmonic effect, the isocurvature bound can be relaxed by many orders of magnitude with respect to the normal scenario. Together with the fact that the final axion abundance is independent of f_ϕ, we have opened up a scenario that allows the axion with $f_\phi \lesssim 10^{11}$ GeV to explain all DM without running afoul of the isocurvature bounds. The price we have to pay is to introduce an extra PQ breaking term with $N^{1/4} r \approx 0.02$ and $|\theta_H| \lesssim 10^{-3}$. This requires a mild tuning of the relative phase of the PQ breaking. Conversely, if θ_H is near the upper limit, it could be observed through nEDM in the near future.

In Chapter 5, we considered an effective potential from the Witten effect of hidden monopole. We obtained the condition that the adiabatic suppression mechanism works by estimating the violation of adiabaticity $\epsilon(t_{\rm def})$. The non-adiabatic regime can be realized by the anharmonic effect, in which case the isocurvature is significantly suppressed in similar to the case of the time-independent potential. We have numerically estimated the abundance and confirmed the consistency with the analytical estimate. In particular, we saw that the exponent of suppression factor is consistent with the inverse of $\epsilon(t_{\rm def})$.

When the axion acquires the potential considered in Chapter 4 and is temporarily trapped at a wrong minimum, the non-adiabatic regime is realized. In this case, the movement of axion is disturbed by the potential barrier and cannot follow the minimum. On the other hand, the non-adiabatic regime is caused by the anharmonic effect in the case of the Witten effect. From these results, we conclude that the adiabaticity can be broken by the non-linearity of the total axion potential. Thus, the properties of axion DM are closely related with corrections to the axion potential induced from a UV physics and can be probed by various future experiments for the axion detection and nEDM measurements.

Acknowledgments

I owe my deepest gratitude to Prof. Fuminobu Takahashi for his excellent guidance throughout my Ph.D. project. Without his enthusiastic guidance, I would never have finished my research. I would like to thank Prof. Kwang Sik Jeong, Dr. Kitajima, Dr. Masaki Yamada, and Dr. Wen Yin, so much for collaborations in my Ph.D. project, daily discussions, and a lot of supports for my everyday life. I also would like to thank all the members of Particle Theory and Cosmology Group in Tohoku University for their help during the Ph.D. project. Finally, I am deeply grateful to my family and friends for your supports. My Ph.D. research project is supported by the Graduate Program on Physics for the Universe of Tohoku University, JST SPRING, Grant Number JPMJSP2114, and JSPS Core-to-Core Program (grant number: JPJSCCA20200002)

Appendix A

Basics for standard cosmology

Here let us briefly summarize standard cosmology for the discussion in this thesis. We consider the homogeneous, isotropic, and flat universe except for the discussion on the axionic fluctuation. It is described by the Friedmann-Lemeître-Robertson-Walker metric, $ds^2 = dt^2 - a^2(t)d\boldsymbol{x}^2$ with $a(t)$ the scale factor. The space-time evolves with various components (baryonic matter, radiation, dark matter, dark energy, and so on) according to the Friedmann equation,

$$H^2(t) = \frac{1}{3M_{\rm Pl}^2}\sum_i \rho_i, \tag{A.1}$$

where $H \equiv \dot{a}/a$ is defined as the Hubble parameter, $M_{\rm Pl} \equiv 1/\sqrt{8\pi G} \simeq 2.4 \times 10^{18}$ GeV denotes the reduced Planck mass with G the Newton constant, and ρ_i represent the energy density for each component.

For later use, let us define the density parameter $\Omega_i \equiv \rho_i/\rho_{\rm crit}$, where the critical energy density is given by

$$\rho_{\rm crit} = 3M_{\rm Pl}^2 H_0^2 \simeq (0.00300\ {\rm eV})^4 h^2, \tag{A.2}$$

with $H_0 \equiv 100h$ km/s/Mpc the present Hubble constant. In the case of the flat universe, the critical density can be simply identified with the total energy density.

Assuming no interaction with each component, the energy density ρ_i of individual component obeys the energy conservation equation,

$$\dot{\rho}_i + 3H(\rho_i + P_i) = 0, \tag{A.3}$$

where P_i represents the pressure. The equation of state is given by $w_i \equiv P_i/\rho_i$. For instance, the energy density for radiation is given by

$$\rho_{\rm rad} = \frac{\pi^2}{30} g_*(T) T^4, \tag{A.4}$$

where g_* is the effective degree of freedom for relativistic particle. This defines the temperature of thermal equilibrium plasma, which determines the typical energy scale of the universe. For $w_{\rm rad} = 1/3$, we obtain $\rho_{\rm rad} \propto a^{-4}$, or $aT \sim$ const that means the radiation energy is redshifted with time.

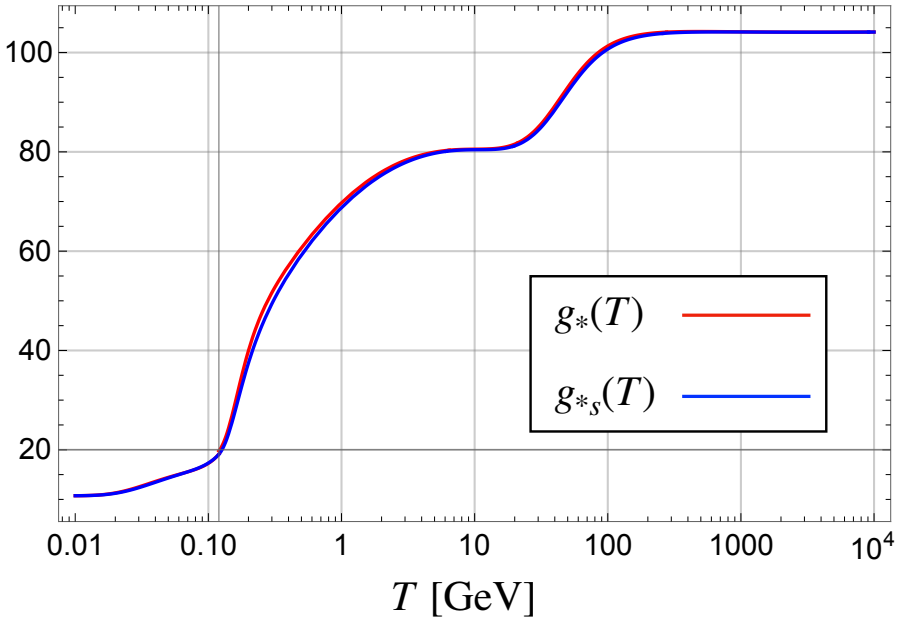

Figure A.1: The effective degree of freedom of relativistic components g_* (red) and g_{*s} (blue) as a function of the temperature [141].

Besides, another conservation equation is associated with entropy density $s(T)$, given by $sa^3 = \text{const}$. The entropy density is given by

$$s(T) = \frac{2\pi^2}{45} g_{*s}(T) T^3, \tag{A.5}$$

where g_{*s} denotes the effective degree of freedom of relativistic components associated with entropy. The effective degrees of freedom g_* and g_{*s} we use in this thesis are estimated by using the lattice result [141]. See Fig. A.1. The entropy conservation is useful for analyzing cosmological quantities.

Appendix B

Vacuum structure in QCD

B.1 Nontrivial gauge configuration

Here let us briefly review a vacuum structure in QCD. The QCD Lagrangian is given by

$$\mathcal{L}_{\text{gauge}} = -\frac{1}{4}G^a_{\mu\nu}G^{a\mu\nu} - \theta\frac{g_s^2}{32\pi^2}G^a_{\mu\nu}\tilde{G}^{a\mu\nu}, \tag{B.1}$$

where the gluon field strength and its dual are respectively written as $G^a_{\mu\nu} = \partial_\mu A^a_\nu - \partial_\nu A^a_\mu + g_s f^{abc}A^b_\mu A^c_\nu$ and $\tilde{G}^a_{\mu\nu} = \frac{1}{2}\epsilon_{\mu\nu\alpha\beta}G^{a\alpha\beta}$. g_s is the gauge coupling constant, and f^{abc} denotes the structure constant for SU(3). The θ term can be written by the Chern-Simons current as [65]

$$G^a_{\mu\nu}\tilde{G}^{a\mu\nu} = \partial_\mu K^\mu = \partial_\mu\epsilon^{\mu\alpha\beta\gamma}\left(A^a_\alpha G^a_{\beta\gamma} - \frac{g_s}{3}f_{abc}A^a_\alpha A^b_\beta A^c_\gamma\right), \tag{B.2}$$

which seems not to contribute to path integral as long as we consider a trivial configuration of gluon fields, $A^a_\mu = 0$, since it is a total derivative. In the Euclidean space, the action is estimated as

$$\int d^4x_E G\tilde{G} = \int d^4x_E \partial_\mu K_\mu = \int_{S_3} d\sigma_\mu K_\mu, \tag{B.3}$$

where S_3 is the 3-dimensional sphere at infinity and $d\sigma_\mu$ is an element of its hypersurface. If the configurations at infinity is trivial, the integral vanishes.

We are interested in configurations of gauge field such that the action is finite. The finite action requires the condition that $G^a_{\mu\nu} \to 0$ at $|\boldsymbol{x}| \to \infty$, and we can obtain nontrivial configurations by a gauge transformation with $G^a_{\mu\nu} = 0$ on S_3 maintained. Defining the gauge field as $A_\mu \equiv A^a_\mu t^a$ in terms of SU(3) generators t^a, it transforms as $A_\mu \to U^{-1}A_\mu U + ig_s^{-1}U^{-1}\partial_\mu U$ where $U(\boldsymbol{x})$ is a unitary matrix. The configurations on the boundary is called pure gauge, $A_\mu|_{S_3} = ig_s^{-1}U^{-1}\partial_\mu U$. To prove that the matrix U is not equivalent to the identity matrix, we consider the SU(2) subgroup of SU(3) for simplicity. The SU(2) configurations are constructed as S_3 at infinity as with SU(3). The transformation matrix can be expanded as $U = a_4 \cdot 1 + ia_i\sigma_i$ where σ_i is the Pauli matrices and the coefficients a_i and a_4 are real constants. The unitarity gives $a_4^2 + |\boldsymbol{a}|^2 = 1$. Thus the gauge configurations are the mapping $S_3 \to S_3$. From the argument of topology, the mapping $U(\boldsymbol{x})$ can be

classified in different homotopy classes by integers which are called winding number. As regards this mapping, the winding number is given by [142]

$$\begin{aligned} n &\equiv \frac{1}{24\pi^2}\int d^3x \mathrm{Tr}[\epsilon^{ijk}(U_{(n)}^{-1}\partial_i U_{(n)})(U_{(n)}^{-1}\partial_j U_{(n)})(U_{(n)}^{-1}\partial_k U_{(n)})] \\ &= \frac{ig_s^3}{24\pi^2}\int d^3x \mathrm{Tr}[\epsilon_{ijk}A^i_{(n)}A^j_{(n)}A^k_{(n)}], \end{aligned} \tag{B.4}$$

where we take pure gauge in the second equality, and the subscripts (n) denote the configurations composed of gauge fields with winding number n. Such configurations are known as instanton which is a solution to classical equation of motion in the Euclidean space. The simplest instanton solution was discovered by the authers in [13]. It is known that the above discussions are applicable to any Lie group which has an SU(2) as its subgroup by Bott's theorem [143].

B.2 θ vacua

In the Minkowski spacetime, let us consider the action again. We take temporal gauge $A_0 = 0$, and the action of the gauge configuration with a winding number ν is given by

$$\begin{aligned} \frac{g_s^2}{32\pi^2}\int d^4x G^a_{\mu\nu}\tilde{G}^{a\mu\nu} &= \frac{g_s^2}{32\pi^2}\int d^4x \partial_0 K^0 = \frac{g_s^2}{32\pi^2}\int d^3x K^0\Big|_{t=-\infty}^{t=\infty} \\ &= n_+ - n_- \equiv \nu \in \mathbb{Z}, \end{aligned} \tag{B.5}$$

where we use $K^0 = (4ig_s/3)\mathrm{Tr}[\epsilon^{ijk}A_iA_jA_k]$, and n_+ (n_-) represents the winding number at $t = \infty$ ($-\infty$). Thus this cofiguration corresponds to the solution of the transition from one vacuum $|n_-\rangle$ to another vacuum $|n_+\rangle$. However, each individual vacuum is not gauge-invariant. Consider a gauge transformation with winding number m. The gauge field transforms as $A^i_{(n)} = ig_s^{-1}U^{-1}_{(n)}\partial^i U_{(n)} \to ig_s^{-1}(U_{(n)}U_{(m)})^{-1}\partial^i(U_{(n)}U_{(m)})$, and we can see that the resultant gauge configuration has winding number $n+m$. In this way, the vaccum is changed by the gauge transformation as $U_{(m)}|n\rangle = |n+m\rangle$. As a physical vacuum, we can consider a linear combination of all vacuum states,

$$|\theta\rangle \equiv \sum_{n=-\infty}^{n=\infty} e^{in\theta}|n\rangle, \tag{B.6}$$

where $\theta \in [0, 2\pi)$ is a constant parameter. This is the θ vacuum. It is obvious that the θ vacuum is not changed.

Let us find an important property of the θ vacuum. We consider the transition amplitude from $|\theta\rangle$ to $|\theta'\rangle$,

$$\langle\theta'|e^{-HT}|\theta\rangle = \sum_{n'=-\infty}^{n=\infty}\sum_{n=-\infty}^{n=\infty} e^{-i(n'\theta'-n\theta)}\langle n'|e^{-HT}|n\rangle, \tag{B.7}$$

where we take Euclidean space. We define the variant of winding number as $\nu \equiv n' - n$,

and then, we can use path integral to obtain

$$\begin{aligned}\langle\theta'|e^{-HT}|\theta\rangle &= \sum_{n'=-\infty}^{n=\infty} e^{-in'(\theta'-\theta)} \sum_{\nu=-\infty}^{\nu=\infty} \int DA_{(\nu)} \exp\left[\int d^4x_E \frac{1}{4} G^a_{\mu\nu} G^{a\mu\nu} - i\nu\theta\right] \\ &= \delta(\theta'-\theta) \int DA \exp\left[-\int d^4x_E \left(\frac{1}{4} G^a_{\mu\nu} G^{a\mu\nu} + i\theta \frac{g_s^2}{32\pi^2} G^a_{\mu\nu} \tilde{G}^{a\mu\nu}\right)\right].\end{aligned} \tag{B.8}$$

$DA_{(\nu)}$ is the pathe integral measure of gauge field with winding number ν and DA is the measure of all the gauge configurations. Note that the delta function indicates the stability of the θ vacuum. As a result, the nontrivial vacumm structures in QCD require the θ term in the QCD Lagrangian.

Appendix C

Useful equations for numerical calculations of abundance

Here we derive a useful equation of motion for numerical calculations. First let us rewrite the equation of motion (2.16) using the dimensionless time $\tau \equiv T_n/T$, where T_n is an arbitrary normalization factor of mass-dimension one [58]. Taking account of the temperature-dependence of g_* and g_{*s}, we obtain the time derivative of the temperature

$$\begin{aligned} \frac{dT}{dt} &= -\frac{\pi}{M_{\rm Pl}}\sqrt{\frac{g_*(T)}{10}}\frac{s(T)}{s'(T)}T^2 \\ &= -HT\left(\frac{3\tau K(\tau)}{\sqrt{g_*(\tau)}}\right), \end{aligned} \tag{C.1}$$

where $K(\tau)$ is defined as

$$K(\tau) \equiv \frac{\sqrt{g_*(\tau)}}{3\tau}\frac{g_{*s}(\tau)}{g_{*s}(\tau) - \tau g'_{*s}(\tau)/3}. \tag{C.2}$$

We refer to Ref. [141] for the detailed temperature dependence of g_* and g_{*s} (see Fig. A.1). Assuming g_{*s} does not depend on the temperature, one can see that this relation is consistent with the usual one, $dT/dt = -HT$ or $H = 1/2t$. In other words, $K(\tau)$ represents the time-dependence of g_{*s}.

Using this relation, we can obtain the derivative of the time t

$$\frac{d}{dt} = \sqrt{\frac{\pi^2 T_n^4}{10M_{\rm Pl}^2}}K(\tau)\frac{d}{d\tau}. \tag{C.3}$$

Thus the equation of motion (2.16) becomes

$$K^2(\tau)\frac{d^2\theta}{d\tau^2} + K(\tau)\left[\frac{dK}{d\tau} + \sqrt{g_*}\tau^{-2}\right]\frac{d\theta}{d\tau} + \frac{10M_{\rm Pl}^2}{\pi^2 T_n^4 f_\phi}V'(\phi) = 0. \tag{C.4}$$

This equation is applicable to a homogeneous scalar field with any differentiable potential. Note that in the above derivation we use only the fact $sa^3(T) = \text{const.}$, so (C.4) generally holds.

Appendix D

Calculations of isocurvature perturbation

The structures in the universe can originate from primordial perturbations generated by scalar fields. The evolution of the perturbations follows the Einstein equation and the conservation laws of energy and momentum. Since the perturbations are generically smaller than the uniform components, perturbative expansion can be applied to these equations. The metric and energy-momentum tensor are respectively expanded as

$$g_{\mu\nu} = \bar{g}_{\mu\nu} + h_{\mu\nu} \tag{D.1}$$
$$T_{\mu\nu} = \bar{T}_{\mu\nu} + \delta T_{\mu\nu}, \tag{D.2}$$

where the quantity with a bar attatched denotes the unperturbed value, and $h_{\mu\nu}$ and $\delta T_{\mu\nu}$ are perturbed values. Hereafter, we define quantities X_i (e.g. n_i, ρ_i, P_i, etc) as $X_i = \bar{X}_i(t) + \delta X_i(t, \mathbf{x})$, where $\bar{X}_i$ and δX_i denote the homogeneous part and the perturbation of X_i, and the subscripts 'i' represents particle species, like radiation, cold dark matter (CDM), etc. Due to the general covariance, we have infinite possibilities to take space-time coordinates, and we should identify which quantities are physical by fixing the gauge in order to estimate observables.

In Sec. D.1, we consider a specific metric of space time, and on the basis of $\delta\mathcal{N}$-formalism, derive a gauge-invariant quantity which is conserved on the superhorizon scale. Next we present a method for calculating the isocurvature power spectrum using perturbation theory in Sec. D.2. Numerical methods are described, and finally the useful analytical formula is derived.

D.1 $\delta\mathcal{N}$-formalism

Let us briefly review the $\delta\mathcal{N}$-formalism [96]. Here $\mathcal{N}$ denotes the local e-folding number as defined below, and we can see that the curvature perturbation is given by the perturbation of the e-folding number.

We use the standard $(3+1)$-decomposition (ADM formalism) [144],[1]

$$ds^2 = -N_\ell^2 dt^2 + a^2(t) e^{2\psi} \tilde{\gamma}_{ij} (dx^i + \beta^i dt)(dx^j + \beta^j dt), \tag{D.3}$$

[1] Throughout the thesis, we use the metric of the mostly minuses, but only in this Appendix, we use the mostly pluses, because I would feel strange if I used the mostly minuses in the cosmological perturbation theory.

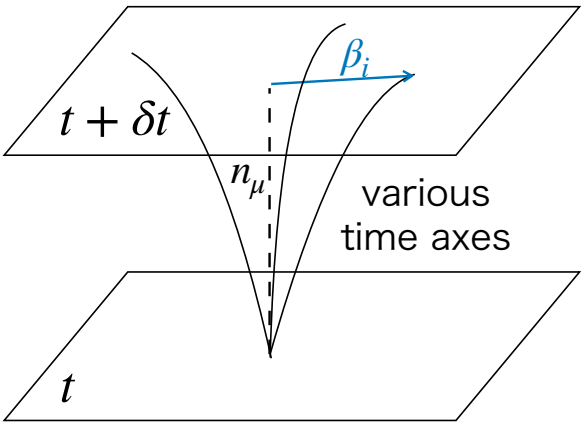

Figure D.1: The schematic picture for the ADM formalism. The two planes are taken at t and $t + \delta t$. The black solid curves represent time axes, and the black dashed line is the vector perpendicular to the constant-time plane. the shift vector β_i is denoted by the blue arrow.

where N_ℓ is the lapse function, $a(t)$ a global scale factor, $\tilde{\gamma}_{ij}$ the spatial metric, β^i the shift vector, and ψ is the perturbation of the expansion rate, or equivalently, the curvature perturbation. We show the schematic picture for the metric we are considering in Fig. D.1. The two planes represent 3-dimensional surfaces in which time is constant. In this figure, time is taken at t and $t+\delta t$ on the constant-time planes with $\delta t/t \ll 1$, and $n_\mu = (-N_\ell, 0)$ is the vector perpendicular to the constant-time plane. The lapse function scales the length of n_μ, depending on how to take the constant-time plane. We can see that the shift vector β_i can represent a deviation of time axis from n_μ, because the worldline can be chosen as we like.

In the ADM formalism, space and time are apparently separated, and we can fix the gauge by specifying a time axis and constant-time planes. The former prescription is called 'to fix the threading', and the latter is 'to fix the slicing'. All the ways to fix the threading are equivalent to the comoving threading in the linear approximation [96].[2] The comoving threading corresponds to the spatial coordinates which comove with fluids. We have a room to choose the time slicing. In the following, we mainly use two kinds of slicing. One is the flat slicing where the curvature perturbation ψ is zero. The other is the uniform-density slicing where the perturbation of total energy density vanishes, $\sum_i \delta\rho_i \equiv \delta\rho = 0$. We can also take only a part of energy density to be zero, $\delta\rho_i = 0$.

Let us consider the relationship between the e-folding number and the curvature perturbation. In the ADM formalism, we can define the local Hubble parameter as

$$\tilde{H}(t, x_i) \equiv \frac{1}{N_\ell}\frac{\dot{\tilde{a}}}{\tilde{a}} = \frac{1}{N_\ell}\left(\frac{\dot{a}}{a} + \dot{\psi}\right), \tag{D.4}$$

where $\tilde{a} = a(t)e^{\psi}$ is the local scale factor. Using the local Hubble parameter, the local

[2] In the $\delta\mathcal{N}$-formalism, we use gradient expansion where the perturbations on the superhorizon scale can be cut off.

e-folding number can be given by

$$\mathcal{N}(t_2, t_1; x_i) \equiv \int_{t_1}^{t_2} N_\ell dt \tilde{H}(t, x_i) = \int_{t_1}^{t_2} dt \left(\frac{\dot{a}}{a} + \dot{\psi} \right). \tag{D.5}$$

Thus we obtain

$$\psi(t_2, x_i) - \psi(t_1, x_i) = \mathcal{N}(t_2, t_1; x_i) - \ln \frac{a(t_2)}{a(t_1)}, \tag{D.6}$$

where time slicings are not fixed. The perturbation of the e-folding number is given by the difference of the curvature perturbations.

Let us derive the important quantity which is conserved on the superhorizon scale. In the linear approximation of the $\delta\mathcal{N}$-formalism, the equation of motion is reduced to the unperturbed form [96], and the energy conservation law is given by

$$\frac{1}{N_\ell} \frac{d\rho}{dt} + 3\tilde{H}(\rho + P) = 0, \tag{D.7}$$

where ρ and P are the total energy density and pressure, respectively. We can rewrite the right-hand side of (D.6) in the integral form as

$$\psi(t_2, x_i) - \psi(t_1, x_i) = -\frac{1}{3} \int_{\rho(t_2)}^{\rho(t_2, x_i)} \frac{d\rho}{\rho + P} + \frac{1}{3} \int_{\rho(t_1)}^{\rho(t_1, x_i)} \frac{d\rho}{\rho + P}. \tag{D.8}$$

From this equation, we can find a conserved quantity,

$$\zeta(x_i) = -\psi(t, x_i) - \frac{\delta\rho(t, x_i)}{3(\rho + P)}. \tag{D.9}$$

If the energy exchange between different components is not allowed, similar conserved quantities ζ_i can be defined for each component. Note that we consider only the superhorizon mode in the $\delta\mathcal{N}$-formalism.

Lastly, let us take an example for later use. We consider two sets of space-time manifold, A and B, where the initial slicing at $t = t_1$ is taken as the flat slicing. If the final slicing in the space time A is taken as the uniform-density slicing and that in the space time B as the $\delta\rho_i = 0$ slicing, then we obtain the difference between them,

$$\zeta_i = \zeta + \mathcal{N}_A - \mathcal{N}_B \equiv \zeta + \delta\mathcal{N}(t_2, t_1; x_i). \tag{D.10}$$

Here we define $\delta\mathcal{N}$ as the difference of the number of e-folds between the uniform-density and $\delta\rho_i = 0$ slicing. The gauge invariant perturbation can be written by the perturbation of $\mathcal{N}$. On the uniform-density slicing, the energy density is given by

$$\rho_i(\mathcal{N}_A, x_i) = \bar{\rho}_i + \delta\rho_i(\mathcal{N}_A, x_i). \tag{D.11}$$

On the other hand, we obtain the energy density on $\delta\rho_i = 0$ slicing,

$$\rho_i(\mathcal{N}_A + \delta\mathcal{N}) = \bar{\rho}_i. \tag{D.12}$$

Assuming $\delta\mathcal{N} \ll 1$ and $\delta\rho_i/\bar{\rho}_i \ll 1$, we obtain [145, 146, 147]

$$\delta\mathcal{N} \simeq -\frac{\delta\rho_i}{\bar{\rho}_i'}, \tag{D.13}$$

where the prime denotes the derivative with respect to $\mathcal{N}_A$. Using this formula, we can calculate the isocurvature power spectrum by following the e-folding number.

D.2 Estimate of power spectrum

Numerical method

Here we present a numerical method for calculating the power spectrum of the axionic isocurvaure perturbation on the basis of the $\delta\mathcal{N}$-formalism described above.

The isocurvature perturbation is defined as

$$S(x_i) \equiv 3(\zeta_{\rm CDM} - \zeta_{\rm rad}). \tag{D.14}$$

Assuming that the other CDM components acquire only adiabatic fluctuations uncorrelated with the axionic fluctuation, we obtain

$$\zeta_{\rm CDM} + \psi = -\frac{\delta\rho_\phi + \delta\rho_m}{\bar{\rho}'_\phi + \bar{\rho}'_m} \simeq -R_\phi \frac{\delta\rho_\phi}{\bar{\rho}'_\phi}, \tag{D.15}$$

with $R_\phi \equiv \Omega_\phi/\Omega_{\rm DM}$. Here $\bar{\rho}_{\phi(m)}$ and $\delta\rho_{\phi(m)}$ denote the homogeneous part and the fluctuation of the axion (the other CDM) energy density, respectively. Note that we have used $\delta\rho_m = 0$ in the second equality. This is because we have approximately $\delta\rho_{\rm rad} = \delta\rho_m = 0$ in the deep radiation dominated era.

Using Eq. (D.13), we obtain the CDM isocurvature perturbation using the fluctuation of the e-folding number $\delta\mathcal{N}$,

$$S(\vec{x}) \simeq -3R_\phi \frac{\delta\rho_\phi}{\bar{\rho}'_\phi} \simeq 3R_\phi \delta\mathcal{N}. \tag{D.16}$$

Note that $\delta\mathcal{N}$ is defined as the fluctuation of the number of e-folds from the initial flat slicing at the horizon exit of the CMB scales to the uniform-ρ_ϕ slicing after the axion abundance gets fixed. We expand $\delta\mathcal{N}$ in terms of the axion fluctuation as

$$\delta\mathcal{N} \simeq \frac{\partial\mathcal{N}}{\partial\phi_*}\delta\phi_* + \frac{1}{2}\frac{\partial^2\mathcal{N}}{\partial\phi_*^2}(\delta\phi_*^2 - \langle\partial\phi_*^2\rangle) + \cdots, \tag{D.17}$$

where $\delta\phi_*$ represents the initial fluctuation of the axion field at the horizon exit, and ϕ_* is identified with the initial position $\phi_{\rm ini}$ in the previous section.

The isocurvature power spectrum is defined as

$$\langle S(\vec{k}_1)S(\vec{k}_2)\rangle \equiv (2\pi)^3\mathcal{P}_S(\vec{k}_1)\delta^{(3)}(\vec{k}_1 + \vec{k}_2), \tag{D.18}$$

where $S(\vec{k})$ denotes the Fourier component of the isocurvature perturbation $S(x_i)$. Taking account of the leading term of (D.17) and using the power spectrum of $\delta\phi_*$, $\mathcal{P}_{\delta\phi_*}(\vec{k}) = H_{\rm inf}^2/2k^3$, we obtain the dimensionless power spectrum,

$$\Delta_S^2 \equiv \frac{k^3}{2\pi^2}\mathcal{P}_S(\vec{k}) \simeq \left(3R_\phi \frac{\partial\mathcal{N}}{\partial\theta_{\rm ini}}\frac{H_{\rm inf}}{2\pi f_\phi}\right)^2 \equiv (R_\phi\Delta_\phi)^2. \tag{D.19}$$

where we have defined Δ_ϕ.

This formula is a useful form to estimate the isocurvature perturbation numerically. Noting that the e-folding number is measured as the difference between the final slicing of $\delta\rho_\phi = 0$ and $\delta\rho = 0$, we can obtain its derivative by taking the difference of the e-folding

numbers for slightly different initial positions. Numerically, it is sufficient to follow each e-folding number until the axion number density becomes equal to a fixed value after n_ϕ/s becomes constant with time. Specifically, we have the relation $n_{\rm I}(T_E) = n_{\rm II}(T_E + \Delta T)$, where T_E is an arbitrary temperature (lower than $T_{\rm osc}$ or $T_{\rm osc2}$) on the final slicing, $n_{\rm I}$ is the number density for the initial position $\theta_{\rm ini}$, and $n_{\rm II}$ is the number density for $\theta_{\rm ini} + \Delta\theta$. After the (final) coherent oscillation started, n_ϕ/s becomes constant with time, and so we get

$$\frac{s(T_E + \Delta T)}{s(T_E)} = \frac{n_{\rm I}/s}{n_{\rm II}/s}. \tag{D.20}$$

Thus the difference of the e-folding number is written by

$$\delta\mathcal{N} = -\frac{1}{3}\ln\left[\frac{s(T_E + \Delta T)}{s(T_E)}\right] = -\frac{1}{3}\ln\left[\frac{n_{\rm I}/s}{n_{\rm II}/s}\right], \tag{D.21}$$

which is independent of the temperature T_E but depends only on $\Delta\theta$ as we expected. Thus we can evaluate the isocurvature perturbation by calculating the ratio of n_ϕ/s for slightly different initial conditions.

Analytical formula

Finally, let us derive the useful analytical formula of the isocurvature power spectrum by using Eq. (D.19) [100]. We assume that the total DM abundance is saturated by the axion and other CDM components, $\Omega_{\rm DM} = \Omega_\phi + \Omega_m$. Since the other components have adiabatic perturbations, the derivatives of energy density satisfies the relation,

$$\frac{\partial\rho_{\rm DM}}{\partial\phi_*} = \frac{\partial\rho_\phi}{\partial\phi_*}, \tag{D.22}$$

or

$$\frac{\partial\mathcal{N}}{\partial\phi_*} = \frac{\partial\mathcal{N}}{\partial\rho_{\rm DM}}\frac{\partial\rho_\phi}{\partial\phi_*} \simeq \frac{1}{3\rho_{\rm DM}}\frac{\partial\rho_\phi}{\partial\phi_*}. \tag{D.23}$$

In the second equality, we use $a(t) \propto \rho_{\rm DM}^{1/3}$ in the approximately matter-dominant universe where the perturbations of our interest enters into the horizon. Thus we obtain the power spectrum,

$$\Delta_S^2 \simeq \left(\frac{1}{\rho_{\rm DM}}\frac{\partial\rho_\phi}{\partial\theta_*}\frac{H_{\rm inf}}{2\pi f_\phi}\right)^2 = \left(R_\phi\frac{\partial\ln\Omega_\phi}{\partial\theta_*}\frac{H_{\rm inf}}{2\pi f_\phi}\right)^2. \tag{D.24}$$

Bibliography

[1] Planck collaboration, N. Aghanim et al., *Planck 2018 results. VI. Cosmological parameters*, *Astron. Astrophys.* **641** (2020) A6 [1807.06209].

[2] K. G. Begeman, A. H. Broeils and R. H. Sanders, *Extended rotation curves of spiral galaxies: Dark haloes and modified dynamics*, *Mon. Not. Roy. Astron. Soc.* **249** (1991) 523.

[3] D. Clowe, M. Bradac, A. H. Gonzalez, M. Markevitch, S. W. Randall, C. Jones et al., *A direct empirical proof of the existence of dark matter*, *Astrophys. J. Lett.* **648** (2006) L109 [astro-ph/0608407].

[4] K. Enqvist, S. Nadathur, T. Sekiguchi and T. Takahashi, *Decaying dark matter and the tension in σ_8*, *JCAP* **09** (2015) 067 [1505.05511].

[5] K. Enqvist, S. Nadathur, T. Sekiguchi and T. Takahashi, *Constraints on decaying dark matter from weak lensing and cluster counts*, *JCAP* **04** (2020) 015 [1906.09112].

[6] S. Alvi, T. Brinckmann, M. Gerbino, M. Lattanzi and L. Pagano, *Do you smell something decaying? Updated linear constraints on decaying dark matter scenarios*, *JCAP* **11** (2022) 015 [2205.05636].

[7] R. D. Peccei and H. R. Quinn, *CP Conservation in the Presence of Instantons*, *Phys. Rev. Lett.* **38** (1977) 1440.

[8] R. D. Peccei and H. R. Quinn, *Constraints Imposed by CP Conservation in the Presence of Instantons*, *Phys. Rev. D* **16** (1977) 1791.

[9] S. Weinberg, *A New Light Boson?*, *Phys. Rev. Lett.* **40** (1978) 223.

[10] F. Wilczek, *Problem of Strong P and T Invariance in the Presence of Instantons*, *Phys. Rev. Lett.* **40** (1978) 279.

[11] S. L. Adler, *Axial vector vertex in spinor electrodynamics*, *Phys. Rev.* **177** (1969) 2426.

[12] J. S. Bell and R. Jackiw, *A PCAC puzzle: $\pi^0 \to \gamma\gamma$ in the σ model*, *Nuovo Cim. A* **60** (1969) 47.

[13] A. A. Belavin, A. M. Polyakov, A. S. Schwartz and Y. S. Tyupkin, *Pseudoparticle Solutions of the Yang-Mills Equations*, *Phys. Lett. B* **59** (1975) 85.

[14] C. G. Callan, Jr., R. F. Dashen and D. J. Gross, *The Structure of the Gauge Theory Vacuum*, *Phys. Lett. B* **63** (1976) 334.

[15] R. Jackiw and C. Rebbi, *Vacuum Periodicity in a Yang-Mills Quantum Theory*, *Phys. Rev. Lett.* **37** (1976) 172.

[16] V. Baluni, *CP Violating Effects in QCD*, *Phys. Rev. D* **19** (1979) 2227.

[17] M. Pospelov and A. Ritz, *Theta vacua, QCD sum rules, and the neutron electric dipole moment*, *Nucl. Phys. B* **573** (2000) 177 [hep-ph/9908508].

[18] J. Dragos, T. Luu, A. Shindler, J. de Vries and A. Yousif, *Confirming the Existence of the strong CP Problem in Lattice QCD with the Gradient Flow*, *Phys. Rev. C* **103** (2021) 015202 [1902.03254].

[19] C. Abel et al., *Measurement of the Permanent Electric Dipole Moment of the Neutron*, *Phys. Rev. Lett.* **124** (2020) 081803 [2001.11966].

[20] A. Arvanitaki, S. Dimopoulos, S. Dubovsky, N. Kaloper and J. March-Russell, *String Axiverse*, *Phys. Rev. D* **81** (2010) 123530 [0905.4720].

[21] J. Preskill, M. B. Wise and F. Wilczek, *Cosmology of the Invisible Axion*, *Phys. Lett. B* **120** (1983) 127.

[22] L. F. Abbott and P. Sikivie, *A Cosmological Bound on the Invisible Axion*, *Phys. Lett. B* **120** (1983) 133.

[23] M. Dine and W. Fischler, *The Not So Harmless Axion*, *Phys. Lett. B* **120** (1983) 137.

[24] R. Mayle, J. R. Wilson, J. R. Ellis, K. A. Olive, D. N. Schramm and G. Steigman, *Constraints on Axions from SN 1987a*, *Phys. Lett. B* **203** (1988) 188.

[25] G. Raffelt and D. Seckel, *Bounds on Exotic Particle Interactions from SN 1987a*, *Phys. Rev. Lett.* **60** (1988) 1793.

[26] M. S. Turner, *Axions from SN 1987a*, *Phys. Rev. Lett.* **60** (1988) 1797.

[27] J. H. Chang, R. Essig and S. D. McDermott, *Supernova 1987A Constraints on Sub-GeV Dark Sectors, Millicharged Particles, the QCD Axion, and an Axion-like Particle*, *JHEP* **09** (2018) 051 [1803.00993].

[28] P. Carenza, T. Fischer, M. Giannotti, G. Guo, G. Martínez-Pinedo and A. Mirizzi, *Improved axion emissivity from a supernova via nucleon-nucleon bremsstrahlung*, *JCAP* **10** (2019) 016 [1906.11844].

[29] L. B. Leinson, *Axion mass limit from observations of the neutron star in Cassiopeia A*, *JCAP* **08** (2014) 031 [1405.6873].

[30] K. Hamaguchi, N. Nagata, K. Yanagi and J. Zheng, *Limit on the Axion Decay Constant from the Cooling Neutron Star in Cassiopeia A*, *Phys. Rev. D* **98** (2018) 103015 [1806.07151].

[31] L. B. Leinson, *Constraints on axions from neutron star in HESS J1731-347*, *JCAP* **11** (2019) 031 [1909.03941].

[32] M. Buschmann, C. Dessert, J. W. Foster, A. J. Long and B. R. Safdi, *Upper Limit on the QCD Axion Mass from Isolated Neutron Star Cooling*, *Phys. Rev. Lett.* **128** (2022) 091102 [2111.09892].

[33] D. H. Lyth, *Axions and inflation: Sitting in the vacuum*, *Phys. Rev. D* **45** (1992) 3394.

[34] K. Strobl and T. J. Weiler, *Anharmonic evolution of the cosmic axion density spectrum*, *Phys. Rev. D* **50** (1994) 7690 [astro-ph/9405028].

[35] K. J. Bae, J.-H. Huh and J. E. Kim, *Update of axion CDM energy*, *JCAP* **09** (2008) 005 [0806.0497].

[36] L. Visinelli and P. Gondolo, *Dark Matter Axions Revisited*, *Phys. Rev. D* **80** (2009) 035024 [0903.4377].

[37] R. Daido, F. Takahashi and W. Yin, *The ALP miracle: unified inflaton and dark matter*, *JCAP* **05** (2017) 044 [1702.03284].

[38] F. Takahashi and W. Yin, *QCD axion on hilltop by a phase shift of π*, *JHEP* **10** (2019) 120 [1908.06071].

[39] R. T. Co, E. Gonzalez and K. Harigaya, *Axion Misalignment Driven to the Hilltop*, *JHEP* **05** (2019) 163 [1812.11192].

[40] P. W. Graham and A. Scherlis, *Stochastic axion scenario*, *Phys. Rev. D* **98** (2018) 035017 [1805.07362].

[41] F. Takahashi, W. Yin and A. H. Guth, *QCD axion window and low-scale inflation*, *Phys. Rev. D* **98** (2018) 015042 [1805.08763].

[42] S. Nakagawa, F. Takahashi and W. Yin, *Stochastic Axion Dark Matter in Axion Landscape*, *JCAP* **05** (2020) 004 [2002.12195].

[43] M. Reig, *The stochastic axiverse*, *JHEP* **09** (2021) 207 [2104.09923].

[44] R. Kallosh, A. D. Linde, D. A. Linde and L. Susskind, *Gravity and global symmetries*, *Phys. Rev. D* **52** (1995) 912 [hep-th/9502069].

[45] T. Banks and N. Seiberg, *Symmetries and Strings in Field Theory and Gravity*, *Phys. Rev. D* **83** (2011) 084019 [1011.5120].

[46] E. Witten, *Symmetry and Emergence*, *Nature Phys.* **14** (2018) 116 [1710.01791].

[47] D. Harlow and H. Ooguri, *Constraints on Symmetries from Holography*, *Phys. Rev. Lett.* **122** (2019) 191601 [1810.05337].

[48] D. Harlow and H. Ooguri, *Symmetries in quantum field theory and quantum gravity*, *Commun. Math. Phys.* **383** (2021) 1669 [1810.05338].

[49] K. S. Jeong, K. Matsukawa, S. Nakagawa and F. Takahashi, *Cosmological effects of Peccei-Quinn symmetry breaking on QCD axion dark matter*, *JCAP* **03** (2022) 026 [2201.00681].

[50] E. Witten, *Dyons of Charge e theta/2 pi*, *Phys. Lett. B* **86** (1979) 283.

[51] W. Fischler and J. Preskill, *DYON - AXION DYNAMICS*, *Phys. Lett. B* **125** (1983) 165.

[52] G. 't Hooft, *Magnetic Monopoles in Unified Gauge Theories*, *Nucl. Phys. B* **79** (1974) 276.

[53] A. M. Polyakov, *Particle Spectrum in Quantum Field Theory*, *JETP Lett.* **20** (1974) 194.

[54] M. Kawasaki, F. Takahashi and M. Yamada, *Suppressing the QCD Axion Abundance by Hidden Monopoles*, *Phys. Lett. B* **753** (2016) 677 [1511.05030].

[55] M. Kawasaki, F. Takahashi and M. Yamada, *Adiabatic suppression of the axion abundance and isocurvature due to coupling to hidden monopoles*, *JHEP* **01** (2018) 053 [1708.06047].

[56] A. D. Linde, *Relaxing the cosmological moduli problem*, *Phys. Rev. D* **53** (1996) R4129 [hep-th/9601083].

[57] K. Nakayama, F. Takahashi and T. T. Yanagida, *On the Adiabatic Solution to the Polonyi/Moduli Problem*, *Phys. Rev. D* **84** (2011) 123523 [1109.2073].

[58] S. Nakagawa, F. Takahashi and M. Yamada, *Trapping Effect for QCD Axion Dark Matter*, *JCAP* **05** (2021) 062 [2012.13592].

[59] J. E. Kim, *Light Pseudoscalars, Particle Physics and Cosmology*, *Phys. Rept.* **150** (1987) 1.

[60] H.-Y. Cheng, *The Strong CP Problem Revisited*, *Phys. Rept.* **158** (1988) 1.

[61] M. Kuster, G. Raffelt and B. Beltran, eds., *Axions: Theory, cosmology, and experimental searches. Proceedings, 1st Joint ILIAS-CERN-CAST axion training, Geneva, Switzerland, November 30-December 2, 2005*, vol. 741, 2008.

[62] J. E. Kim and G. Carosi, *Axions and the Strong CP Problem*, *Rev. Mod. Phys.* **82** (2010) 557 [0807.3125].

[63] D. J. E. Marsh, *Axion Cosmology*, *Phys. Rept.* **643** (2016) 1 [1510.07633].

[64] L. Di Luzio, M. Giannotti, E. Nardi and L. Visinelli, *The landscape of QCD axion models*, *Phys. Rept.* **870** (2020) 1 [2003.01100].

[65] W. A. Bardeen, *Anomalous Currents in Gauge Field Theories*, *Nucl. Phys. B* **75** (1974) 246.

[66] K. Fujikawa, *Path Integral Measure for Gauge Invariant Fermion Theories*, *Phys. Rev. Lett.* **42** (1979) 1195.

[67] M. A. B. Beg and H. S. Tsao, *Strong P, T Noninvariances in a Superweak Theory*, *Phys. Rev. Lett.* **41** (1978) 278.

[68] H. Georgi, *A Model of Soft CP Violation*, *Hadronic J.* **1** (1978) 155.

[69] R. N. Mohapatra and G. Senjanovic, *Natural Suppression of Strong p and t Noninvariance*, *Phys. Lett. B* **79** (1978) 283.

[70] A. E. Nelson, *Naturally Weak CP Violation*, *Phys. Lett. B* **136** (1984) 387.

[71] S. M. Barr, *Solving the Strong CP Problem Without the Peccei-Quinn Symmetry*, *Phys. Rev. Lett.* **53** (1984) 329.

[72] C. Vafa and E. Witten, *Restrictions on Symmetry Breaking in Vector-Like Gauge Theories*, *Nucl. Phys. B* **234** (1984) 173.

[73] C. Vafa and E. Witten, *Parity Conservation in QCD*, *Phys. Rev. Lett.* **53** (1984) 535.

[74] J. E. Kim, *Weak Interaction Singlet and Strong CP Invariance*, *Phys. Rev. Lett.* **43** (1979) 103.

[75] M. A. Shifman, A. I. Vainshtein and V. I. Zakharov, *Can Confinement Ensure Natural CP Invariance of Strong Interactions?*, *Nucl. Phys. B* **166** (1980) 493.

[76] A. R. Zhitnitsky, *On Possible Suppression of the Axion Hadron Interactions. (In Russian)*, *Sov. J. Nucl. Phys.* **31** (1980) 260.

[77] M. Dine, W. Fischler and M. Srednicki, *A Simple Solution to the Strong CP Problem with a Harmless Axion*, *Phys. Lett. B* **104** (1981) 199.

[78] P. Di Vecchia and G. Veneziano, *Chiral Dynamics in the Large n Limit*, *Nucl. Phys. B* **171** (1980) 253.

[79] G. Grilli di Cortona, E. Hardy, J. Pardo Vega and G. Villadoro, *The QCD axion, precisely*, *JHEP* **01** (2016) 034 [1511.02867].

[80] M. Gorghetto and G. Villadoro, *Topological Susceptibility and QCD Axion Mass: QED and NNLO corrections*, *JHEP* **03** (2019) 033 [1812.01008].

[81] RM123 collaboration, G. M. de Divitiis, R. Frezzotti, V. Lubicz, G. Martinelli, R. Petronzio, G. C. Rossi et al., *Leading isospin breaking effects on the lattice*, *Phys. Rev. D* **87** (2013) 114505 [1303.4896].

[82] MILC collaboration, S. Basak et al., *Electromagnetic effects on the light hadron spectrum*, *J. Phys. Conf. Ser.* **640** (2015) 012052 [1510.04997].

[83] R. Horsley et al., *Isospin splittings of meson and baryon masses from three-flavor lattice QCD + QED*, *J. Phys. G* **43** (2016) 10LT02 [1508.06401].

[84] C. G. Callan, Jr., R. F. Dashen and D. J. Gross, *Toward a Theory of the Strong Interactions*, *Phys. Rev. D* **17** (1978) 2717.

[85] C. Bonati, M. D'Elia, M. Mariti, G. Martinelli, M. Mesiti, F. Negro et al., *Axion phenomenology and θ-dependence from $N_f = 2 + 1$ lattice QCD*, *JHEP* **03** (2016) 155 [1512.06746].

[86] S. Borsanyi et al., *Calculation of the axion mass based on high-temperature lattice quantum chromodynamics*, *Nature* **539** (2016) 69 [1606.07494].

[87] P. Petreczky, H.-P. Schadler and S. Sharma, *The topological susceptibility in finite temperature QCD and axion cosmology*, *Phys. Lett. B* **762** (2016) 498 [1606.03145].

[88] C. Bonati, M. D'Elia, G. Martinelli, F. Negro, F. Sanfilippo and A. Todaro, *Topology in full QCD at high temperature: a multicanonical approach*, *JHEP* **11** (2018) 170 [1807.07954].

[89] F. Burger, E.-M. Ilgenfritz, M. P. Lombardo and A. Trunin, *Chiral observables and topology in hot QCD with two families of quarks*, *Phys. Rev. D* **98** (2018) 094501 [1805.06001].

[90] D. J. Gross, R. D. Pisarski and L. G. Yaffe, *QCD and Instantons at Finite Temperature*, *Rev. Mod. Phys.* **53** (1981) 43.

[91] G. Ballesteros, J. Redondo, A. Ringwald and C. Tamarit, *Standard Model—axion—seesaw—Higgs portal inflation. Five problems of particle physics and cosmology solved in one stroke*, *JCAP* **08** (2017) 001 [1610.01639].

[92] T. Hiramatsu, M. Kawasaki, K. Saikawa and T. Sekiguchi, *Production of dark matter axions from collapse of string-wall systems*, *Phys. Rev. D* **85** (2012) 105020 [1202.5851].

[93] M. Kawasaki, K. Saikawa and T. Sekiguchi, *Axion dark matter from topological defects*, *Phys. Rev. D* **91** (2015) 065014 [1412.0789].

[94] T. S. Bunch and P. C. W. Davies, *Quantum Field Theory in de Sitter Space: Renormalization by Point Splitting*, *Proc. Roy. Soc. Lond. A* **360** (1978) 117.

[95] K. A. Malik and D. Wands, *Evolution of second-order cosmological perturbations*, *Class. Quant. Grav.* **21** (2004) L65 [astro-ph/0307055].

[96] D. H. Lyth, K. A. Malik and M. Sasaki, *A General proof of the conservation of the curvature perturbation*, *JCAP* **05** (2005) 004 [astro-ph/0411220].

[97] P. J. Steinhardt and M. S. Turner, *Saving the Invisible Axion*, *Phys. Lett. B* **129** (1983) 51.

[98] A. D. Linde, *Generation of Isothermal Density Perturbations in the Inflationary Universe*, *Phys. Lett. B* **158** (1985) 375.

[99] Planck collaboration, Y. Akrami et al., *Planck 2018 results. X. Constraints on inflation*, *Astron. Astrophys.* **641** (2020) A10 [1807.06211].

[100] T. Kobayashi, R. Kurematsu and F. Takahashi, *Isocurvature Constraints and Anharmonic Effects on QCD Axion Dark Matter*, *JCAP* **09** (2013) 032 [1304.0922].

[101] G. Grilli di Cortona, E. Hardy, J. Pardo Vega and G. Villadoro, *The QCD axion, precisely*, *JHEP* **01** (2016) 034 [1511.02867].

[102] "AxionLimits website." https://cajohare.github.io/AxionLimits/.

[103] I. Stern, *ADMX Status*, *PoS* **ICHEP2016** (2016) 198 [1612.08296].

[104] MADMAX Working Group collaboration, A. Caldwell, G. Dvali, B. Majorovits, A. Millar, G. Raffelt, J. Redondo et al., *Dielectric Haloscopes: A New Way to Detect Axion Dark Matter*, *Phys. Rev. Lett.* **118** (2017) 091801 [1611.05865].

[105] ABRACADABRA collaboration, R. Henning et al., *ABRACADABRA, A Search for Low-Mass Axion Dark Matter*, in *13th Patras Workshop on Axions, WIMPs and WISPs*, pp. 28–31, 2018, DOI.

[106] CAST collaboration, V. Anastassopoulos et al., *New CAST Limit on the Axion-Photon Interaction*, *Nature Phys.* **13** (2017) 584 [1705.02290].

[107] S.-F. Ge, K. Hamaguchi, K. Ichimura, K. Ishidoshiro, Y. Kanazawa, Y. Kishimoto et al., *Supernova-scope for the Direct Search of Supernova Axions*, *JCAP* **11** (2020) 059 [2008.03924].

[108] IAXO collaboration, E. Armengaud et al., *Physics potential of the International Axion Observatory (IAXO)*, *JCAP* **06** (2019) 047 [1904.09155].

[109] S. M. Barr and D. Seckel, *Planck scale corrections to axion models*, *Phys. Rev. D* **46** (1992) 539.

[110] R. Holman, S. D. H. Hsu, T. W. Kephart, E. W. Kolb, R. Watkins and L. M. Widrow, *Solutions to the strong CP problem in a world with gravity*, *Phys. Lett. B* **282** (1992) 132 [hep-ph/9203206].

[111] M. Kamionkowski and J. March-Russell, *Planck scale physics and the Peccei-Quinn mechanism*, *Phys. Lett. B* **282** (1992) 137 [hep-th/9202003].

[112] M. Kamionkowski and J. March-Russell, *Are textures natural?*, *Phys. Rev. Lett.* **69** (1992) 1485 [hep-th/9201063].

[113] L. M. Carpenter, M. Dine and G. Festuccia, *Dynamics of the Peccei Quinn Scale*, *Phys. Rev. D* **80** (2009) 125017 [0906.1273].

[114] F. Takahashi and M. Yamada, *Strongly broken Peccei-Quinn symmetry in the early Universe*, *JCAP* **10** (2015) 010 [1507.06387].

[115] Particle Data Group collaboration, R. L. Workman et al., *Review of Particle Physics*, *PTEP* **2022** (2022) 083C01.

[116] J. Fuentes-Martín, M. Reig and A. Vicente, *Strong CP problem with low-energy emergent QCD: The 4321 case*, *Phys. Rev. D* **100** (2019) 115028 [1907.02550].

[117] C. Csáki, M. Ruhdorfer and Y. Shirman, *UV Sensitivity of the Axion Mass from Instantons in Partially Broken Gauge Groups*, *JHEP* **04** (2020) 031 [1912.02197].

[118] M. A. Buen-Abad and J. Fan, *Dynamical axion misalignment with small instantons*, *JHEP* **12** (2019) 161 [1911.05737].

[119] S. Nakagawa, F. Takahashi, M. Yamada and W. Yin, *Axion dark matter from first-order phase transition, and very high energy photons from GRB 221009A*, 2210.10022.

[120] Y. Nomura, S. Rajendran and F. Sanches, *Axion Isocurvature and Magnetic Monopoles*, *Phys. Rev. Lett.* **116** (2016) 141803 [1511.06347].

[121] T. Higaki, K. S. Jeong, N. Kitajima and F. Takahashi, *Quality of the Peccei-Quinn symmetry in the Aligned QCD Axion and Cosmological Implications*, *JHEP* **06** (2016) 150 [1603.02090].

[122] N. Kitajima and F. Takahashi, *Primordial Black Holes from QCD Axion Bubbles*, *JCAP* **11** (2020) 060 [2006.13137].

[123] L. Di Luzio, B. Gavela, P. Quilez and A. Ringwald, *Dark matter from an even lighter QCD axion: trapped misalignment*, *JCAP* **10** (2021) 001 [2102.01082].

[124] B. T. McAllister, G. Flower, J. Kruger, E. N. Ivanov, M. Goryachev, J. Bourhill et al., *The ORGAN Experiment: An axion haloscope above 15 GHz*, *Phys. Dark Univ.* **18** (2017) 67 [1706.00209].

[125] D. J. E. Marsh, K.-C. Fong, E. W. Lentz, L. Smejkal and M. N. Ali, *Proposal to Detect Dark Matter using Axionic Topological Antiferromagnets*, *Phys. Rev. Lett.* **123** (2019) 121601 [1807.08810].

[126] J. Schütte-Engel, D. J. E. Marsh, A. J. Millar, A. Sekine, F. Chadha-Day, S. Hoof et al., *Axion quasiparticles for axion dark matter detection*, *JCAP* **08** (2021) 066 [2102.05366].

[127] S. Chigusa, T. Moroi and K. Nakayama, *Axion/hidden-photon dark matter conversion into condensed matter axion*, *JHEP* **08** (2021) 074 [2102.06179].

[128] DMRadio collaboration, L. Brouwer et al., *Projected sensitivity of DMRadio-m3: A search for the QCD axion below 1 μeV*, *Phys. Rev. D* **106** (2022) 103008 [2204.13781].

[129] D. Alesini, D. Babusci, D. Di Gioacchino, C. Gatti, G. Lamanna and C. Ligi, *The KLASH Proposal*, 1707.06010.

[130] nEDM collaboration, M. W. Ahmed et al., *A New Cryogenic Apparatus to Search for the Neutron Electric Dipole Moment*, *JINST* **14** (2019) P11017 [1908.09937].

[131] n2EDM collaboration, N. J. Ayres et al., *The design of the n2EDM experiment: nEDM Collaboration*, *Eur. Phys. J. C* **81** (2021) 512 [2101.08730].

[132] D. Wurm et al., *The PanEDM Neutron Electric Dipole Moment Experiment at the ILL*, *EPJ Web Conf.* **219** (2019) 02006 [1911.09161].

[133] T. Higaki, K. S. Jeong, N. Kitajima and F. Takahashi, *The QCD Axion from Aligned Axions and Diphoton Excess*, *Phys. Lett. B* **755** (2016) 13 [1512.05295].

[134] S. Nakagawa, F. Takahashi and M. Yamada, *Cosmic Birefringence Triggered by Dark Matter Domination*, *Phys. Rev. Lett.* **127** (2021) 181103 [2103.08153].

[135] S. M. Carroll, G. B. Field and R. Jackiw, *Limits on a Lorentz and Parity Violating Modification of Electrodynamics*, *Phys. Rev. D* **41** (1990) 1231.

[136] S. M. Carroll and G. B. Field, *The Einstein equivalence principle and the polarization of radio galaxies*, *Phys. Rev. D* **43** (1991) 3789.

[137] D. Harari and P. Sikivie, *Effects of a Nambu-Goldstone boson on the polarization of radio galaxies and the cosmic microwave background*, *Phys. Lett. B* **289** (1992) 67.

[138] S. M. Carroll, *Quintessence and the rest of the world*, *Phys. Rev. Lett.* **81** (1998) 3067 [astro-ph/9806099].

[139] A. Lue, L.-M. Wang and M. Kamionkowski, *Cosmological signature of new parity violating interactions*, *Phys. Rev. Lett.* **83** (1999) 1506 [astro-ph/9812088].

[140] T. Fujita, Y. Minami, K. Murai and H. Nakatsuka, *Probing axionlike particles via cosmic microwave background polarization*, *Phys. Rev. D* **103** (2021) 063508 [2008.02473].

[141] K. Saikawa and S. Shirai, *Primordial gravitational waves, precisely: The role of thermodynamics in the Standard Model*, *JCAP* **05** (2018) 035 [1803.01038].

[142] R. J. Crewther, *Effects of Topological Charge in Gauge Theories*, *Acta Phys. Austriaca Suppl.* **19** (1978) 47.

[143] R. Bott, *On the iteration of closed geodesics and the sturm intersection theory*, *Commun. Pure. Appl. Math* **9 (2)** (1956) 171.

[144] R. L. Arnowitt, S. Deser and C. W. Misner, *The Dynamics of general relativity*, *Gen. Rel. Grav.* **40** (2008) 1997 [gr-qc/0405109].

[145] M. Kawasaki, K. Nakayama, T. Sekiguchi, T. Suyama and F. Takahashi, *Non-Gaussianity from isocurvature perturbations*, *JCAP* **11** (2008) 019 [0808.0009].

[146] D. Langlois, F. Vernizzi and D. Wands, *Non-linear isocurvature perturbations and non-Gaussianities*, *JCAP* **12** (2008) 004 [0809.4646].

[147] M. Kawasaki, K. Nakayama, T. Sekiguchi, T. Suyama and F. Takahashi, *A General Analysis of Non-Gaussianity from Isocurvature Perturbations*, *JCAP* **01** (2009) 042 [0810.0208].